CENTRAL NERVOUS SYSTEM REGULATION OF MUSCLE ATROPHY

by

Theodore Paul Braun

A DISSERTATION

Presented to the Department Cell and Developmental Biology

and the Oregon Health & Science University

School of Medicine

in partial fulfillment of

the requirements for the degree of

Doctor of Philosophy

April 2012

CERTIFICATE OF APPROVAL

This is to certify that the PhD dissertation of

Theodore P. Braun

has been approved

Advisor, Daniel Marks, MD, PhD

Member and Chair, Caroline Enns, PhD

Member, Kevin Grove, PhD

Member, David Jacoby, MD

Member, Anthony Barnes, PhD

TABLE OF CONTENTS

LIST OF FIGURES AND TABLES

Appendix B

LIST OF ABBRIVIATIONS

ACTH	Adrenocorticotropic Hormone
ADX	Adrenalectomy
AgRP	Agouti Related Peptide
AMPK	AMP Activated Protein Kinase
ARC	Arcuate Nucleus of the Hypothalamus
ATP	Adenosine Triphosphate
BBB	Blood Brain Barrier
BCAT2	Branched Chain Amino-Acid Transferase
BMD	Bone Mineral Density
BMI	Body Mass Index
Bnip3	BCL2/adenovirus E1B 19 kDa protein-interacting protein 3
BSA	Bovine Serum Albumin
CART	Cocaine and Amphetamine Regulated Transcript
CHF	Congestive Heart Failure
CLP	Cecal Ligation and Puncture
CNS	Central Nervous System
COX	Cyclooxygenase
CRH	Corticotropin Releasing Hormone
CSA	Cross Sectional Area
CstL	Cathepsin L
Depp	Decidual Protein Regulated by Progesterone
Dex	Dexamethasone
DIO	Diet Induced Obesity
EDL	Extensor Digitorum Longus

FOXO	Forkhead Box Protein O1
GABARAPL1	GABA(A) Receptor-Associated Protein Like 1
GAPDH	Glyceraldehyde 3-Phosphate Dehydrogenase
GHSR-1a	Growth Hormone Secretagogue Receptor 1a
Gn	Gastrocnemius
GR	Glucocorticoid Receptor
GRE	Glucocorticoid Response Element
HFD	High Fat Diet
HPA	Hypothalamic Pituitary Adrenal
i.c.v.	Intracerebroventricular
i.p.	Intraperitoneal
Id3	Inhibitor of DNA Binding 3
IGF-1	Insulin-Like Growth Factor 1
IKK	Inhibitor of Kappa Kinase
IL-1R1	Interleukin-1 Receptor 1
IL-1Ra	Interleukin-1 Receptor Antagonist
IL-1α	Interleukin-1 Alpha
IL-1β	Interleukin-1 Beta
IL-6	Interleukin 6
IRES	Internal Ribosome Entry Sight
IRS	Insulin Receptor Substrate
IκBα	Inhibitor of kappa-B alpha
KLF15	Krüpple-Like Factor 15
KY	Kyphoscoliosis Peptidase
LC3	Microtubule-Associated Protein 1 Light Chain 3 Beta

Lcn2	Lipocalin 2
LIF	Leukemia Inhibitory Factor
LLC	Lewis Lung Carcinoma
LMA	Locomoter Activity
LOD	Limit of Detection
LPS	Lipopolysaccharide
MAFbx	Muscle Atrophy F Box
MC4R	Type 4 Melanocortin Receptor
MC4RKO	Type 4 Melanocortin Receptor Knockout
mGRKO	Muscle-Specific Glucocorticoid Receptor Knockout
mMyD88KO	Muscle-Specific MyD88 knockout
MR	Mineralocorticoid Receptor
Mt2	Metallothionein 2
MTII	Melanotan II
mTOR	Mamalian Target of Rapamycin
MuRF1	Muscle Ring Finger Protein 1
MyD88	Myeloid Differentiation Factor 88
MyD88KO	Myeloid Differentiation Factor 88 Knockout
NFκB	Nuclear Factor Kappa-B
NPY	Neuropeptide Y
p38 MAPK	P38 Mitogen Activated Protein Kinase
PF	Pair Fed
PGE2	Prostaglandin E2
PI3K	Phosphatidylinositol 3-Kinases
POMC	Proopiomelanocortin

PVN	Paraventricular Nucleus
REDD1	Regulated in DNA Damage Responses1
RIA	Radioimmunoassay
SERGMs	Selective Glucocorticoid Receptor Modulator
Sesn1	Sestrin 1
SGK1	Serum and Glucocorticoid-Induceible Kinase 1
SNS	Sympathetic Nervous System
SOCS3	Suppressor of Cytokine Signaling 3
TA	Tibialis Anterior
TAK1	Transforming Growth Factor Beta Activated Kinase 1
TGF-β	Transforming Growth Factor Beta
TLR4	Toll-Like Receptor 4
TNF	Tumor Necrosis Factor
TRAF6	Tumor Necrosis Factor Associated Factor
Ucp3	Uncoupling Protein 3
Veh	Vehicle
WGn	White Gastrocnemius
WT	Wild Type
ZT	Zeitgeber
α-MSH	Alpha Melanocyte Stimulating Hormone

ACKNOWLEDGEMENTS

I owe a debt of gratitude to many people for their help during the course of my graduate work. Firstly, I would like to thank my mentor Dr. Daniel Marks for his incredible support. I first met Dan as an interviewing student, and it was immediately impressed upon me that he was someone who would hold me to a high standard. From the start, Dan has believed in me. He allowed me to do a rotation as a medical student when others told me I could not. He somehow gave me enough rope in the lab to find my own way (and gain confidence from it), but not so much as to allow me to drift off track. Dan always had time to talk with me about my work and to deal with whatever I happened to be worked up about at the time, irrespective of his myriad of other responsibilities. As I move forward in my career and face the prospect of mentoring others myself, I hope to be able to emulate in some way, the mentorship that Dan has provided to me.

I would also like to thank my thesis committee members, Dr. Caroline Enns, Dr. David Jacoby, Dr. Kevin Grove and Dr. Anthony Barnes. I greatly appreciate the time they have spent in guiding the development of the research contained in this thesis. The input they have provided has pushed me to consider alternate approaches and interpretations that I would not have otherwise.

My co-workers in the Marks Lab are also provided invaluable support throughout the entirety of my graduate career. Many thanks to Xin Xia, Stephanie, Peter, Wilmon, My Linh, Maynika, Gabe, Lindsey and Cindy. Whether it be help with an experiment, editing of manuscript, or simply providing friendship, they are responsible for the creation of a lab environment that was a positive and exciting place to be. I would particularly like to say thanks to two individuals. The first is Marek Szumowski, a technician who worked

with me during the final two years of graduate school. The animal experiments described in this thesis and numerous others that do not appear here require attention to detail, responsibility and hard labor. Marek provided all of this without complaint. I could not have accomplished half of what I did during the last year of my PhD without his help.

The second individual who I would like to specially thank is Aaron Grossberg. Graduate training and in particular MD/PhD training can be a lonely undertaking. I was incredibly fortunate to be joined during my journey by another individual who was also undertaking the same journey himself. I cannot think of a single experiment that appears in this thesis in that Aaron did not participate in the design of to some degree. He was not only an incredibly important part of my development as a scientist, but also a close friend. My experience as a graduate student would have been fundamentally different had I not shared it with Aaron.

Finally I would like to thank my family for their support. My father and mother have been supportive of my career ambitions my entire life and have done everything in their power to allow me to focus on my work. My wife Julia has equally been supportive. She has been there for me equally during times of elation and frustration. Truly, I would not have been able to accomplish anything without her love and understanding. It is to my daughter Isabel that I would like to dedicate this thesis. Although she does not realize it yet, she is going to have an interesting ride as the child of two scientists. I hope she is understanding.

ABSTRACT

Chronic disease is marked by perturbations in both behavior and systemic metabolism. A loss of muscle mass, decreased food intake, and decreases in daily activity are collectively referred to as cachexia. The presence of cachexia likely has a significant impact on disease survival. While the features of cachexia are conserved, the underlying diseases that cause cachexia are varied. Illnesses such as cancer, renal failure, heart failure and chronic infection all result in sickness behavior and muscle atrophy. Despite significant variation in the underlying disease pathology, conditions associated with cachexia are all marked by systemic inflammation. The infusion of inflammatory cytokines into experimental animals reproduces the features of cachexia. Despite this, the mechanisms by which inflammation produces cachexia remain unclear and treatment options are very limited. The goal of this thesis was to define the anatomic sites where cytokines act to produce the different features of cachexia.

One of the primary focuses of the work described here was the investigation of muscle atrophy from a systems perspective. The vast majority of work investigating the mechanisms of inflammatory muscle atrophy has been appropriately performed at the level of the skeletal myocyte. However, little attention has been directed at other tissues as mediators of muscle wasting. We investigated the role of the brain as an intermediary between inflammatory cytokines and the loss of muscle mass. This work demonstrated that inflammation in the brain only was sufficient to produce rapid muscle atrophy at the molecular and gross level. We further identified glucocorticoids as a fundamental mediator of this process, as adrenalectomized animals fail to catabolize muscle in response to central inflammation. We demonstrated that CNS cytokine signaling is an essential player in the atrophy response to systemic inflammation as well. Muscle-specific deletion of the glucocorticoid receptor prevents atrophy in response to systemic

inflammatory challenges. Further, it appears that increased levels of glucocorticoids are all that is required for muscle atrophy. Treatment of rats with glucocorticoids at a dose that reproduces the circulating levels seen in response to inflammation produces severe wasting of muscle mass.

We also performed a series of experiments to examine the cell types that respond directly to cytokines and produce sickness behavior. We generated mice lacking the adaptor protein MyD88 (which is requisite for interleukin-1 signaling) in neurons. Despite the fact that mice lacking MyD88 in all tissues do not display any features of cachexia in response to IL-1β administration, our data demonstrate that MyD88 is not required in neurons for sickness behavior.

The data described in this thesis provide insight into the cellular and tissue sites-of-action for inflammatory cytokines in mediating cachexia. Collectively, they demonstrate that the CNS is a fundamental regulator of cachexia, mediating both sickness behavior and muscle atrophy. Furthermore, these data highlight the critical role of glucocorticoids as mediators of inflammation-induced atrophy and support therapeutic interventions targeting this hormonal system.

CHAPTER 1

INTRODUCTION

1. Significance

Decreased appetite (Anorexia) and catabolism of lean tissues are common co-morbidities of a multitude of chronic diseases. In diseases such as cancer, congestive heart failure (CHF), chronic renal failure and sepsis, the synergistic effects of decreased energy intake on the one hand, and increased energy expenditure on the other generate an ongoing loss of body weight (1). In contrast with starvation, where weight is lost primarily in the form of fat, inflammation exhibits a special proclivity for the loss of skeletal muscle mass (2). The loss of muscle mass accompanying involuntary weight loss in chronic disease is known as cachexia. The consensus definition of cachexia is "... a complex metabolic syndrome associated with underlying illness and characterized by the loss of muscle with or without loss of fat mass" (3). Although cachexia is not always associated with overt anorexia, they often occur together (4). Potentially exacerbated by decreased food intake, weight loss is a serious contributor to the morbidity and mortality of inflammatory diseases. In cancer patients, 30-80% experience weight loss depending on the type of cancer (5). Patients diagnosed with pancreatic and gastric cancer are the most likely to experience weight loss. In pancreatic cancer, weight loss is a presenting symptom with a median weight loss in 14.2% in patients with unresectable tumors, progressing to 24.5% at the time of last assessment (6). Weight loss also occurs in many other forms of chronic disease. In CHF, 16% of patients in one study were identified as having undergone significant weight loss (7).

The presence of cachexia is a negative prognostic indicator in a multitude of conditions including cancer (8-10), chronic renal failure (11), CHF) (7), and HIV (12). These observations have lead to the suggestion that, in cancer, 20% of deaths are the direct result of cachexia (13). It was recently found that the treatment of muscle loss in experimental cancer cachexia dramatically improves survival independent of

tumor progression providing the first evidence of the causal relationship between cachexia and disease mortality (14). Unfortunately, despite the clear clinical need, successful pharmacotherapy for cachexia has been difficult to achieve. Given the lack of treatment options and an incomplete understanding of disease mechanisms, further work on the fundamental physiology of cachexia is needed.

2. Cachexia as an Inflammatory Disease

2.1 Circulating Inflammatory Cytokines are Markers of Cachexia

Cachexia is found in response to a multitude of primary disease states with fundamentally different underlying pathology. Despite this, the behavioral and metabolic features are markedly conserved between diseases states. Thus commonalities between the conditions serve as an important guide to understanding the fundamental mechanisms of cachexia. One of these shared features is an increase in the levels of circulating inflammatory cytokines. In CHF, circulating levels of tumor necrosis factor (TNF) (15-17) and interleukin-6 (IL-6) (16) are increased and correlate with the degree of exercise impairment in these patients. In chronic renal failure, increased levels of C reactive protein are correlated with increased mortality (18). Likewise, in cancer patients suffering from cachexia, the cytokines IL-6 (19, 20) and TNF (21, 22) have been found at increased levels relative to non-cachectic cancer patients. Furthermore, multiple studies have implicated leukemia inhibitory factor (LIF) as a pathogenic factor in cancer cachexia. LIF is found at high levels in cancer patients (23) and is released from human tumor cell lines (24). While serum LIF levels are a negative prognostic indicator in sepsis (25), no studies have been performed to date correlating the circulating LIF levels with the degree of cancer cachexia. Others have failed to find elevated levels of the aforementioned

inflammatory mediators in cancer cachexia, likely reflecting heterogeneity in the type and severity of cancer studied as well as the intermittent nature of inflammatory processes (22, 26).

2.2 Cachexia Is an Evolved Response to Infection

It has been argued that the behavioral and metabolic response to inflammation is adaptive and evolved resulting in increased fitness. For instance, the decrease in appetite associated with inflammation may function to decrease essential nutrients (i.e. iron, zinc ect.) necessary for the growth of microorganisms (27). Experimental evidence in support of this hypothesis has shown that decreases in food intake are positively associated with survival during bacterial infection. Mice starved prior to inoculation with *Lysteria monocytogenes* showed increased survival relative to fed controls (28). When food intake in mice infected with Lysteria is maintained by gavage feeding, increased mortality is observed relative to mice allowed to undergo normal decreases in nutritional intake (29). It has also been suggested that anorexia reduces foraging behavior during acute infection, offsetting an increase in the risk of predation (27).

Understanding the teleology of muscle wasting is a less straightforward proposition. It is tempting to explain inflammation-induced muscle wasting as a mobilization of energy reserves consequent to the concurrent decrease in food intake. However, inflammation consistently produces excessive muscle wasting when compared to animals that have been restricted to a similar level of food intake (pair feeding) (30). Furthermore, decreased food intake is not always associated with muscle mass loss in cancer patients (31). Indeed, correction of the nutritional deficit by IV nutrition in cachexia, while beneficial, has been unsuccessful in completely

reversing the catabolic features of this syndrome (32). Hence, decreased nutritional intake alone cannot be the sole driver of wasting.

In cancer cachexia, the energy demands of the tumor provide another potential explanation for muscle wasting. Cancer cells produce ATP predominantly via glycolytic metabolism: a phenomenon known as the Warburg Effect. It has been proposed that muscle atrophy occurs to liberate amino acids that can be utilized for tumor glycolysis with hepatic gluconeogenesis as an intervening step (33). However, this is a somewhat unsatisfying explanation for muscle wasting as it suggests that preventing muscle wasting should prevent tumor growth. Multiple studies have examined the growth of tumors in experimental animals in which lean mass loss was attenuated or blocked, and decreased tumor growth has not been observed (14, 34-36). Thus, it is unlikely that tumor metabolism and the subsequent flow of nutrients by mass action can explain the totality of muscle atrophy in cancer cachexia.

An explanation that seems more in line with the evidence comes from the comparison of the starved state and systemic inflammation, both of which induce muscle atrophy. While starvation results in immunosupression (37) and decreases in metabolic rate, inflammation results in an immediate acute phase and febrile response, both of which have significant energetic demand. Fever is estimated to result in a 13% increase in metabolic rate for every 1° rise in body temperature (38). This would be expected to increase the utilization of all nutrient stores including skeletal muscle, especially in the setting of decreased food intake. Additionally, nearly every component of innate and adaptive immunity requires de-novo protein synthesis (39). While it is nearly impossible to de-convolute the protein cost of immune activation from the metabolic cost of fever, it is clear that significant protein mass is produced acutely and that skeletal muscle represents the major body store for amino

acids. While all of these explanations are speculative and difficult to prove, they do provide a conceptual understanding for the underlying purpose of cachexia.

3. Mechanisms of Muscle Catabolism

3.1 Protein Degradation Underlies Muscle Atrophy

In muscles undergoing rapid weight loss, myofibrillar atrophy is the predominant feature. While the absolute number of muscle fibers does not change, the individual fibers decrease in size with concurrent decreases in protein content (40). This does not occur equally in all muscle. Fast twitch, glycoclytic muscle undergoes atrophy at a far more rapid rate than does slow twitch, oxidative muscle (41-43). Muscle atrophy in response to inflammation occurs as the concerted result of increases in protein breakdown often accompanied by decreases in protein synthesis (44-47). A common molecular mechanism is responsible for the degradation of myofibrillar protein. The ubiquitin proteasome system is responsible for the degradation of the majority of cellular proteins and contractile proteins are no exception (48). This pathway requires adenosine triphosphate (ATP), the protein ubiquitin, and the 26s proteasome (49). The 26s proteasome is a cylindrical, multi-subunit complex which contains 3 distinct proteolytic activities. Protein substrates are marked by the covalent attachment of a chain of ubiquitin in a process that requires three enzymatic steps. The three enzymatic activities require 3 separate enzymes: the ubiquitin-activating enzyme (E1) the ubiquitin conjugating enzyme (E2) and the ubiquitin ligase (E3). The E3 is thought to confer a significant amount of specificity to the proteasome pathway, by forming a bridge between the E2 and the substrate (49). While there is only one E1 and several E2s, thousands of E3 ligases are encoded by the genome reflecting the diversity of protein substrates degraded by the proteasome.

Work describing the molecular mechanisms of skeletal muscle atrophy began to make rapid progress in the 1990s with the discovery that the increased rate of myofibrillar protein breakdown observed in explanted muscles as a result of tumor growth (43, 50, 51), acidosis (52), fasting (53), denervation (54) or disuse (55) was largely blocked by ATP depletion. While the ATP dependence of protein breakdown implicated the ubiquitin-proteasome system, confirmation of this fact awaited the development of specific proteasome inhibitors. Once this was achieved, it was found that muscle protein degradation in acute diabetes (56), metabolic acidosis (57), denervation, hyperthyroidism and sepsis (48) was blocked by proteasome inhibitors. Although multiple proteasomal subunits and ubiquitin itself are upregulated in atrophying muscle, the factors controlling the specificity of this reaction for contractile proteins were unclear (52, 56). Believing that the ultimate degradation of myofibrillar protein constituted a conserved process regardless of the atrophic stimulus, two groups examined genes that were similarly induced in several models of atrophy (58, 59). The result of these screens was the identification of two E3 ubiquitin ligases that were expressed specifically in muscle and were dramatically upregulated in response to atrophic stimuli. Muscle atrophy F box (MAFbx or Atrogin-1) is an E3 of the SCF class of ubiquitin ligases and associates with Skp1 via its F box domain. MAFbx expression increases at least 7-fold in response to fasting, as well as in response to every other form of atrophy examined (58). Muscle ring finger protein-1 (MuRF1) belongs to the family of ring-based ubiquitin ligases and is a member of a subfamily of closely related E3 ligases MuRF1, MuRF2 and MuRF3. While MuRF2 and MuRF3 appear to be regulated under certain atrophic conditions, MuRF1 is the only member of the subfamily that is consistently upregulated in atrophic muscle (59). MAFbx and MuRF1 are both fundamental components of the atrophy process, as gene knockout at either locus substantially protects against atrophy (59). While it has been largely

assumed that these E3 ligases are responsible for the degradation of contractile protein via direct ubiquitin ligase activity, this is not exclusively the case. Prior to its identification as an atrophy regulated gene, MuRF1 was identified by a yeast-2-hybrid screen as associating with the M-line protein Titin, which forms a single continuous filament system along the entirety of the myofibril (60). Over expression of MuRF1 results in destabilization of the sarcomeric structure, suggesting Titin as a MuRF1 target. However, in another report, over expression of MuRF1 failed to result in atrophy, instead altering genes associated with carbohydrate metabolism (61). MuRF1 is also critical for the organized disassembly of thick filament, first ubiquitinating the stabilizing proteins myosin binding protein C and myosin light chains 1 and 2 (62). After the degradation of these stabilizing proteins, myosin heavy chain is also ubiquitinated and targeted for proteasomal degradation (62, 63). This process is summarized in Figure 1. There is some debate as to the involvement of MuRF1 in the degradation of thin filament proteins. Some studies have demonstrated specific ubiquitination of troponin I in cardiac muscle by MuRF1 (64), while there is no evidence for this in skeletal muscle (62). Actin has also been proposed as a target of MuRF1 (65), however actin was not been identified as a MuRF1 target in other studies (62).

MAFbx on the other hand has never been associated with the ubiquitination of contractile proteins. The only identified substrates for MAFbx are the regulatory proteins such as eIF3-f (66), the muscle differentiation transcription factor MyoD (67) and IκBα (68). The targeting of IκBα is of particular interest (as discussed below), as MuRF1 is a known NFκB target gene, suggesting the possibility of crosstalk between these two E3 ligases. Interestingly, MAFbx also is a co-activator of Foxo transcription factors in cardiac muscle, suggesting possible feed forward activation of the atrophy program (the role of Foxo transcription factors are discussed in detail below) (69).

MAFbx over expression alone does not result in atrophy in myotubes, however, these data are only reported as an unpublished observation (70). Despite the fact that MAFbx does not appear to target myofibrillar proteins for ubiquitination, it is a larger contributor to denervation-induced atrophy. Mice lacking MAFbx demonstrate a 56% sparing of muscle mass in response to denervation, while mice lacking MuRF1 only demonstrated a 36% sparing (59). It is unclear whether this relative contribution is unique to denervation atrophy, or whether it extends to other forms of atrophy as well. While MAFbx and MuRF1 are doubtlessly only a part of the mechanism by which contractile elements are degraded, they are inseparable from the atrophy process. There are no experimental models that have been reported to date that do not demonstrate the induction of MAFbx and MuRF1 during the active loss of muscle mass. Therefore, these two genes serve as excellent markers of active muscle wasting.

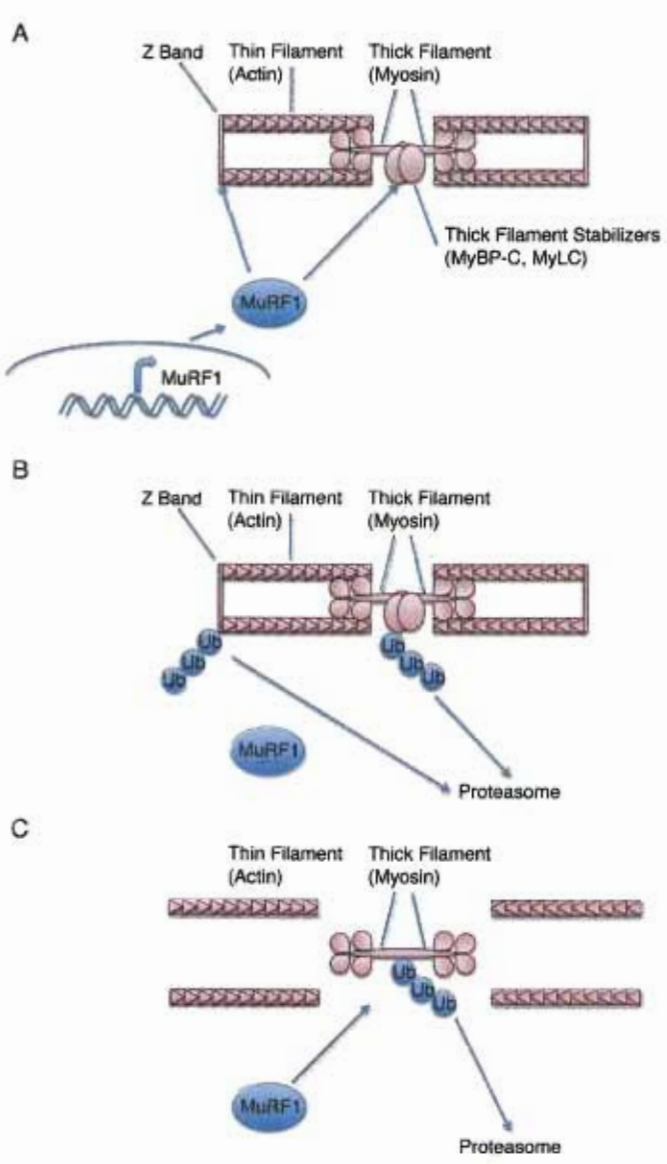

Figure 1. MuRF1 is an E3 ubiquitin ligase responsible for targeting the contractile apparatus to the proteasome

(A) Under catabolic conditions, MuRF1 transcription increases. (B) MuRF1 first targets structural and regulatory elements within the myofibril, such as myosin binding proteins and Titan in the z-band. (C) Once these structural elements have been degraded, the thick filament is freed and subsequently ubiquitinated under the direction of MuRF1 and subjected to proteasomal degradation.

3.2 The Molecular Regulation of Atrophy: Cytokines, Hormones and Transcription Factors

Despite the fact that cachexia is clearly a disease of systemic inflammation, the means by which the atrophic signal is delivered to muscle is not necessarily inflammatory cytokines themselves. Early studies utilizing parabiosis demonstrated that the signals mediating cachexia were contained within the systemic circulation (71). As described above, inflammatory cytokines clearly fit this definition. However, a number of other endocrine signals have important roles in the regulation of muscle mass and are altered under conditions of inflammation. The following section will discuss extracellular signals that regulate protein balance in skeletal muscle, as well as the intracellular signaling networks that govern the process of atrophy.

3.2.1 Insulin-like Growth Factor Signaling at the Crossroads of Muscle Anabolism and Catabolism

Insulin and Insulin-like Growth Factor (IGF-1) have been extensively studied with regard to their role in regulating the anabolic/catabolic balance in skeletal muscle. Insulin was shown very early on to stimulate protein synthesis and inhibit protein breakdown in isolated muscle in short term culture (72). Interestingly however, mice lacking insulin receptor in skeletal muscle do not demonstrate atrophy, suggesting that the lack on insulin signaling per-se does not result in muscle catabolism (73). IGF-1 signaling also significantly regulates muscle mass. Muscle specific over expression of IGF-1 leads to massive hypertrophy (74, 75) and prevents muscle atrophy in response to a variety of stimuli (76). The binding of insulin and IGF-1 to their cognate receptors recruits insulin receptor substrate (IRS) proteins to the membrane, activating phosphatidylinositol 3-kinase (PI3K) (40). The phosphorylation of membrane inositides by PI3K creates a docking site for protein kinase B (PKB/Akt)

which directly phosphorylates many downstream targets critical for cell growth. The anabolic activity of IGF-1 requires activation of both PI3K and Akt (77). Furthermore, isolated activation of Akt is sufficient to produce hypertrophy. The activity of the IGF-1/PI3K/Akt pathway in muscle is actively restrained by proteasomal degradation of IRS-1 mediated by the ubiquitin ligase Fbxo40 (78). When Fbxo40 is knocked down, significant hypertrophy results.

A central regulator of the anabolic activity downstream of IGF-1/PI3K/Akt signaling is the mammalian target of rapamycin (mTOR) complex, which occupies a central position in multiple metabolic signaling cascades, integrating signals from growth factors, nutrient availability, and energy status (79-81). Multiple signals including increased levels of glucocorticoids and decreased insulin/IGF-1 signaling result in the inhibition of mTOR. Two distinct protein complexes contain mTOR: the rapamycin sensitive mTORC1 that contains raptor and the rapamycin insensitive mTORC2 that contains rictor. mTORC1 is generally agreed to be more important for the maintenance of skeletal muscle mass, while mTORC2 appears dispensable (82). Signaling downstream of the IGF-1 receptor results in PI3K dependent phosphorylation of Akt, and activation of mTOR signaling via the tuberous sclerosis complex (40). mTOR then drives bulk protein synthesis via the regulation of translation through several parallel pathways. mTOR inhibits 4E-BP1 binding to eIF4e, freeing it to participate in translational initiation (79). Furthermore, mTOR activates $p70^{S6K}$ which also drives translation (79). mTOR signaling is necessary for muscle hypertrophy in response to IGF-1 or constitutively active Akt (77, 79). While this process appears to be critical for adaptive hypertrophy, treatment with rapamycin and subsequent mTOR inhibition does not lead to atrophy in adult animals, suggesting it may not be critical to the normal maintenance of skeletal muscle (79). The local levels of branched chain amino acids also regulate mTOR. It was recently

reported that the transcription factor Krüpple like factor 15 (KLF15) increases the expression of branched chain amino transferase-2 (BCAT2), resulting in the catabolism of branched chain amino acids and decreased mTOR activity (81).

Critical to the regulation of protein balance by Akt is a family of transcription factors known as forkhead box or Foxo transcription factors. This family contains 3 members: Foxo1, Foxo3a and Foxo4. All three are phosphorylated by Akt and excluded from the nucleus (70, 83, 84). When Akt signaling is lost, Foxo enters the nucleus and drives the transcription of multiple genes. Both MAFbx and MuRF1 promoters contain forkhead binding sites, and are transcriptionally regulated by Foxo (70, 84). Foxo transcription factors are sufficient to induce atrophy, as adenoviral transduction of a constitutively active Foxo3a is sufficient to induce atrophy in cultured myotubes and electroporetic transfection of adult myofibers *in vivo* results in significant atrophy (70). Foxo transcription factors are also necessary for atrophy, as transduction of myotubes with a dominant negative Foxo3a which lacks a transactivation domain prevents atrophy in response to dexamethasone treatment (70). Additionally, dominant negative inhibition of Foxo1, protects against sepsis and tumor-induced muscle atrophy (85). The Foxo family members exert overlapping control over the MAFbx gene, as RNAi against either Foxo1 or Foxo3a alone only partially protects against the activation of a MAFbx-luciferase reporter in fasting animals, while RNAi against both simultaneously completely prevents fasting mediated induction of MAFbx-luciferase activity (70). Furthermore, mutation of putative forkhead binding elements in the MAFbx promoter prevents activation of MAFbx-luciferase activity *in vivo* (70). There is some debate as to whether Foxo signaling is sufficient to induce atrophy, as different effects have been reported on MAFbx expression after the transduction of myotubes with a constitutively active Foxo

(70, 86). However, it is agreed upon that Foxo signaling is necessary for dexamethasone-induced atrophy of myotubes.

MuRF1 is also a target of Foxo transcription factors. The MuRF1 promoter contains numerous conserved forkhead-binding elements. Foxo1 is constitutively present on the MuRF1 promoter, and it's binding increases with dexamethasone treatment (84). The activity of MuRF1 luciferase constructs can be increased by Foxo1, Foxo3a and Foxo4 over expression *in vitro* (84). Consistent with the regulation of the MAFbx gene, increased MuRF1 gene expression in response to dexamethasone treatment is also blocked by IGF-1 treatment. Foxo1 transcription factors also play a critical role in the atrophy process independent from their role in transactivating MAFbx and MuRF1. Muscle specific over expression of Foxo1 *in vivo* leads to reduced muscle size without increases in MAFbx or MuRF1 gene expression, suggesting E3 ligase independent functions of Foxo1 (87). Furthermore, expression of Foxo1 increases in numerous atrophy states, and unlike MAFbx and MuRF1 it remains elevated after the bulk of protein loss (81, 88, 89).

3.2.2 Endogenous and Exogenous Glucocorticoids Promote Muscle Atrophy

Circulating glucocorticoids are also important systemic metabolic regulators. Cortisol in humans or corticosterone in rodents is produced in the adrenal gland under the neuroendocrine control of the central nervous system (CNS) (90). Corticotrophin releasing hormone (CRH) neurons within the paraventricular nucleus (PVN) of the hypothalamus release CRH into the pituitary portal vasculature. CRH acts on anterior pituitary corticotrophs to release adrenocorticotropic hormone (ACTH) into the systemic circulation. ACTH travels to the adrenal gland, where it acts on cells of the zona fasciculata to release cortisol. Cortisol is released in response to a number of psychological and physiologic stressors and mediates numerous stress responses

(90). Glucocorticoids also play a critical role in mediating normal metabolic function, as they are released in a circadian fashion, with a zenith at dawn and a nadir at dusk (This is reversed in rodents were activity and dormancy cycles occur during the night and day respectively). This circadian variation in cortisol levels likely has a significant impact on muscle physiology, as multiple metabolically active, glucocorticoid responsive transcripts are regulated in skeletal muscle across the day/night cycle including the muscle specific E3 ligases MAFbx and MuRF1 (91).

The role of glucocorticoids in mediating muscle atrophy has been studied in two major paradigms: exogenous administration and blockade of signaling. In most studies involving glucocorticoid administration the synthetic glucocorticoid dexamethasone is predominantly utilized. While this has the advantage of being a long half-life compound and highly specific for the glucocorticoid receptor (GR), it has the obvious caveat of overt pharmacology. When high dose dexamethasone is administered to rodents, or applied to myotubes in culture, pronounced atrophy occurs, accompanied by increased protein turnover (59, 92). Elevated glucocorticoid levels are found in a number of animal models associated with overt muscle catabolism, including sepsis (93), cancer (94), fasting (53, 95), metabolic acidosis (96), and uncontrolled diabetes (95). When glucocorticoid signaling is blocked either via pharmacologic antagonism or adrenalectomy in these conditions, muscle atrophy is attenuated. Several studies have examined the contribution of glucocorticoid signaling to muscle atrophy in cancer (97, 98). In both cases, no statistically significant effect of glucocorticoid blockade was seen in any of the measured parameters of muscle wasting, leading to the generally accepted conclusion that glucocorticoids do not participate in cancer cachexia (33).

A conserved glucocorticoid response element (GRE) is present in the MuRF1 gene, immediately adjacent to a forkhead-binding site. This GRE is near perfectly

conserved between mouse, rat and human and is an essentially perfect consensus GRE, which is quite rare in glucocorticoid response genes (84). Potent synergy exists between GR and Foxo1 mediated activation of the MuRF1 gene, as demonstrated by a dramatic increase in MuRF1-luciferase activity in the presence of both transcription factors. MAFbx on the other hand does not contain a GRE, yet is dramatically induced by glucocorticoid treatment. A possible explanation for the induction of MAFbx by glucocorticoids is the degradation of IRS-1 by Fbxo40 (78). Although the regulation of Fbxo40 in response to glucocorticoids has not been examined, it is theoretically possible that decreased phosphorylated Akt levels are the result of increased Fbxo40 mediated degradation of IRS-1. Protein synthesis is also decreased by glucocorticoids. Both KLF15 and regulated in DNA damage responses-1 (REDD1) expression increases in muscle in response to glucocorticoid treatment. REDD1, a direct inhibitor of mTOR, is directly transactivated by ligand bound GR (81). KLF15 is also a directly transactivated by GR, influencing mTOR activity via alterations in the levels of branched chain amino acids (81).

Glucocorticoids contribute to muscle atrophy in a number of disease states. In acute diabetes, muscle wasting is prevented by adrenalectomy, yet glucocorticoid signaling is not believed to be sufficient to explain this effect (95). Diabetic adrenalectomized mice show a restoration of muscle wasting in response to a low dose of dexamethasone, which is estimated to mimic endogenous pathophysiologic concentrations of glucocorticoids. However, in non-diabetic animals, this dose is insufficient to induce atrophy. The authors explain this effect via a non-genomic interaction between glucocorticoid and insulin signaling at the level of IRS-1, where GR competes with PI3K for the available IRS-1. The resulting decrease in Akt phosphorylation increases Foxo transactivation of MAFbx. While this finding does suggest an increased sensitivity to glucocorticoid-induced atrophy during diabetes, it

is impossible to know whether the dose of dexamethasone given accurately reflects the endogenous production of glucocorticoids during stress. Further, dexamethasone differs from the endogenous glucocorticoid corticosterone in a number of critical ways including receptor affinity, biological half-life, and potency at other steroid receptors. Given the synergy between Foxo1 and GR mediated transactivation of MuRF1, this increased sensitivity to glucocorticoid-induced atrophy is not surprising in acute diabetes, where profound insulinopenia would be expected to significantly increase nuclear Foxo.

3.2.3 Inflammatory Cytokines as Direct Mediators of Muscle Atrophy

The direct action of inflammatory cytokines on the skeletal myocyte is the dominant hypothesis for the mechanism by which inflammation mediates muscle atrophy. The application of inflammatory cytokines onto cultured myotubes results in a loss of cross sectional area and activation of the atrophy program at the molecular level (42, 99, 100). *In vivo*, inflammatory cytokines are both necessary for tumor-induced atrophy, and sufficient in isolation to cause atrophy (30, 101). The most studied transcriptional mediator of inflammatory signaling in muscle atrophy is Nuclear Factor Kappa-B (NFκB). Often referred to as the master inflammatory regulator, NFκB signaling occurs via two principle pathways: canonical and non canonical. The canonical pathway is the best characterized with regard to its role in the atrophy process. The alternate or non canonical pathway appears to be more relevant to the regulation of mitochondrial function (102). In the absence of inflammatory signaling, the canonical NFκB heterdodimer composed of p65 (product of the RelA gene) and p50 are retained in the cytosol via binding to inhibitor of kappa B alpha (IκBα) (103). Inflammatory signals converge on the inhibitor of kappa B kinase (IKK) complex. The beta subunit is phosphorylated, and then phosphorylates

IκBα, targeting it for ubiquitination and subsequent proteasomal degradation, freeing the p65/p50 heterodimer to translocate to the nucleus and drive inflammatory gene expression. Muscle specific expression of a constitutively active IKKβ results in a profoundly cachectic phenotype with marked muscle atrophy (104). Furthermore, muscle specific expression of a non-phosphorylatable dominant negative IκBα protects against muscle atrophy in response to denervation and tumor growth. Interestingly, in the setting of NFκB gain-of-function, MuRF1 but not MAFbx is induced. Consistent with this the MuRF1 but not MAFbx promoter is transcriptionally activated by NFκB (70, 104) and MuRF1 knockout mice resist the atrophy induced by constitutive activation of NFκB signaling. Basal levels of MuRF1 transcription and expression are also substantially decreased in the setting of dominant negative inhibition of NFκB, demonstrating an important role for this pathway in the maintenance of MuRF1 expression independent from catabolic stimuli (104). Protein synthesis is not decreased by constitutive activation of NFκB signaling and is instead increased demonstrating that alternate signaling mechanisms underlie the decrease in protein synthesis accompanying inflammation (104).

Signaling via the p38 mitogen-activated protein kinase (MAPK) pathway downstream of inflammatory cytokine receptors has also been implicated in mediating the atrophy response. In addition to the activation of NFκB, the binding of TNF to its cognate receptor also activates p38 MAPK. In cultured myotubes, treatment with a p38 MAPK inhibitor prevents in the induction of MAFbx mRNA and atrophy in response to TNF stimulation (105). These findings have also been extended to interleukin 1 beta (IL-1β) and LPS, which also activate MAFbx via p38 (99, 106). Systemic treatment with p38 MAPK inhibitors also prevents muscle atrophy in response to inflammatory stimuli (106). Recently, these findings have been extended to cancer cachexia as well. Muscle atrophy in response to tumor growth can also be

prevented by systemic p38 inhibition (107). The p38 dependent activation of MAFbx in tumor bearing mice is dependent on C/EBPβ, as C/EBPβ knockout mice also resist tumor-induced atrophy. Caution must be used however in the interpretation of these data. The *in vitro* studies clearly show an important role for p38 in mediating the direct effects of cytokines on cultured muscle cells. However, systemic inhibition of p38 MAPK likely alters the action of inflammatory signaling in other cell types as well. Cytokine production, HPA axis activation and IGF production are all likely affected by this treatment, yet they were not examined in these studies. It is therefore difficult to describe the role of p38 MAPK in the skeletal myocyte in mediating atrophy *in vivo*.

3.2.4 Krüpple-Like Factor 15 in the Regulation of Muscle Mass

MAFbx and MuRF1 are also regulated by KLF15, a transcription factor that was previously mentioned in relation to the regulation of protein synthesis. KLF15 binding sites are present in the promoters of MAFbx and MuRF1, and are requisite for KLF15 mediated transactivation of both genes (81). Transfection of myotubes with KLF15 siRNA, provides a near complete block to the induction of both MAFbx and MuRF1 by dexamethasone. KLF15 over expression is sufficient to drive atrophy gene expression and myofibrillar atrophy in adult skeletal muscle. Furthermore, synergy exists between KLF15 and Foxo1, as AAV transduction of adult muscle with a constitutively activate Foxo1 and KLF15 increases MAFbx and MuRF1 expression more than the sum of either construct alone. Therefore it appears that KLF15 represents another critical node of regulation for the atrophy process.

3.2.5 Activin and Myostatin in the Regulation of Muscle Mass

Myostatin is a transforming growth factor-β (TGF-β) family member that is critical for the maintenance of muscle mass. Myostatin is expressed almost exclusively skeletal and cardiac muscle. Mice lacking myostatin demonstrate massive muscular hypertrophy (108). Systemic administration of myostatin results in significant muscle atrophy (109). Furthermore, pharmacological antagonism of myostatin signaling in adult animals produces profound muscle hypertrophy and improves muscle mass in multiple models of atrophy including cancer, renal failure and unloading (14, 110-113). As previously mentioned, myostatin antagonism was recently demonstrated to improve survival in tumor bearing animals (14). However, these results do not necessarily implicate myostatin overactivity in the pathogenesis of cachexia. Inhibition of myostatin signaling in healthy animals is powerfully anabolic, and it is possible that this anabolic effect simply compensates for ongoing wasting. On the other hand, several lines of evidence do indicate that myostatin signaling may play a role in mediating muscle wasting. Myostatin mRNA and protein are both increased in the skeletal muscle of tumor bearing animals or animals with experimental chronic renal failure (14, 113). Furthermore, myostatin knockout mice do not display a decrease in muscle mass in response to dexamethasone treatment (114). However, other investigators demonstrated that myostatin knockout mice lose more muscle mass in response to tumor growth than do wild type mice (112). Further complicating the interpretation of studies involving myostatin inhibition is the finding that myostatin antagonism reduces systemic inflammation in chronic kidney disease, clouding the issue of where myostatin falls in the hierarchy of local and systemic factors involved in muscle wasting (113). Another potential complication is the role of paraneoplastic anemia, which is a common finding in tumor models such as the landmark paper by Zhou et al (14, 115). Activin family antagonists (such as the soluble ActRIIb) are potent inhibitors of cancer-induced anemia, and are currently in

clinical trial for this very indication. This generates further doubt about the true etiology of improved survival in tumor bearing mice treated with anti-myostatin therapy (116, 117).

The lack of precise molecular mechanism by which myostain mediates muscle atrophy further complicates our understanding of the role of myostatin signaling in the pathogenesis of cachexia. As a member of the TGFβ family, myostain signals via SMAD proteins. Forced activation of SMAD signaling *in vivo* produces muscle atrophy with weak MAFbx activation and an absence of MuRF1 induction (118).Yet myostatin treatment of cultured myotubes induces MAFbx and MuRF1 via decreases in Akt mediated phosphorylation of the Foxo transcription factors (119). Consistent with this, inhibition of myostatin signaling increases Akt and Foxo phosphorylation decreasing E3 ubiquitin ligase expression in cancer cachexia (14, 113). Given the discrepancies in the mechanistic studies, it is clear that further work is required to understand the mechanism underlying myostatin signaling in muscle atrophy. Regardless of whether myostatin over activation plays a key role in cachexia, it is clear that antagonism of myostatin signaling represents a significant therapeutic opportunity for the treatment of muscle wasting diseases. Given the extensive interest in myostain biology from a basic science and pharmaceutical standpoint additional future studies will likely detail the role of myostatin signaling in cachexia.

3.2.6 The Autophagy-Lysosome System Plays an Emerging Role in Muscle Atrophy

The lysosomal system was initially discounted as playing a major role in mediating the loss of muscle protein during atrophy, due to the large component of net protein degradation that was prevented by the use of proteasome inhibitors. However, recent evidence suggests that lysosomal proteolysis and autophagy are an

integral component of the atrophy response. While the proteasome is believe to be responsible for the degradation of short-lived proteins, the autophagy-lysosome system degrades mostly longer-lived proteins and organelles (120). Like the proteasome system, autophagy is also an energy dependent process. Activated small ubiquitin-like molecules such as microtubule-associated protein 1 light chain 3 (LC3) and Gaba receptor A associated protein (GABARAP) (and others) are covalently bound to phosphatidylethanolamine and are transferred from a conjugation system to membranes, forming a critical step in the creation of the autophagosome (121). Importantly, these proteins are short lived, as they are consumed by the process of autophagosome formation. Autophagy genes are upregulated in muscle atrophy (122). However, unlike the ubiquitin-proteasome system where critical regulatory machinery is upregulated under conditions of atrophy, the autophagy system shows selective upregulation of transcripts coding for these short lived ubiquitin-like molecules.

Autophagy is induced in concert with activation of the ubiquitin-proteasome system (85) and is regulated by the same families of transcription factors that also control the proteasome system in muscle. The Foxo transcription factors are also responsible for directing transcriptional activation of the autophagy system, as Foxo3a is both necessary and sufficient for the induction of muscle cell autophagy in response to starvation *in vitro* and *in vivo* (123). In non-muscle cells, inflammatory signaling pathways also play a role in the activation of autophagy. Hepatocyte-specific deletion of IKK beta prevents autophagy induction in response to starvation (124). Furthermore, the induction of autophagy in response to nutrient deprivation *in vitro* depends on IKK activation but not on NFκB signaling (125). The precise role of autophagy in the atrophy process has remained somewhat elusive. The overlapping transcriptional control mechanisms make separation of the specific role of the

autophagy/lysosome system difficult. It is clear however, that complete absence of autophagy in muscle results in multiple pathological features. Muscle specific deletion of the unique E1 enzyme Atg7 results in profound weakness and myopathy in mice, underscoring the importance of autophagy in the maintenance of normal muscle (126).

4. The Role of the Central Nervous System in Cachexia

4.1 Inflammatory Signaling in the Central Nervous System Regulates Sickness Behavior

While skeletal muscle is the best described target of cytokine signaling with regard to atrophy, inflammatory signaling in the CNS has been extensively studied in mediating sickness behavior. The peripheral administration of cytokines such as IL-1β (127-129) and TNF (129), or the inflammatory bacterial cell wall product lipopolysaccharide (LPS) (127, 128) potently induce anorexia in laboratory animals. Furthermore, intercerebroventricular (i.c.v.) injection of inflammatory cytokines such as IL-1β (130), LIF (131), and TNF (132) also reduce food intake, suggesting that the brain can respond directly to inflammatory signals. Peripheral or central cytokine injection leads to a rapid induction of cFOS immunoreactivity (cFOS-IR, a marker of neuronal activation (133)) in multiple brain regions, including areas that are critical for food intake and energy metabolism such as the ARC (134). A negative correlation has been reported in tumor-bearing animals between food intake and interleukin 1 alpha (IL-1α) concentration, further implicating inflammatory cytokines in the pathogenesis of anorexia (135).

Additional studies have shown that inflammatory cytokine production in the CNS itself is critical in the generation of the anorectic response. Animals injected

peripherally with LPS display a rapid increase in the expression of inflammatory cytokines in the hypothalamus (127, 128). IL-1β is particularly critical, as i.c.v. infusion of IL-1 receptor antagonist (IL-1Ra) significantly reduces the anorexia resulting from peripheral LPS administration and normalizes hypothalamic cytokine expression (136). Myeloid differentiation primary response protein 88 (MyD88) is a signaling adaptor downstream of Toll-Like Receptor-4 (the cellular receptor for LPS) and the type 1 interleukin-1 receptor (IL-1R1). Mice lacking functional MyD88 are completely resistant to LPS or IL-1β-induced anorexia and show attenuated induction of hypothalamic cytokine production (127, 128). These results demonstrate that local cytokine production within the brain may function as a critical signaling intermediate and a feed forward mechanism for sustaining the response to inflammation.

The induction of IL-1β (137, 138) and TNF (138) expression in the hypothalamus has been documented in tumor bearing animals as well. Further support for the critical nature of hypothalamic cytokines comes from experiments demonstrating that i.c.v. administration of the TNF neutralizing antibody infliximab or IL-1Ra increases food intake and reduces the febrile response in a cecal ligation and puncture model of sepsis modestly increasing survival (139). Additionally, ICV infliximab or IL-1Ra improve food intake and survival in animals implanted with the Walker-256 tumor (139), in which hypothalamic levels of TNF and IL-1β are both increased. While promising, the modest effects seen in these experiments point to likely redundancies in the inflammatory control of anorexia in more complex disease models. Many cytokines have the capability of inducing anorexia when injected centrally and the mRNA for multiple inflammatory mediators are simultaneously induced in the hypothalamus after peripheral LPS challenge or in tumor-bearing animals. It is therefore likely that anorexia in disease is due to the additive or synergistic effects of multiple inflammatory cytokines. Indeed, infusion of multiple

cytokines at doses that provoke only slight anorexia alone, can lead to dramatic anorexia when given in combination (130). Further, the chronic administration of IL-1β, TNF, IL-6 or Interleukin-8 results in an initial anorectic period with rapid desensitization and complete recovery of food intake by the end of one week (140, 141). In contrast, AAV-mediated delivery of LIF into the CNS can generate chronic anorexia and weight loss that shows no signs of desensitization (142). These findings indicate that the generation of long-lived disease-associated anorexia likely results from the complex interplay of multiple CNS cytokines that are likely specific to the patient and condition.

4.2 Afferent Pathways for the Detection of Systemic Inflammation

4.2.1 Neural Pathways

Visceral sensory afferents are a potential mechanism by which peripheral inflammation generates an anorectic response. In particular, the vagus nerve appears to play a role in mediating behavioral responses to inflammation. Sub-diaphragmatic vagotomy attenuates the induction of IL-1β mRNA expression in the hypothalamus after intraperitoneal (i.p.) LPS challenge (143) or IL-1β injection (144). However, other studies have demonstrated that vagotomy does not prevent increases in hypothalamic IL-1β protein content in i.p. LPS treated animals (145). Some have shown that vagotomy attenuates the anorexia seen with i.p. LPS administration (146), while others have seen no alteration in the anorectic response to i.p. LPS or other peritoneal inflammatory stimuli in vagotomized animals (147). An explanation for the discordance of these studies is not immediately apparent; however these data are suggestive of a vagally mediated anorectic pathway in response to inflammatory stimuli that may be critical under certain circumstances, particularly in the case of

peritoneal inflammation. It seems clear however, that the vagus is not necessary for the anorectic response to intravenous IL-1β (148). There is some evidence to showing that tumor growth stimulates anorexia via a vagal pathway. Anorexia was attenuated in tumor-bearing rats when a subdiaphragmatic vagotomy was performed prior to tumor implantation, or when vagal afferents were chemically ablated (149).

4.2.2 Humoral Pathways

In contrast multiple lines of evidence demonstrate that circulating cytokines act directly on CNS neurons. The best-studied cytokine with regard to its neuronal action is leptin, a negative regulator of body mass and appetite. Leptin has been implicated as a mediator of uremic cachexia (150) and elevated levels of leptin have been reported in CHF (151). Studies demonstrating the critical role for leptin in the pathogenesis of other forms of cachexia have yet to be performed. However, leptin is closely related to IL-6 and LIF in structure and signaling (152). Thus leptin serves as an effective prototype for cytokine access to the CNS, despite the lack of extensive evidence for it being an essential mediator of cachexia. Inflammatory cytokines are generally believed to be too large to cross the blood brain barrier (BBB) by simple diffusion (153). However, CNS structures collectively referred to as circumventricular organs have specialized fenestrated capillaries. The median eminence is one such region, where the permeable capillaries of the portal vasculature play a critical role in the neuroendocrine communication between the hypothalamus and the anterior pituitary. Neurons in the adjacent ARC are thought to have processes that lie outside of the BBB (154) and are also responsive to circulating factors via median eminence capillary fenestrations (153). Furthermore, the ARC is a critical site for the integration of physiologic leptin signals, suggesting that it may also respond to inflammatory cytokines. Additional areas of the brain respond directly to leptin signals (155, 156),

yet lie behind the BBB. Active transport across the BBB and the blood-CSF barrier is well characterized for leptin (157, 158). In addition, cytokines such as IL-1β (159), IL-6 (160), and TNF (161) are also actively transported into the CNS. Collectively, these data suggest that areas of the brain that are behind the BBB may be able to respond to circulating cytokines.

4.2.3 Blood Brain Barrier Permeant Second Messengers

Another mechanism by which inflammatory cytokines can influence neuronal activity is the synthesis of prostaglandins along the BBB, either in endothelial cells or perivascular macrophages. Prostaglandins are small lipid soluble inflammatory mediators that diffuse across the BBB (162, 163). Consistent with the notion that prostaglandins serve as a signaling intermediate, endothelial and perivascular cells express the receptors for inflammatory cytokines (164, 165), and are activated under inflammatory conditions (164, 166). Further, inflammatory insults activate endothelial cells more rapidly than neurons. This suggests that under inflammatory conditions, endothelial cells may be responsible for conveying the activating signal to neurons (166). In accordance with this, neurons are known to express receptors for prostaglandins (167). Under inflammatory conditions, the biosynthetic enzymes for prostaglandin E2 (PGE2, the most studied of the centrally acting prostaglandins), are induced in endothelial cells and perivascular macrophages (168). When cyclooxygenase (COX), the proximal biosynthetic enzyme for prostaglandins, is blocked pharmacologically, animals display attenuated anorectic responses to peripheral IL-1β (169) and LPS (170, 171). In some studies, tumor-bearing animals display attenuated anorexia and weight loss when treated with COX inhibitors (172, 173). The precise mechanisms by which COX inhibition is protective remains somewhat unclear, as certain tumors show attenuated growth when treated with COX

inhibitors (174), suggesting that tumor regression rather than inhibition of anorectic pathways may be responsible for these effects. Further, some experimental tumors produce anorexia and weight loss in a COX-independent manner, as COX inhibition is not effective in reversing anorexia or weight loss in these models (172). Additional evidence for the role of prostaglandins in driving anorexia and weight loss comes from studies in mice lacking the terminal biosynthetic enzyme for PGE2, microsomal prostaglandin E synthase. These mice display complete resistance to anorexia from LPS injection or tumor implantation (175). Interestingly, hypothalamic expression of inflammatory cytokines is normally induced under inflammatory conditions in these animals suggesting parallel pathways for prostaglandin and cytokine signaling.

4.3 Neural Targets of Inflammatory Signaling

4.3.1 The Central Melanocortin System

One important target for inflammatory signaling in the CNS is the hypothalamic central melanocortin system, which consists of two neuronal populations expressing peptide neurotransmitters with opposing actions. Proopiomelanocortin (POMC) neurons are located in the ARC, and the nucleus of the solitary tract of the brain stem (176). These neurons express the POMC precursor peptide, which is cleaved into many bioactive products including the anorectic peptide alpha melanocyte-stimulating hormone (α-MSH). The anorectic effect of α-MSH is exerted by binding to its cognate receptor, the type four melanocortin receptor (MC4R), which is expressed in a broad array of hypothalamic and extra-hypothalamic areas in the CNS (177). The net effect of signaling at the MC4R is decreased appetite (178) and increased energy expenditure (179). It should be noted that the POMC peptide is cleaved into multiple smaller peptides with diverse CNS and peripheral

functions. However, these other cleavage products are not well described in cachexia, and have been extensively reviewed elsewhere (180). Lying adjacent to the arcuate POMC neurons, are the Agouti-Related Peptide/Neuropeptide Y (AgRP/NPY) neurons, which have orexigenic activity (176). While NPY acts on specific NPY receptors, AgRP is an inverse agonist at the MC4R, increasing food intake and decreasing energy expenditure (181). Importantly, α-MSH and AgRP immunoreactive fibers project to many of the same locations across the CNS, although AgRP projections are less dense (182-184). In addition, AgRP neurons send inhibitory projections to neighboring POMC neurons, creating an additional level of control (185). Both neuronal populations are cytokine responsive. Further, both play a critical role in normal energy homeostasis in the response to leptin and the maladaptive energetic response to inflammatory cytokines. In particular, POMC neurons express the IL-1R1, and increase their spontaneous firing rate in response to IL-1β administration. The release of α-MSH from hypothalamic explants after IL-1β treatment is also increased (186). The converse is true of AgRP neurons, which, like POMC neurons express the IL-1R1, but instead decrease the spontaneous release of AgRP in response to IL-1β (187). Presumably, the net result of IL-1β action on these two neuronal populations is to dramatically increase signaling at the MC4R, resulting in anorexia. In addition, recent work has shown that the acute anorectic effects of exogenous LIF are entirely mediated by LIF receptor signaling on POMC neurons (131), further underscoring the importance of the melanocortin system in mediating the response to cytokines. Consistent with this mechanism, mice lacking functional MC4R resist anorexia associated with tumor growth (35, 188), chronic renal failure (150), or LPS administration (35, 188). In addition, ICV administration of exogenous AgRP, or synthetic melanocortin antagonists also ameliorates anorexia induced by

LPS, inflammatory cytokines (129, 189, 190) chronic renal failure (150), and tumor growth (35, 36).

As a result of these findings, multiple preclinical studies have begun to examine the potential therapeutic benefit of melanocortin antagonism in cachexia. Melanocortin antagonists have been developed that improve food intake and prevent the loss of lean mass when administered peripherally to tumor bearing mice (190, 191). Recently, melanocortin antagonists have been developed with oral bioavailability that attenuate anorexia and lean mass loss in tumor bearing animals (192). Preclinical studies have also demonstrated the efficacy of melanocortin antagonism in chronic renal failure. Peripheral administration of melanocortin antagonists improves food intake and prevents the loss of lean mass in subtotal nephrectomy-induced chronic renal failure (193, 194). As the preclinical data demonstrate, melanocortin antagonism is an exciting treatment possibility for anorexia associated with chronic disease. Future clinical studies will likely begin to explore the efficacy of melanocortin antagonism as a therapeutic modality in human cachexia.

4.3.2 Neuropeptide Y

NPY is another well-studied orexigenic neuropeptide, which increases food intake when administered exogenously. Co-expressed in the same neurons as AgRP, NPY is also regulated by inflammatory stimuli. Globally, NPY acts to increase food intake and administration of exogenous NPY leads to hyperphagia and obesity (195). Unlike starvation, which induces NPY mRNA in the hypothalamus, inflammatory stimuli such as LPS or IL-1β either produce no change (196) or demonstrate a reduction (197) in NPY mRNA levels. Furthermore, tumor-bearing animals show either no change (34), a decrease (198) or a slight increase (199) in NPY mRNA, depending on the report. Irrespective of the directionality of the change, inflammatory

anorexia results in a marked suppression of NPY mRNA expression relative to that seen in animals restricted to an equivalent level of food intake where NPY is dramatically induced. This shows that inflammatory signaling disrupts the normal regulation of NPY in response to negative energy balance. A functional antagonism has been demonstrated between IL-1β and NPY, where IL-β decreases the NPY-induced feeding response in a dose dependent manner (130). A reduction is seen in the NPY content of hypothalamic microdialysates from tumor bearing animals, suggesting impaired NPY release in cachectic states (200). However, several studies have demonstrated a decreased efficacy of exogenous NPY in tumor bearing animals as compared with healthy controls, suggesting functional resistance to the peptide in cachexia (36, 200). Furthermore, resistance to continuous infusion of NPY develops rapidly in tumor-bearing animals (200), demonstrating that an NPY deficiency is not solely responsible for the anorexia in tumor-bearing animals. In accordance with these studies, radioligand binding assays performed in anorectic tumor bearing rats showed a dramatic decrease in NPY receptor affinity with a moderate reduction in receptor number (201). Finally, decreases in NPY immunoreactive projections to various hypothalamic nuclei have been documented in anorectic animals (198). These data collectively demonstrate that NPY is aberrantly regulated in cachectic states. There is evidence for both a decrease in NPY production and a decreased sensitivity to NPY in cachexia. Given the presence of apparent resistance to NPY in cachexia, a therapeutic strategy involving exogenous NPY replacement without correction of the underlying downstream defects may not be viable.

4.3.3 Ghrelin

Ghrelin is a growth hormone releasing peptide, which is produced in the stomach in response to hunger or starvation (202). Ghrelin is present in two forms: acylated ghrelin, which is active, and desacyl ghrelin, which is inactive. Acyl ghrelin binds to the growth hormone secretogogue receptor-1a (GHSR-1a) which is found on ARC AgRP/NPY neurons, increasing their activity and peptide release (203). There is some experimental evidence for the involvement of ghrelin the in the pathophysiology of cachexia. Ghrelin exerts anti-inflammatory effects on immune cells and endothelium (204), decreasing proinflammatory cytokine production. In animals and humans experiencing anorexia due to inflammatory arthritis, serum ghrelin levels are decreased compared with controls (205). Furthermore, ghrelin levels are acutely decreased by LPS administration (206), as the result of a prostacyclin-dependent signaling mechanism decreasing ghrelin secretion by the stomach (207). In addition, exogenous ghrelin administration attenuates the anorectic response to LPS (204), most likely due to an attenuation of the inflammatory response and activation of hypothalamic AgRP/NPY neurons.

Despite the acute decreases in ghrelin brought about by inflammation, plasma levels of ghrelin are increased in patients with cachexia from multiple etiologies as compared with non-cachectic patients suffering from the same underlying conditions (208-211). It has been reported however, that levels do indeed fall in advanced cancer patients (212). Therefore, in cachexia ghrelin may be elevated as a compensatory mechanism for negative energy balance. Based on these human data, an overt ghrelin deficiency does not appear to be involved in the pathogenesis of anorexia associated with chronic disease, although the possibility remains that the ghrelin response is inappropriately low given the degree of negative energy balance. Despite the lack of conclusive evidence for a clear role for ghrelin in anorexia of chronic disease, multiple preclinical studies have demonstrated promising results in

experimental models of cachexia. When administered to tumor-bearing animals (34, 213, 214) or rats with chronic renal failure (215), ghrelin ameliorates anorexia and improves lean mass. Ghrelin administration improves skeletal muscle mitochondrial oxidative capacity independent of food intake (216), suggesting that ghrelin may have peripheral anti-catabolic effects, or engage a presently unknown hypothalamic anti-catabolic pathway. When utilized in an experimental model of CHF, ghrelin treatment improves muscle mass (208) and overall lean mass (217). These promising data have resulted in multiple clinical trials examining the efficacy of ghrelin in cachexia of multiple etiologies.

4.3.4 The Hypothalamic-Pituitary-Adrenal Axis

One of the best-understood neuroendocrine responses to inflammation is the activation of the hypothalamic-pituitary-adrenal axis (HPA), resulting in the release of glucocorticoids. The reciprocal relationship between glucocorticoids and inflammatory mediators was initially found in the fact that glucocorticoids inhibit the production of chemotactic factors, as well as inhibiting their action on target cells (218). It was later discovered that the degree of the immune response *in vivo* directly correlated with the level of circulating glucocorticoids (219, 220). Causality was demonstrated by experiments showing that monocyte culture supernatants administered systemically could not activate the HPA axis in the presence of IL-1β neutralizing antibodies. Administration of recombinant IL-1β was later shown to be sufficient to activate the HPA axis (221). Furthermore, this appeared to occur at the level of the hypothalamus, as both ACTH and CRH were released simultaneously with corticosterone, and immunoneutralization of CRH blocked the release of corticosterone (222, 223). It also appears that IL-1β does not activate the HPA axis via signaling at the level of the pituitary as IL-1β fails to induce the release of ACTH from corticotroph cell lines or

primary pituitary cultures. It also seems unlikely that direct IL-1β action on the adrenal gland plays a significant role in this effect, since CRH neutralization completely blocks the release of glucocorticoids. It has subsequently become apparent that other cytokines can cause the release of glucocorticoids (224, 225). Furthermore it appears that some cytokines can directly activate the pituitary gland. Both IL-6 and LIF appear capable of direct stimulation of pituitary corticotrophs, releasing ACTH (226, 227).

Despite the potential for direct stimulation of the pituitary, the best-studied mechanisms by which inflammation activates the HPA axis are those at the level of the hypothalamus. Initially, believing that cytokines were too large to pass across the blood brain barrier (228), work focused primarily on prostaglandins (163). Through a series of detailed neuroanatomical studies using cFos as a marker of neuronal activation, a mechanistic link was established between catecholaminergic neurons of the ventrolateral medulla of the spinal cord and CRH neurons of the hypothalamus. When ascending connections between these two cell groups are cut, intravenous (i.v.) IL-1β fails to induce cFos in CRH neurons (229). Implicating prostaglandins, cyclooxygenase inhibition prevented the ability i.v. Il-1β to induce cFos in the PVN. Further studies have refined the cell types involved with this process, suggesting a critical role for IL-1β signaling in both endothelium and perivascular macrophages in activation of the HPA axis via prostaglandins (168, 230). Despite this extensive histologic evidence for the importance of prostaglandins, the corticosterone response to systemic inflammation is only modestly attenuated by systemic COX inhibition (231). This suggests that alternate, prostaglandin independent pathways play a role in mediating the HPA response to systemic inflammation.

5. An Integrated Model of the Systemic Physiology of Cachexia

5.1 Central Control of Peripheral Metabolic Function via the Autonomic Nervous System

Sickness behavior and muscle atrophy are often considered to be isolated processes of the brain and muscle respectively. Indeed, many studies of muscle atrophy in particular focus on the cell autonomous action of inflammatory cytokines on skeletal muscle. When considering cachexia from a systems perspective however, it seems unlikely that any of these processes occur in isolation or without feedback regulation. A growing body of evidence suggests that the CNS regulates peripheral metabolic function in a coordinated manner. While the majority of the insight regarding the central regulation of peripheral metabolism has come from the obesity literature, the same principles are likely applicable in the context of cachexia. Indeed, the ability to melanocortin antagonism to protect lean mass in experimental models of cachexia suggests a hypothalamic mechanism for muscle catabolism.

While little data exists regarding the central control of muscle mass, the obesity field has made great strides in understanding the regulation of body fat by the brain. Such studies have demonstrated a role for CNS neuropeptide signaling in the regulation of fat mass and cholesterol homeostasis (232, 233) via the autonomic nervous system. In particular, there is extensive evidence to suggest that the process of lipogenesis and lipolysis in white adipose tissue are regulated by preautonomic MC4R positive neurons in hypothalamus. Using retrograde tract-tracing with pseudorabies virus, a series of elegant studies mapped the neuroanatomic circuit between neurons of the PVN and adipose tissue (234-236). This innervation has physiologic relevance, as the sympathetic nervous system (SNS) regulates fat cell number (237). Stimulation of the MC4R increases white adipose tissue sympathetic nerve firing, favoring lipolysis via activation of beta adrenoreceptors (232). Given that metabolic changes rarely occur in isolation, it is possible that the same neurocircuitry

involved in the regulation of fat mass may also regulate the anabolic/catabolic balance in skeletal muscle as a part of the concerted regulation of whole body energy homeostasis.

5.2 Autonomic Regulation of Muscle Mass

5.2.1 Adregnergic Receptors and Skeletal Muscle

Very few studies have examined the role of the autonomic nervous system in the regulation of muscle mass. Both the sympathetic and parasympathetic nervous system have the potential to influence the metabolic activity of skeletal muscle. While the sympathetic nervous system is well studied with regard to skeletal muscle, there is almost no data with regard to parasympathetic nervous system providing input to muscle. β-adrenergic receptors are present on skeletal muscle, with a preponderance of the type 2-receptor (238). β receptor density is greater in slow than it is in fast muscle (239), although paradoxically β agonists have greater effects in fast twitch muscle (240, 241). α1 receptors are also present in the sarcolemma of skeletal muscle, but are found almost exclusively in slow twitch muscle (242). β agonists are anabolic to skeletal muscle and produce significant hypertrophy over time (243, 244). Multiple preclinical studies have documented the potential of beta agonists to increase skeletal muscle mass and function in numerous catabolic states such as cancer (245, 246), muscular dystrophy (247), aging (248, 249) and burn injury (250). Interestingly, drugs targeting the β2 adrenergic receptor have the opposite effects on adipose tissue, decreasing fat mass and leading many to refer to beta agonists as repartitioning agents (244). This of course is consistent with the known physiology of β adrenergic receptors on adipose tissue as discussed above. However, this is not entirely consistent with a model wherein melanocortin signaling in the brain increases

SNS output resulting in the mobilization of energy reserves from both adipose tissue and skeletal muscle in concert.

5.2.2 Effects of Endogenous Autonomic Activity on Skeletal Muscle

Only a few studies have explored the role of endogenous catecholamines on skeletal muscle. In rats, treatment with guanethidine (which depletes noradrenergic terminals) results in significant increase in skeletal muscle protein breakdown (251). Likewise, chemical or surgical sympathectomy results in significant decreases in protein breakdown (252). What is difficult to discern from these two studies is whether this effect is derived from autonomic nerve endings in skeletal muscle or from circulating catecholamines. Both severing of the sympathetic trunk and administration of guanethidine decrease circulating catecholamine levels which are derived from he adrenal medulla. Regardless, these data demonstrate that muscle receives tonic anabolic input from endogenous catecholamines.

Alpha-adrenergic receptors also influence the metabolism of skeletal muscle. When administered into the CNS, leptin increases skeletal muscle glucose uptake via the activation of AMPK. This effect can be blocked by surgical denervation of the hind limb muscle, or by administration of the α antagonist phentolamine (253). Consistent with the expression of the receptor primarily in slow twitch muscle, this effect occurs predominantly in oxidative rather than glycolytic muscles.

6. Summary

Substantial evidence exists to implicate cytokine signaling in the CNS and in particular the hypothalamus in the regulation of skeletal muscle mass. Skeletal muscle receives input in the form of hormonal signals from IGFs and glucocorticoids, as well as receiving neural input. However, the role of the CNS in the regulation of

muscle mass has not been completely described. Compounds with a CNS site-of-action are being developed as therapeutic agents for cachexia, yet we know very little about the underlying mechanisms by which metabolic signals are relayed from the brain. Therefore, it was the purpose of this thesis to better characterize the CNS substrates for cytokine action in mediating the metabolic response to sickness and to delineate central pathways pathway mediating muscle atrophy.

CHAPTER 2

Manuscript #1

Central Nervous System Inflammation Induces Muscle Atrophy via Activation of the Hypothalamic-Pituitary-Adrenal Axis

Theodore P. Braun[1,2], Xinxia Zhu[1], Marek Szumowski[1], Gregory D. Scott[2,3], Aaron J. Grossberg[1,2], Peter R. Levasseur[1], Kathryn Graham[4], Sheehan Khan[5], Sambasivarao Damaraju[4], William F. Colmers[6], Vickie E. Baracos[4] and Daniel L. Marks[1*]

Papé Family Pediatric Research Institute[1], MD/PhD Program[2] and Department of Pulmonary and Critical Care[3], Oregon Health & Science University, Portland, Oregon, 97239, USA.
Department of Oncology[4], Department of Computer Science[5] and Department of Pharmacology[6], University of Alberta, Edmonton, Alberta, T6G 2H7, Canada.

Chapter 2 is modified from the original paper published in *The Journal of Experimental Medicine* Nov 14th, 2011.

Abstract

Skeletal muscle catabolism is a co-morbidity of many chronic diseases and is the result of systemic inflammation. While direct inflammatory cytokine action on muscle promotes atrophy, non-muscle sites of action for inflammatory mediators are less well described. Here we demonstrate that central nervous system-delimited interleukin-1 beta (IL-1β) signaling alone can evoke a catabolic program in muscle, rapidly inducing atrophy. This effect is dependent on hypothalamic-pituitary-adrenal (HPA) axis activation, as CNS IL-1β-induced atrophy is abrogated by adrenalectomy. Furthermore, we identified a glucocorticoid-responsive gene expression pattern conserved in models of acute and chronic inflammatory muscle atrophy. In contrast with reports suggesting that the direct action of inflammatory cytokines on muscle is sufficient to induce catabolism, adrenalectomy also blocks the atrophy program in response to systemic inflammation, demonstrating that glucocorticoids are requisite for this process. Additionally, circulating levels of glucocorticoids equivalent to those produced under inflammatory conditions are sufficient to cause profound muscle wasting. Together, these data suggest that a significant component of inflammation-induced muscle catabolism occurs indirectly via a relay in the central nervous system.

Introduction

Loss of muscle mass is a defining feature of cachexia of chronic disease. Patients suffering from cancer, chronic heart disease, COPD, sepsis and many other conditions experience involuntary weight loss and loss of muscle mass, which contributes significantly to mortality (reviewed recently in (33, 254)). A decrease in volitional food intake is often associated with cachexia, but is not solely responsible for the loss of muscle mass, as nutritional supplementation fails to substantially reverse changes in body weight (32). A common pathologic feature of these disparate conditions is an increase in circulating inflammatory cytokines. Systemic administration of cytokines results in muscle catabolism in experimental animals (42). Further, genetic (255)or pharmacologic blockade (101) of cytokine signaling attenuates experimental cachexia. Numerous studies have demonstrated that inflammatory cytokines can cause atrophic changes in cultured myotubes, and *in vivo* studies have demonstrated that activation of inflammatory signaling pathways are fundamental to the atrophy process (42, 106, 256, 257). However, the catabolic effects of inflammation *in vivo* have not been shown to depend exclusively on direct cytokine action on skeletal muscle.

Despite the well-documented role of the brain in regulating whole body metabolism, the contribution of CNS inflammation to muscle atrophy has not been examined. The central nervous system is a known target of cytokine signaling in cachexia, where cytokines act on neural feeding circuits to mediate anorexia (131, 186). Multiple inflammatory cytokines are induced in the hypothalami of animals treated peripherally with lipopolysaccharide (LPS) (127), or in tumor-bearing animals (138). When CNS IL-1 receptors are pharmacologically antagonized during systemic inflammation, anorexia and alterations in peripheral protein metabolism are

ameliorated (136, 258), suggesting CNS inflammation plays a critical role in integrating the host response to disease.

Here we present evidence that CNS inflammation is sufficient to induce muscle atrophy independent of substantial peripheral inflammation. Activation of the hypothalamic-pituitary-adrenal (HPA) axis is both necessary and sufficient to explain the catabolic action of central inflammation. Consistent with the role of the brain as a central regulator of metabolic homeostasis, this work implicates CNS cytokine signaling in regulating the muscle catabolism in response to systemic inflammation.

Results

CNS Inflammation and Muscle Catabolism are Coincident States

CNS inflammation and muscle catabolism are common features in experimental models of cachexia. Mice treated with LPS (250 μg/kg) or implanted with the Lewis Lung Carcinoma (LLC) robustly increase the expression of inflammatory cytokines in the hypothalamus (Figure 2 a, c). LPS administration results in generalized inflammation, as evidenced by the upregulation of both IL-1β and TNF. In contrast, tumor growth resulted only in the upregulation of IL-1β. Furthermore, after systemic LPS administration, IL-1β expression is strongly induced within the hypothalamic arcuate nucleus as shown by in situ hybridization, demonstrating endogenous production within the CNS (Figure 2 b). Muscle loss in cachexia occurs as a result of a decrease in protein synthesis and a concomitant increase in protein degradation that occurs principally via the ubiquitin proteasome system (43, 52, 56). Muscle-specific E3 ubiquitin ligases, muscle atrophy F-box (MAFbx or atrogin-1) and muscle ring finger protein 1 (MuRF1) (58, 59) are induced in catabolic muscle and are regulated by the Forkhead Box (Foxo) family of transcription factors (70). Increased expression of MAFbx and MuRF1 occurs in all forms of atrophy studied (122). Simultaneous with central inflammation, the atrophy program is activated in skeletal muscle, marked by the upregulation of MAFbx, MuRF1 and Foxo1 (Figure 2 a, c), which in the case of tumor-bearing animals occurs in the context of muscle mass loss (Figure 2 d).

Acute and Chronic Central Administration of IL-1β Results in Muscle Atrophy

To determine whether inflammatory signaling in the CNS plays a role in directing muscle catabolism, mice were administered IL-1β (10 ng) or vehicle (Veh) by intracerebroventricular (i.c.v.) injection. To control for the anorectic effects of IL-1β,

food was removed from all cages at the time of injection. Central administration of IL-1β led to a significant and rapid induction of MAFbx, MuRF1 and Foxo1 mRNA in gastroncnemius (Gn) muscle 4-8 h after the injection (Figure 3 a), demonstrating rapid activation of the catabolic program in skeletal muscle in response to central inflammation. Given the known role of PI3K/Akt signaling in the regulation of muscle mass, we examined Akt phosphorylation in muscle by Western blot after acute i.c.v. IL-1β (Figure 3 b). No changes were observed in the phosphorylation of Akt at any time point after i.c.v. IL-1β injection. To rule out the possibility that centrally administered IL-1β was leaking into the systemic circulation and having a direct impact on muscle, we examined p38 MAPK phosphorylation in muscle. Signaling via this pathway occurs downstream of the type I IL-1 receptor (IL-1R1), and has been implicated in the regulation of MAFbx (105, 106). No changes were observed in p38 phosphorylation at any time point after central IL-1β injection, suggesting that centrally injected cytokine is unlikely to be directly signaling in muscle (Figure 3 b). We also examined circulating IL-1β levels after acute central IL-1β injection, and found no changes at any time point examined (Table 1).

We next examined whether the catabolic molecular mechanisms that are rapidly engaged after bolus i.c.v. IL-1β injection can bring about muscle atrophy with time. Rats were infused with IL-1β into the lateral ventricle for 3 days via osmotic minipumps at a dose (10 ng/hr) thought to mimic endogenous pathophysiologic concentrations under inflammatory conditions (141). This dose is also far below those given peripherally to induce muscle catabolism or anorexia (59, 129). To control for the effects of IL-1β on food intake, a subset of Veh treated animals were pair fed (PF) to the IL-1β treated animals. Central IL-1β treatment led to a sustained decrease in food intake over the course of the 3-day study. While Veh treated animals consumed 78.6±2.2 g of food over the 3-day period, IL-1β treated animals only consumed

45.29±4.0 g. Similar to acute injection, chronic i.c.v. infusion of IL-1β increased the expression of MAFbx, MuRF1 and Foxo1 mRNAs in muscle (Figure 3 c). The most pronounced differences were seen in the Gn and extensor digitorum longus (EDL), which are predominantly composed of fast twitch fibers. These effects were largely independent from food intake as PF animals failed to show similar changes in gene expression. In contrast, the induction of MAFbx, MuRF1 and Foxo1 in the soleus was relatively small. Central IL-1β infusion also resulted in significant alterations in body composition, resulting in significant food intake-independent losses of both body weight and lean mass (Figure 3 d). While significant fat mass loss occurred with IL-1β treatment, these changes were paralleled by the PF group. Concurrent with the changes in body composition, significant food intake-independent loss of Gn and EDL muscles were observed (Figure 3 e). To examine whether the loss of muscle mass seen with i.c.v. IL-1β treatment is the result of myofibrillar atrophy, fiber cross sectional area (CSA) was measured in regions of the Gn and soleus muscle composed of fast (white Gn, WGn) and slow (soleus) fibers. WGn Fiber CSA was significantly reduced by IL-1β treatment, but unaltered in PF animals (Figure 3 f, g). In contrast, soleus fiber CSA was only mildly reduced (Figure 3 f).

To confirm that centrally infused IL-1β is not diffusing systemically and acting directly on muscle, we infused IL-1β intraperitoneally (i.p.) at the same dose given i.c.v (10ng/hr) for 3 days. This peripheral IL-1β treatment did not induce MAFbx, MuRF1 or Foxo1 mRNA in the Gn, soleus or EDL (Figure 4 a). Unlike i.c.v. infusion, i.p. IL-1β delivered at this dose did not affect Gn, soleus and EDL weights (Figure 4 b). In addition, peripheral IL-1β infusion did not significantly alter body weight, lean mass or fat mass (Figure 4 c), and failed to alter fiber CSA in the WGn or soleus (Figure 4 d, e). To determine whether low dose systemic IL-1β infusion was causing increases in circulating IL-1β levels, we measured IL-1β in the plasma of these

animals. Circulating IL-1β levels were below the limit of detection in all samples (LOD= 93.6 pg/mL, data not shown). Collectively, these data demonstrate that inflammation in the CNS is sufficient to induce muscle atrophy, predominantly in fast twitch fibers. Furthermore, IL-1β is a far more potent catabolic mediator when administered centrally than when given peripherally.

Central Melanocortin Signaling Is Not Necessary for IL-1β-Induced Muscle Atrophy

Pharmacologic blockade of the type 4 melanocortin receptor (MC4R) prevents IL-1β-induced anorexia and attenuates lean mass loss in experimental cachexia (35, 36, 150). Furthermore, the MC4R is critical to the CNS regulation of many other facets of metabolism (232, 233). Finally, inflammatory challenges specifically upregulate IL-1β mRNA in the arcuate nucleus, which contains the proximal neurons of the central melanocortin system. Based on this, we sought to examine whether the acute, food intake-independent changes in muscle catabolism initiated by IL-1β are dependent on signaling at the MC4R. WT mice and mice lacking a functional MC4R (MC4RKO) were injected i.c.v. with IL-1β (10 ng) and were sacrificed 8 h after injection. Surprisingly, IL-1β led to a similar increase in the mRNA for MAFbx, MuRF1 and Foxo1 in the Gn of both WT and MC4RKO mice (Figure 5 a). To further examine the role of the central melanocortin system in regulating muscle catabolism independent from its effects on food intake, rats were injected i.c.v. with melanotan II (MTII, 1 nmol), an agonist at the type 3 and 4 melanocortin receptors, and were sacrificed 6 h after injection. MTII failed to increase the mRNA for MAFbx, MuRF1 or Foxo1 in the Gn (Figure 5 b). To determine the impact of increased signaling via the MC4R in the chronic state, MTII (1 nmol) was administered i.c.v. every 12 h for 36 h (4 injections), and animals were sacrificed 2 h after the final injection. To control for the decreased food intake associated with MTII treatment, aCSF-injected control

animals were PF with MTII-treated animals. Chronic MTII failed to increase the mRNA for MAFbx or Foxo1 relative to pair fed controls, but led to a small increase in MuRF1 mRNA in the Gn (Figure 5 c). No changes in the expression of MAFbx, MuRF1, or Foxo1 were seen in the soleus (Figure 5 c). Both MTII-treated and pair fed animals lost weight over the course of the experiment, but there was no difference between groups (Figure 5 d). MTII treatment also did not lead to significant food intake-independent losses of fat mass, lean mass, Gn or soleus weight (Figure 5 d, e). These results argue that the CNS mechanism by which IL-1β induces food intake-independent muscle catabolism is not dependent on signaling at the MC4R.

Central IL-1β Injection Induces a Transcriptional Program in Skeletal Muscle, Which Is Analogous to That Seen in Other Forms of Atrophy

Changes in the mRNA profile of skeletal muscle undergoing atrophy have been extensively characterized, revealing a conserved pattern of gene expression (122). To gain insight into how central IL-1β induces muscle catabolism, we performed cDNA microarray analysis of mouse skeletal muscle RNA at 2, 4 and 8 h after i.c.v. IL-1β injection. Statistical analysis with a false discovery rate of 1% yielded 494 significantly regulated genes. This list was further narrowed to 100 genes by restricting it to genes that were at least 1.75 fold up- or down-regulated at any of the three time points (Figure 6, Figure 10 and Table 4). The expression pattern of 10% of these genes was confirmed by real time PCR (denoted in red). The complete data set has been deposited in the GEO Omnibus database (GEO Series accession number GSE26766). Significantly regulated genes were grouped based on their known functions in skeletal muscle. At the 2 and 4 h time points there was a pronounced regulation of genes involved in regulating the inflammatory/anti-inflammatory balance. At the 4 and 8 h time points, alterations in nutrient signaling were evident, with

changes in mammalian target of rapamycin (mTOR) and AMP activated protein kinase pathway members. An oxidative stress response was also observed at later time points. Genes involved in cell cycle regulation and myogenic differentiation were significantly affected, suggesting alterations in muscle regeneration. Comparison of this data set with two separate gene expression array studies evaluating muscle gene expression in response to glucocorticoid administration revealed multiple glucocorticoid-responsive genes (marked by §) (259, 260). These data implicate HPA axis activation in mediating the changes in gene expression in skeletal muscle after central IL-1β treatment.

Regulation of Circulating Growth Factors and Cytokines After i.c.v. IL-1β

Plasma levels of IL-6 were examined by ELISA after acute i.c.v. IL-1β injection, as circulating IL-6 increases after central IL-1β administration (261), and IL-6 has been implicated in mediating muscle catabolism (101). A small induction of circulating IL-6 was observed at early time points, with a peak of 298 ± 35 pg/mL at 2 h vs 13 ± 3 pg/mL in vehicle-treated animals, with levels returning to baseline by 8 h (Table 1). Despite a marked increase, these levels of IL-6 are quite low in comparison to those found in animals undergoing systemic inflammatory challenge, where peak serum values approach 7,000 pg/mL. To examine whether significant IL-6 production or signaling was occurring in muscle after central IL-1β treatment, we measured the expression of IL-6 and its downstream feedback inhibitor suppressor of cytokine signaling 3 (SOCS3). We found no changes in either IL-6 or SOCS3 gene expression in muscle at any time point after central injection of IL-1β, suggesting that significant IL-6 signaling does not occur in muscle after i.c.v. IL-1β injection (data not shown). Additionally, sustained delivery of IL-1β into the CNS, did not lead to an increase in circulating IL-6 levels at the end of three days of i.c.v. infusion (Table 2), suggesting

that the elevation of IL-6 after acute central IL-1β treatment is a transient phenomenon.

Circulating insulin-like growth factor-1 (IGF-1) contributes to the regulation of the anabolic/catabolic balance in skeletal muscle (77). No differences in IGF-1 were observed between vehicle and IL-1β treated animals at any time point, with all values falling in the expected normal range (Table 1). IGF-1 levels were also measured in animals infused i.c.v. with IL-1β for 3 days. Serum IGF-1 levels were unaffected by chronic IL-1β administration relative to ad lib fed controls (Table 2).

Glucocorticoids are known mediators of muscle catabolism (59), and inflammation activates the HPA axis. Given the significant glucocorticoid-regulated gene expression signature seen in response to central inflammation, we measured serum corticosterone (the predominant circulating glucocorticoid in rodents) by radioimmunoassay. Similar to IL-6, serum corticosterone levels were highest at 2 h after acute i.c.v. IL-1β, reaching 397 ± 30 ng/mL vs 104 ±16 ng/mL in vehicle treated animals, and had returned to baseline by 8 h after injection (Table 1). In contrast with plasma IL-6 levels, chronic i.c.v. infusion of IL-1β led to a sustained increase in circulating corticosterone at the time of sacrifice relative to vehicle-treated animals, (183 ± 40 ng/mL for IL-1β infused animals vs 37 ± 21 ng/mL for vehicle treated animals (Table 2)).

Activation of the HPA Axis is Necessary for the Muscle Catabolic Effects of i.c.v. IL-1β

To explore the involvement of HPA axis activation in i.c.v. IL-1β-induced muscle catabolism, mice received acute i.c.v. injections of IL-1β (10ng) and were treated with the glucocorticoid/progesterone antagonist mifepristone. Mifepristone treatment attenuated the induction of MAFbx, MuRF1 and Foxo1 mRNA by i.c.v. IL-1β (Figure 7 a and Table 3). To confirm these findings, we utilized adrenalectomized

(ADX) mice with low physiologic corticosterone replacement. This allowed us to examine whether tonic glucocorticoids are a permissive factor in muscle catabolism or whether an increase in circulating corticosterone is the driver of atrophy. In ADX animals, i.c.v. IL-1β failed to induce MAFbx to the same degree as seen in sham-operated animals, and the induction of MuRF1 and Foxo1 by i.c.v. IL-1β injection was completely blocked (Figure 7 b and Table 3). In addition, the induction of the catabolic transcription factor Krüpple-Like Factor 15 (KLF15), which transactivates MAFbx and MuRF1 (81), was blocked by ADX. These data demonstrate that an increase in circulating glucocorticoids is necessary for the acute activation of the atrophy program in response to i.c.v. IL-1β.

To determine if intact adrenals are necessary for food intake-independent myofibrillar atrophy, we infused i.c.v. IL-1β (10ng/ hr) or vehicle for three days in ADX, corticosterone replaced rats. To control for the effects of food intake, Veh-treated animals were PF to IL-1β treated animals. No significant differences were observed in the expression of MAFbx, MuRF1 or Foxo1 in the Gn, soleus, or EDL (Figure 7 c). There were statistically non-significant trends toward an increase in the levels of MAFbx and MuRF1 mRNA in the Gn (MAFbx mRNA P=0.09, and MuRF1 mRNA P=0.12) and EDL (MAFbx mRNA P=0.19, MuRF1 mRNA P=0.34). Central IL-1β infusion failed to generate a significant decrease in body weight, fat mass or lean mass beyond that seen in PF animals (Figure 7 d), although a statistically non-significant trend was seen toward the loss of lean mass (P=0.13). No differences were observed in the weights of Gn, soleus or EDL muscles (Figure 7 e). Muscle fiber CSA was also not significantly decreased by IL-1β infusion relative to pair fed controls in either the WGn or soleus (Figure 7 f-g). Centrally infused IL-1β was not leaking systemically, as the majority (19/20) of animals had plasma IL-1β levels below the limit of detection (LOD= 93.6 pg/mL, data not shown).

Central IL-1β Induces a Glucocorticoid-Dependent Transcriptional Program That Is Common to Models of Acute and Chronic Systemic Inflammation

To study the extent to which the transcriptional program initiated by central IL-1β is dependent on glucocorticoid signaling, we selected several genes identified by the array analysis to examine in ADX mice. The adipokine lipocalin-2 (Lcn2), and the steroid hormone responsive transcript decidual protein regulated by progesterone (Depp) were highly induced by central IL-1β administration, a response only slightly attenuated by adrenalectomy (Figure 8 a and Table 3). In contrast, the induction of the oxidative stress response genes metallothionein-2 (Mt2) and uncoupling protein-3 (Ucp3) was completely blocked by ADX. The upregulation of mammalian target of rapamycin (mTOR) pathway members sestrin-1 (Sesn1) and Regulated in Development and DNA Damage Responses (REDD1 or Ddit4) as well as the downstream target Foxo3 were also inhibited by ADX. The anti-myogenic basic helix-loop-helix transcription factor inhibitor of DNA binding-3 (Id3) was also induced by central IL-1β treatment in a glucocorticoid-dependent manner. The cytoskeletal protein kyphoscoliosis peptidase (KY) is dramatically downregulated by central inflammation an effect partially blocked by ADX. We also examined myostatin gene expression in skeletal muscle, given its known critical role in the regulation of muscle mass (14, 113). Myostatin was modestly induced by central IL-1β administration and this induction was completely blocked by adrenalectomy (Figure 8a). Collectively, these genes show a pattern of regulation that is largely dependent on an intact HPA axis, although some features are independently regulated. To confirm this expression pattern in a model of systemic inflammation, we examined the expression of these genes in LPS and tumor-associated muscle catabolism (Figure 8 b, c). An identical pattern of regulation was observed in LPS-treated animals, suggesting a significant

glucocorticoid effect on skeletal muscle in response to peripheral inflammation. Despite the low-grade peripheral inflammation in tumor bearing animals, many of the genes examined (5/9) were regulated in skeletal muscle. Importantly, the glucocorticoid dependent mTOR regulators Sesn1 and REDD1 were up regulated in the muscle of tumor-bearing animals demonstrating that glucocorticoid signaling may contribute to the pathogenesis of cancer cachexia.

HPA Axis Activation is Necessary and Sufficient for Muscle Wasting Driven by Central and Peripheral Inflammation

To examine the role of HPA axis activation in peripheral inflammation-induced activation of the atrophy program, LPS (250 μg/kg) was administered to ADX mice. The LPS-mediated induction of MAFbx was attenuated in ADX mice, and the induction of MuRF1 and Foxo1 were completely prevented in ADX animals (Figure 9 a). The induction of KLF15, REDD1 and Sestrin-1 by LPS was also completely blocked in ADX mice. Collectively, this demonstrates that peripheral inflammation-mediated activation of the atrophy program requires intact adrenal glands.
While high-dose administration of synthetic glucocorticoids induces substantial atrophy, it remains unknown whether the lower levels of circulating corticosterone evoked by inflammation are sufficient to induce atrophy. To examine this possibility, rats were implanted with sustained release cort pellets at a dose known to produce circulating concentrations approximating levels seen in inflamed animals (145, 262). Rats were implanted with 100 mg or 2 X 100 mg (200 mg) corticosterone tablets, achieving mean circulating levels of 321.8±43.0 ng/mL and 908.5±223.7 ng/mL respectively vs undetectable levels (LOD=25 ng/mL) in sham animals. Both treatments significantly induced MAFbx, MuRF1 and Foxo1 to largely the same degree (Figure 9 b). We additionally assessed the expression of the mTOR regulators

REDD1, Sestrin-1 and KLF15, as well as the glucocorticoid responsive anti-inflammatory mediator IκBα (263), in Gn after corticosterone treatment. All 4 genes were significantly elevated by 100 mg and 200 mg corticosterone treatment (Figure 9 b). Significant weight loss was observed in the Gn and EDL muscle with relative sparing of the soleus (Figure 9 c). Both 100 mg and 200 mg treatments also resulted in a significant loss of body weight, fat mass and lean mass (Figure 9 d). Significant myofibrillar atrophy was evident in the WGn from both corticosterone treatment groups, but was largely absent in the soleus (Figure 9 e, f). In nearly all cases, little difference was seen between 100 mg and 200 mg treatments, demonstrating that the atrophy program is maximally activated by corticosterone levels within the physiologic range evoked by inflammation.

Discussion

The CNS serves as a central regulator of whole body energy balance coordinating metabolic homeostasis in multiple peripheral tissues (232, 253, 264). Under normal physiologic conditions, anabolism and catabolism are regulated such that energy needs are met. During acute infection, skeletal muscle is mobilized to provide substrates to fuel the necessary increases in immune function. However, in cases of chronic disease where inflammation persists, muscle protein is excessively mobilized, leading to profound muscle atrophy. The regulation of protein mobilization by inflammation occurs at numerous levels. The direct action of inflammatory signaling molecules on skeletal muscle has been extensively examined, as has the contribution of IGF1 signaling (42, 77, 99, 105, 106). The data we present here demonstrate that CNS integration of inflammatory signaling also plays a critical role in regulating the anabolic/catabolic balance in muscle via activation of the HPA axis. Given that a multitude of inflammatory diseases with underlying muscle catabolism are also marked by CNS inflammation, a central mechanism must now be considered when describing muscle atrophy.

To model endogenous production of IL-1β in the CNS and its impact on skeletal muscle, we utilized i.c.v. injection to deliver physiologically relevant doses of this prototypical inflammatory cytokine. Central injection of IL-1β is believed to mimic its production by the choroid plexus and circumventricular organs (265) and is therefore a model of endogenous inflammation. Hypothalamic IL-1β production is a conserved feature of a multitude of conditions associated with muscle catabolism, including cancer cachexia (Figure 2 and (137, 138)), peripheral cytokine administration (197) and endotoxemia (Figure 2 and (127)). Additionally, antagonism of central IL-1 signaling attenuates many of the behavioral (136) and metabolic (258, 266) features of inflammatory disease. Our data show that central inflammation

initiates significant muscle atrophy. Although we have demonstrated that central IL-1β is sufficient for this effect, it is unlikely to be the only mediator during systemic inflammation, as many cytokines activate the HPA axis (224). We demonstrate specific production of IL-1β within the arcuate nucleus under inflammatory conditions. The arcuate also contains two neuronal groups that are known to express the IL-1R1: POMC and AgRP (187) neurons. The net effect of IL-1β on these two neuronal groups is to increase signaling at the MC4R, decreasing food intake. In accordance with this, the anorexia associated with IL-1β administration is completely prevented by blockade of the MC4R (129). Furthermore, the loss of lean mass associated with cancer cachexia and LPS administration is prevented by blockade of the MC4R (35, 36). Surprisingly, we found that signaling at the MC4R is not necessary for central IL-1β-induced muscle catabolism, and MC4R activation is not sufficient to produce significant muscle catabolism. These results are in disagreement with previous work showing a protective effect of melanocortin blockade on body weight and lean mass in experimental cachexia. However, these prior studies did not separate the powerful effects of melancortin blockade on food intake from its effects on body composition. Given the minor regulation of MuRF1 by the central melanocortin system, and the effects of the melanocortin system on food intake, it is possible that the protective effects of melanocortin blockade in experimental cachexia are the result of the combination of these two factors alone.

The precise neuroanatomic substrate via which IL-1β exerts its catabolic effect remains unknown. However, given that the major downstream mediator of central inflammation-induced muscle catabolism is activation of the HPA axis, there is significant evidence to implicate endothelial IL-1R1 as a crucial mediator of this effect. Activation of corticotrophin releasing hormone neurons in the paraventricular nucleus (the hypothalamic component of the HPA axis) by central or peripheral IL-1β is

blocked by knockdown of endothelial IL-1R1 (230). Furthermore, a component of this effect is mediated via endothelium-derived prostaglandin signaling in medullary catecholaminergic neurons projecting to paraventricular neurons, activating the HPA axis (163, 168). Future loss-of-function studies will likely examine the role of inflammatory signaling at the level of the cerebrovascular endothelium in mediating muscle catabolism. In addition, there is a great deal of evidence that pituitary corticotrophs can be directly activated by inflammatory cytokines. Both leukemia inhibitory factor and IL-6 can directly activate pituitary corticotrophs, leading to the release of ACTH independent of hypothalamic signaling (226, 227).

Increased levels of circulating glucocorticoid are necessary for muscle catabolism due to fasting (53), sepsis (93) and acute diabetes (95), as adrenalectomy or administration of mifepristone attenuates muscle wasting in these states. Consistent with this, we found that central inflammation also requires an intact HPA axis to induce muscle catabolism. Furthermore, models of peripheral inflammation-induced muscle-wasting share a similar glucocorticoid-responsive gene expression signature, suggesting this response relies on HPA axis activation. Surprisingly, induction of the atrophy program by LPS was almost entirely blocked by adrenalectomy. LPS has been proposed to induce muscle catabolism via direct action on muscle, or via the production of cytokine intermediates such as TNF or IL-1β, which act directly on muscle (99, 105, 106). Our data suggest that HPA axis activation is an integral part of the catabolic response to inflammation and that glucocorticoids may synergize with cytokines acting directly on muscle to promote atrophy. Interestingly, muscle specific loss of function of the cytokine receptor adaptor protein TRAF6 ameliorated tumor-induced muscle atrophy, implicating cytokine action on the myocyte as a mediator of atrophy (267). However, atrophy due to denervation is also attenuated in muscle specific TRAF6 knockout mice. Given that denervation atrophy

is not believed to occur via systemic inflammation, this finding suggests that TRAF6 may play some as yet unspecified role in muscle atrophy independent of its role in transducing inflammatory cytokine signals. Indeed, the inflammatory signaling apparatus has been generally implicated in mediating the atrophic response in skeletal muscle. NF-κB activity is increased in the muscle of tumor-bearing mice, and dominant negative inhibition of NF-κB signaling blocks tumor-associated muscle atrophy (104). NF-κB also plays a critical role in the atrophy process in response to denervation and unloading, both of which are not thought to rely on systemic inflammation (268, 269). Therefore, it is likely that signaling via TRAF6 and NF-κB plays a fundamental role in atrophy beyond their role in the transduction of systemic inflammatory signals.

Despite the fact that elevated glucocorticoid levels are found in models of cancer cachexia (270), it is widely accepted that they do not participate in muscle atrophy associated with tumor growth (97, 98). However, it is difficult to rule out a role for endogenous glucocorticoids on the basis of these studies. Two of these studies utilized the same tumor model (YAH-130), which grows in the peritoneal cavity, and likely directly impacts organ function. Furthermore, food intake was not removed as a variable in these studies. Despite this, a trend toward improvement was observed in ADX tumor-bearing animals with regard to skeletal muscle protein content (98). Pharmacologic blockade of glucocorticoid receptors with mifepristone has been unsuccessful in cancer cachexia, however given the 1-2 h half life of this drug in rodents (271), the once daily dosing was likely sub-therapeutic in these studies. Given the glucocorticoid responsive gene expression signature seen in the skeletal muscle of tumor-bearing animals and the limitations of the aforementioned studies, the involvement of glucocorticoids in tumor-associated muscle wasting appears likely.

Future genetic loss-of-function studies will likely shed light on the contribution of glucocorticoids to muscle wasting in cancer.

The molecular mechanisms underlying glucocorticoid-induced atrophy have been extensively studied at the level of skeletal muscle, and are driven to a large degree by transcriptional changes. Our array analysis is unique in the literature in that it offers insight into these early transcriptional events that take place after endogenous activation of the HPA axis. The upregulation of catabolic machinery after central IL-1β administration likely occurs via a number of molecular mechanisms. Glucocorticoids directly transactivate the MuRF1 gene in synergy with Foxo1 (84). In addition, Foxo1 expression is induced by both central IL-1β and low-dose glucocorticoids. While the principle mechanism for the regulation of the activity of Foxo transcription factors with regard to their catabolic activity is via Akt-dependent phosphorylation and nuclear exclusion (70), we saw no evidence for alterations in the IGF1/Akt signaling pathway in response to central inflammation. However, increased levels of Foxo1 have been extensively correlated with atrophy (81, 89, 122, 272). Furthermore, over expression of Foxo1 in muscle is sufficient to produce atrophy (87). Myostatin is another mediator of skeletal muscle catabolism that is induced by central inflammation in an HPA axis-dependent manner. Blockade of myostatin signaling attenuates the induction of MAFbx and MuRF1 in a variety of catabolic states (14, 113). KLF15 is another transcription factor that has recently been implicated in the regulation of skeletal muscle catabolism. KLF15 is directly induced by glucocorticoids, and transactivates both MAFbx and MuRF1 (81). The suppression of protein synthesis by glucocorticoids is also executed via several distinct mechanisms, all converging to inhibit mTOR signaling. REDD1 is directly transactivated by the glucocorticoid receptor, and inhibits mTOR activity via the tuberous sclerosis complex (273). Sestrin-1 is another negative regulator of mTOR signaling in response to

genotoxic stress via activation of the tuberous sclerosis complex and AMPK (274). An integral role for sestrin signaling in the catabolic process has not yet been described, however their role in metabolic signaling cascades make them likely targets of future studies. Protein synthesis via the mTOR complex is also regulated by the transcription factor KLF15 (81). The concerted upregulation of multiple inhibitors of mTOR signaling suggests that central inflammation elicits concerted decreases in protein synthesis and increases in protein breakdown to evoke atrophy.

We found a distinct set of genes that were regulated in skeletal muscle after IL-1β treatment and were not returned to baseline by adrenalectomy. While a causative role cannot be ascribed to any of these genes in central IL-1β-induced muscle catabolism, this pattern does demonstrate a glucocorticoid-independent effect of i.c.v. IL-1β on skeletal muscle. Recent work has shown that two discrete events are necessary for muscle catabolism in acute diabetes, where both a loss of skeletal muscle insulin signaling and pathophysiologic levels of glucocorticoids are required (95). Critical to the interpretation of these studies is the distinction between physiologic levels and pharmacologic dosing of glucocorticoids. It is well known that administration of the synthetic glucocorticoid dexamethasone, in doses far exceeding the physiologic range, is sufficient to induce muscle atrophy (59). However, when dexamethasone is given at a dose estimated to mimic endogenous activation of the HPA axis, no muscle atrophy is observed (95). In contrast, we demonstrated that administration of the endogenous glucocorticoid corticosterone, at a dose that mimics the inflammatory activation of the HPA axis, produces dramatic muscle atrophy. This discrepancy is likely due to the differences between dexamethasone and corticosterone including potency, metabolism and activity at the mineralocorticoid receptor. Regardless, the levels of circulating corticosterone we achieved in this study are well within the physiologic range, and comparable to those seen in a multitude of

diseases associated with muscle wasting (97, 115). Therefore, it is likely that glucocorticoids are necessary and sufficient to explain a significant portion of muscle catabolism in many forms of chronic disease. However, the incomplete blockade of atrophy gene induction by ADX during both central and systemic inflammation demonstrates that other mechanisms play critical roles in regulating catabolism in response to inflammation.

The finding that CNS inflammation elicits muscle atrophy illustrates a new anatomic target for cytokine-induced muscle catabolism. This study is the first to demonstrate that inflammatory cytokines cause muscle breakdown by acting within the brain. In addition to the direct effects of inflammatory cytokines on skeletal muscle, the action of cytokines in the CNS to influence skeletal muscle metabolism must now be considered. The upregulation of inflammatory cytokines in the CNS in disease models of cachexia is well documented, indicating that this pathway is generally activated in diseases associated with muscle wasting. Further studies will likely examine the general contribution of the CNS mediated muscle wasting in cachexia, and may discover new therapeutic targets for muscle wasting diseases.

Materials and Methods

Animals

Wild type C57BL/6J mice (20-25g) were obtained from Jackson Laboratories (Bar Harbor, ME). Sprague Dawley rats (250-350g) were purchased from Charles River Laboratories (Wilmington, MA). MC4RKO mice were as used as previously reported (275). MC4RKO mice were backcrossed at least 10 generations into the C57BL/6J strain. All animals were maintained on a normal 12:12 hr light/dark cycle and provided *ad libitum* access to water and food (Purina rodent diet 5001; Purina Mills, St. Louis, MO), except in the case of pair fed animals in which food intake was restricted to that consumed by the indicated group. Rats were sacrificed by decapitation under isoflurane anesthesia, and mice were sacrificed by decapitation under anesthesia from a ketamine cocktail. Experiments were conducted in accordance with the National Institutes of Health Guide for the Care and Use of Laboratory Animals, and approved by the Animal Care and Use Committee of Oregon Health & Science University.

Real Time PCR

Total muscle RNA was extracted using the RNeasy fibrous tissue mini kit (Qiagen, Valencia, CA) and hypothalamic RNA was extracted using an RNeasy mini kit according to the manufacturer's instructions. cDNA was transcribed using Taqman reverse transcription reagents and random hexamers according to the manufacturers instructions. PCR reactions were run on an ABI 7300, using Taqman universal PCR master mix, using Taqman gene expression assays: mouse GAPDH (Mm99999915_g1), mouse MAFbx (Mm00499518_m1), mouse MuRF1 (Mm01185221_m1), mouse Foxo1 (Mm00490672_m1), Mouse Lcn2 (Mm01324470_m1), Mouse Mt2 (Mm00809556_s1), Mouse Sesn1

(Mm01185732_m1), Mouse DEPP (Mm04206895_m1), Mouse UCP3 (Mm00494077_m1), Mouse Foxo3 (Mm01185722_m1), Mouse Selp (Mm00441295_m1), Mouse Nfkbia (Mm00477798_m1), Mouse Id3 (Mm00492575_m1), Mouse Ky (Mm00600373_m1), Mouse REDD1 (Mm00512504_g1), Mouse KLF15 (Mm00517792_m1), Rat GAPDH (Rn99999916_s1) Rat MAFbx (Rn00591730_m1, Rat MuRF1 (Rn00590197_m1), rat Foxo1 (Rn01494868_m1), Rat IL-1β (Rn00580432_m1), Rat KLF15 (Rn00585508_m1), Rat REDD1 (Rn01433735_g1), Rat Sesn1 (Rn01440906_m1), Rat Nfkbia (Rn01473657_g1), (Applied Biosystems, Carlsbad, CA). Relative expression was calculated using the delta-delta Ct method, and was normalized to vehicle treated control. Statistical analysis was performed on the normally distributed delta-Ct values. For analyses involving 2-variables, raw data and two-way ANOVA results can be found in supplemental table 1.

Microarray Analysis

Gene expression microarrays were performed in the Department of Oncology at the University of Alberta, Canada.

Synthesis of cRNA and cDNA, labeling and hybridization of arrays: Protocols and temperature cycling conditions for cDNA synthesis and *in vitro* transcription of cRNA, hydrolysis of cRNA (by RNase H) and fragmentation (by APE 1) as well as labeling of single stranded cDNA were as described by the manufacturer (Ambion/Applied Biosystems, Ontario, Canada) and the Ambion WT Expression Kit (Product Number 411974). The reaction mix contained 500 ng of total RNA. The reaction mix was spiked with Poly-A RNA (Product Number 900433) to monitor the amplification and labeling process independent of the quality of the initial total RNA used in the reactions. Reaction products at each of the synthesis steps were quantified using the

NanoDrop 1000 spectrophotometer. Samples were biotinylated using the WT Terminal Labeling Kit (Affymetrix, Product Number 900671) adhering to the experimental protocols described by the supplier. Samples were hybridized using the Affymetrix Gene Chip Hybridization Control Kit (Product Number 900454) and the GeneChip Hybridization, Wash and Stain Kit (Product Number, 900720). Arrays were scanned using the Affymetrix GeneChiP Scanner 3000 7G.

Gene expression arrays: The total RNA was quantified using a NanoDrop 1000 Spectrophotometer (NanoDrop Technologies, Wilmington, DE, USA) and its integrity evaluated using a Bioanalyzer 2100 (Agilent Technologies, Santa Clara , CA, USA) according to the manufacturer's protocols. RNA samples with RNA Integrity Numbers (RIN) greater than 5.0 were used in this study (average of 28 samples is 6.68; maximum value at 8.3 and minimum at 5.1). Mouse expression array (GeneChip Mouse Exon 1.0 ST Array, Affymetrix) were used to capture gene expression profiles in the sample sets. These arrays are designed to capture all exons, each with multiple probes per exon, and are amenable to analysis both for alternatively spliced transcripts (all exons individually) as well as gene-level expression from multiple probes from exons to yield a single expression level data point reflecting transcripts derived from a single gene. For the current analysis, we used gene-level expression analysis (core analysis) and deferred the exon/splice variant analysis for future data mining pending development of new analytical tools. The complete data set has been deposited in the GEO Omnibus database (GEO Series accession number GSE26766).

Data processing: The gene expression data were normalized and transformed using GeneSpring GX 11.5. Using a Core analysis, the data was summarized using RMA16, log transformed and baselined to the median in all samples. A one-way ANOVA was performed on the $\log_2$-normalized intensities. After correcting the p

values for multiple comparisons using the Benjamini-Hochberg correction at a false discovery rate of 1%, 494 probes were declared significantly expressed ($p<2.8X10^{-5}$). Only probes that showed 1.75 fold up-or down-regulation at any of the time-points were considered. Genes were organized into functional categories based on GeneRIFs (NCBI) and reported function in skeletal muscle.

Immunohistochemistry

Cryosections of gastocnemius/soleus complex were cut in cross section. For laminin staining, 20 µm sections were fixed for 15 minutes in 4% PFA, then blocked in PBS (10 mM NaPO4, 150 mM NaCl)/ 10% BSA for 1 hour at room temperature. Sections were then incubated overnight at room temperature with a rabbit anti-laminin antibody (Sigma, St. Louis, MO) diluted 1:50 in PBS/0.1% BSA, washed with PBS/0.025% triton-X-100, and incubated in a goat anti-rabbit Alexafluor-488 or 555 nm labeled secondary antibody (Invitrogen, Carlsbad, CA) diluted 1:500 in PBS/10% BSA. Sections were mounted with Vectashield fluorescent mounting media (Vector Labs, Burlingame, CA). For analysis of muscle fiber type, 9 µm unfixed cryosections were blocked for 1 hour in PBS/1% BSA/10% goat serum, and then incubated overnight in primary antibody diluted 1:250 in PBS/1% BSA/10% goat serum. The following primary antibodies were used: SC-71 for myosin IIa, BF-F3 for myosin IIb (Developmental Studies Hybridoma Bank, University of Iowa, Iowa City, Iowa), and anti Myosin I (Vector Labs, Burlingame, CA). Sections were washed in PBS/0.025% triton-X-100, and incubated with a goat anti-mouse Alexafluor-488 nm labeled secondary antibody (Invitrogen, Carlsbad, CA) diluted 1:500 in PBS/10% BSA. Sections were mounted with Vectashield fluorescent mounting media (Vector Labs, Burlingame, CA). Fiber area was measured in images that were acquired on a Leica DM4000 B microscope, using a Leica DFC340 FX camera at ambient temperature at

100X magnification using Leica Applications Suit 3.6 software (Leica, Buffalo Grove, IL). Images were segmented in ImageJ using a coherence enhanced diffusion filter. Images were pseudocolored using ImageJ. Images demonstrating fiber type distribution were obtained using a FW1000 confocal microscope, at 100X using Fluoview software (Olympus, Center Valley, PA).

Lewis Lung Carcinoma Tumor Implantation

C57BL/6J mice were injected with ($1X10^7$ cells per site) Tumors were allowed to grow for 21 days and animals were sacrificed. Tumor weight at sacrifice averaged 2.4 ±0.4g. Gastrocnemius muscle and hypothalamic blocks were stored in RNAlater (Ambion, Austin, Tx) according to the manufacturer's instructions.

Intracerebroventricular Injection

26-gauge lateral ventricle cannulas (mice) and 22 gauge lateral ventricle cannulas (rats) (PlasticsOne, Roanoke VA.) under isoflurane anesthesia, using a stereotactic alignment instrument (Kopf, Tujunga, CA) at the following coordinates relative to bregma: for mice, -1.0 mm X, -0.5 mm Y, and -2.25 mm Z; for rats, -1.5 mm X, -1.0 mm Y, and -4.0 mm Z. 10 ng mouse IL-1β (R&D, Minneapolis, MN) injections were given in 1 µL total volume. IL-1β was dissolved in artificial cerebrospinal fluid (aCSF, 150 mM NaCl, 3 mM KCl, 1.4 mM $CaCl_2$, 0.8mM $MgCl_2$, 1.0 mM $NaPO_4$) with 0.1% endotoxin free BSA. MTII (Phoenix Pharmaceuticals, Burlingame, CA), was dissolved in aCSF and administered at 1 nmol/5uL volume. Chronic injections were performed by administering MTII every 12 h for 36 h (4 injections total). Mifepristone (Sigma, St Louis, MO) (10 mg/kg) was dissolved in sesame oil, and administered 30 minutes prior to i.c.v. injection, and 4 h after i.c.v. injection.

Chronic lateral ventricle infusions were performed in Sprague Dawley rats using brain infusion kits (Brain Infusion Kit II) and osmotic minipumps (Model 2001), (Alzet, Cupertino, CA). Cannulas were implanted into the lateral ventricle under isoflurane anesthesia, using a stereotactic alignment instrument (Kopf, Tujunga, CA) at the following coordinates relative to bregma: -1.5 mm X, -1.0 mm Y, and -4.0 mm Z. Mini osmotic pumps delivering 10 ng rat IL-1β per hour (R&D, Minneapolis, MN) were connected via polyethylene catheters to the cannulas and implanted subcutaneously. Body composition analysis was performed 2 days prior to surgery, and again immediately before sacrifice using an EchoMRI 4-in-1 NMR system (EchoMRI, Houston, Tx).

Peripheral Infusions

Mini osmotic pumps (Model 1003D, Alzet, Cupertino, CA) delivering 10 ng rat IL-1β per hour were implanted into the peritoneal cavity of Sprague Dawley rats under isoflurane anesthesia. Body composition analysis was performed as per chronic i.c.v. infusion.

LPS treatment:

Mice were injected with 250 µg/kg LPS (Sigma, St Louis, MO) dissolved in normal saline/0.5% BSA, and sacrificed 8 h later. For studies examining hypothalamic gene expression, animals were perfused with DEPC treated PBS prior to the dissection of hypothalamic blocks, to remove circulating immune cells from the tissue.

Adrenalectomy

Adrenalectomized animals were purchased from Charles River Laboratories. Animals were implanted with 21-day sustained release corticosterone tablets (Innovative Research of America, Sarasota, FL) immediately after arrival.

Corticosterone Pellet Implantation

For corticosterone replacement in adrenalectomized animal, rats were implanted with 35 mg tablets and mice were implanted subcutaneously with 1.5 mg tablets, both of which are known to produce low physiologic levels of corticosterone (262, 276). Animals were maintained with 0.9% saline drinking water, and allowed to recover at least one week prior to cannula implantation. To achieve stressed levels of circulating corticosterone, Sprague Dawley rats were implanted with 100 mg or 2X 100mg corticosterone tablets which are known to produce circulating levels approximating those seen in stressed animals (262).

Western Blotting

Muscles were homogenized in RIPA buffer [50mM Tris pH 7.4, 150mM NaCl, 1mM EDTA, 1% Triton X, 0.25% Na Deoxycholate, 1mM NaF, and supplemented with Complete protease inhibitors and Phosphastop phosphatase inhibitor (Roche, Indianapolis, IN)] for 5 minutes using a Polytron homogenizer (Kinematica, Bohemia, NY). Samples were incubated on ice for 1 hr, and centrifuged at 13,000 RPM for 10 minutes at 4C. 50 ug of total protein per lane was run on NuPage Bis-Tris 4-12% gradient polyacrylamide gels (Invitrogen, Carlsbad, CA), and transferred to Immobilon-FL PVDF membranes (Millipore, Billerica, MA). Proteins were detected using the following antibodies, and quantitated using an Odyssey System (Li-Cor, Lincoln, NE): Rabbit anti phospho AKT Ser473 D9E, Mouse anti Pan AKT 40D4,

Rabbit anti phospho p38 Thr180/Tyr182 D3F9 (Cell Signaling, Danvers, MA), E7 Tubulin (Developmental Studies Hybridoma Bank, Iowa City, Iowa), IRDye 800CW goat anti-mouse IgG, IRDye 680LT Goat anti-Rabbit IgG (Li-Cor, Lincoln, NE).

Plasma ELISA and RIA

Interleukin-6 and IGF-1 were measured by ELISA (R&D, Minneapolis, MN) according to the manufacturer's instructions. Plasma corticosterone levels were measured by RIA (MP Biomedicals, Solon, OH) according to the manufacturer's instructions.

In Situ Hybridization

Rats were injected with LPS (250μg/kg) and sacrificed 8 h after injection. Coronal sections (20 μm) were cut on a cryostat and thaw-mounted onto Superfrost Plus slides (VWR Scientific, West Chester, PA). Hypothalamic sections were collected in a 1:6 series from the diagonal band of Broca (bregma 0.50 mm) caudally through the mammillary bodies (bregma - 5.00 mm). Antisense 33P-labeled rat IL-1β riboprobe (corresponding to bases 316-762 of rat IL-1b; GenBank accession no. NM_031512.2) (0.15 pmol/ml) was denatured, dissolved in hybridization buffer along with tRNA (1.7 mg/ ml), and applied to slides. Slides were covered with glass coverslips, placed in a humid chamber, and incubated overnight at 55 °C. The following day, slides were treated with RNase A and washed under conditions of increasing stringency. Slides were dipped in 100% ethanol, air dried, and then dipped in NTB-2 liquid emulsion (Eastman Kodak Co., Rochester, NY). Slides were developed 4 d later and coverslipped.

Statistical Analysis

Data are expressed as mean ±SEM. Statistical analysis was performed using Prism software (Version 4.0, Prism Software Corp., Irvine, CA). All data were analyzed with either an unpaired t test, one-way ANOVA followed by a post hoc analysis using a Bonferroni corrected t test, or a two-way ANOVA followed with post hoc analysis using a Bonferroni corrected t test. For the measurements of serum growth factors and hormones, some samples had undetectable levels of the analyte. For these analyses, normal distribution of the data cannot be assumed, and a Kruskal-Wallis test was utilized with a Dunn's multiple comparison post-test. For all analyses, significance was assigned at the level of $P<0.05$.

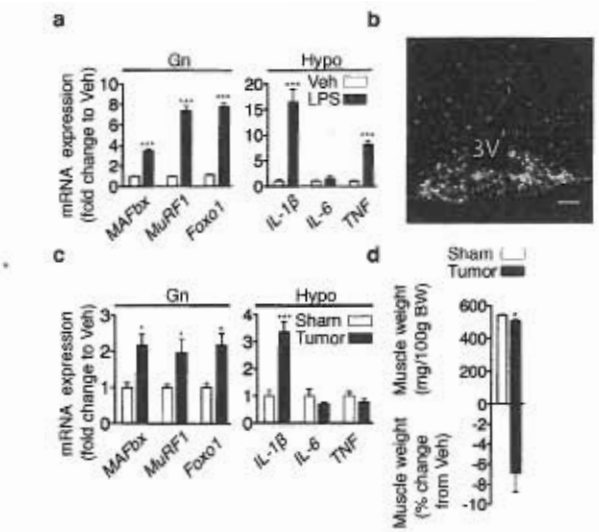

Figure 2. CNS inflammation and muscle catabolism occur simultaneously

(**a**) Atrophy gene expression in mouse gastrocnemius muscle (Gn) and cytokine expression in mouse hypothalamic blocks (Hypo) 8 h after i.p. LPS (250 μg/kg) or vehicle (Veh) were measured by real-time PCR (n=5-7/group for Gn and 5/group for Hypo). Values are relative to GAPDH for Gn and 18s RNA for Hypo. (**b**) In situ hybridization for IL-1β mRNA in the arcuate nucleus of the hypothalamus (-2.80 relative to bregma, 3V= 3rd ventricle) 8 h after LPS administration. Veh treated animals showed no specific signal at this exposure time. (**c**) Atrophy gene expression in Gn, and cytokine expression in hypothalamic blocks in mice bearing LLC tumors (or sham) were measured by real-time PCR (n=5-9/group). Values are relative to GAPDH for Gn and 18s RNA for Hypo. (**d**) Gastrocnemius muscle weight normalized to initial body weight (BW) and muscle weight change relative to vehicle in LLC tumor bearing animals (n=5-9/group). Scale bar =100 μm. Data represented as mean ± s.e.m. *=P<0.05, ***=P<0.001 as calculated by unpaired t-test. Reprinted with permission from Rockefeller University Press, Braun TP et al. *J Exp Med.* 2011;208(12):2449–2463.

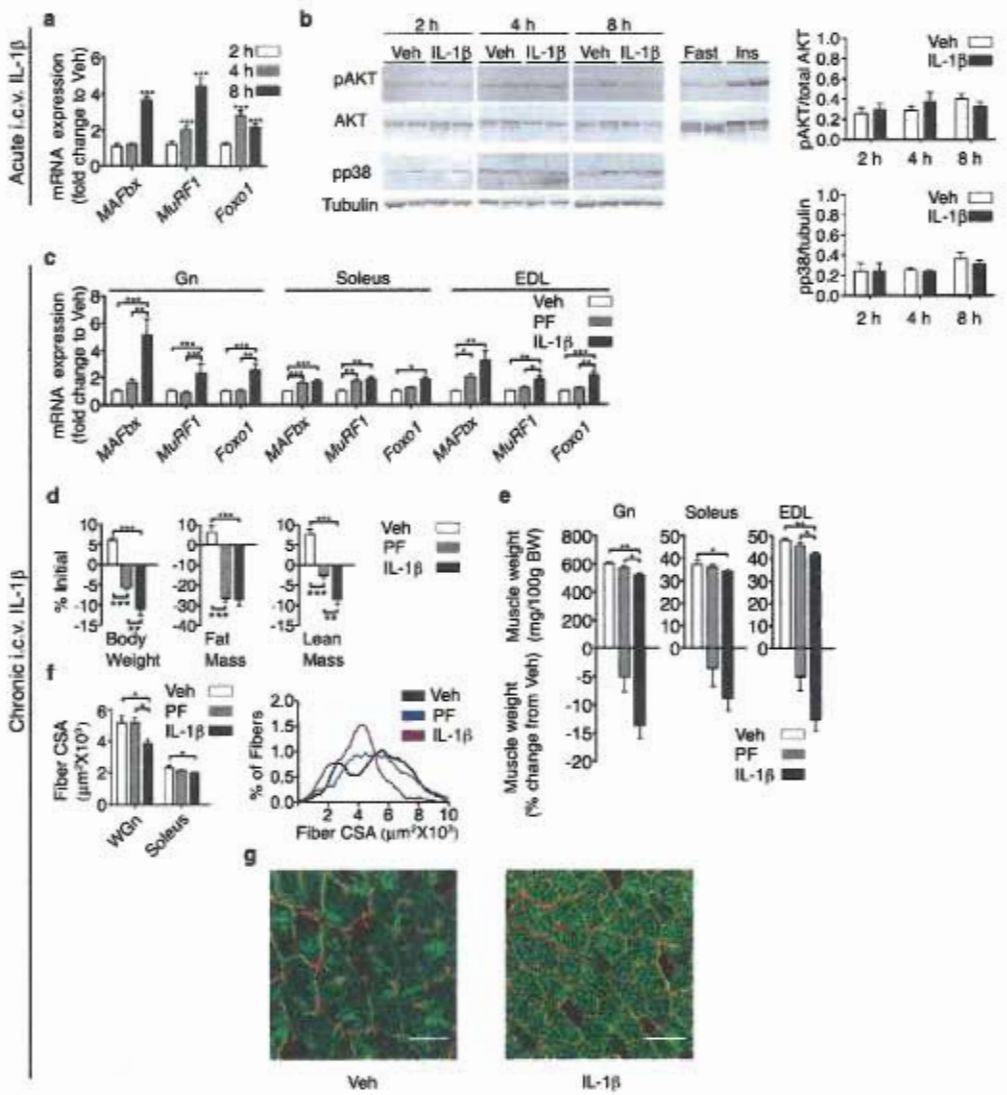

Figure 3. IL-1β signaling in the CNS produces muscle catabolism

(**a**) Atrophy gene expression in mouse gastrocnemius muscle (Gn) after acute intracerebroventricular (i.c.v.) IL-1β injection (10 ng, n=6-9/group) or vehicle (Veh). (**b**) Akt and p38 phosphorylation in Gn after acute i.c.v. IL-1β was measured by western blot (n=6-9/group). (**c-g**) Rats were i.c.v. infused for 3-days with IL-1β (10 ng/h) or Veh (n=8-11/group). A subset of Veh treated animals were pair fed (PF) to IL-1β treated animals. (**c**) Atrophy gene expression in rat muscle (Gn, Soleus, and extensor digitorum longus [EDL]) after 3-day i.c.v. IL-1β or Veh infusion was measured by real-time PCR. Reported values are relative to GAPDH. (**d**) Body composition after 3-day IL-1β infusion. (**e**) Muscle weight normalized to

initial body weight (BW) and weight change relative to vehicle. (**f**) Average fiber cross sectional area (CSA) in white Gn (WGn) and soleus and frequency distribution in Gn. (**g**) WGn immunostained for laminin (red) delineating fiber area, and Myosin IIb (green). Scale bar =100 μm. Data represented as mean ± s.e.m. *=P<0.05, **=P<0.01, ***=P<0.001 calculated by one-way (**c-f**) or two-way (**a, b**) ANOVA with Bonferroni corrected t-test. Reprinted with permission from Rockefeller University Press, Braun TP et al. *J Exp Med*. 2011;208(12):2449–2463.

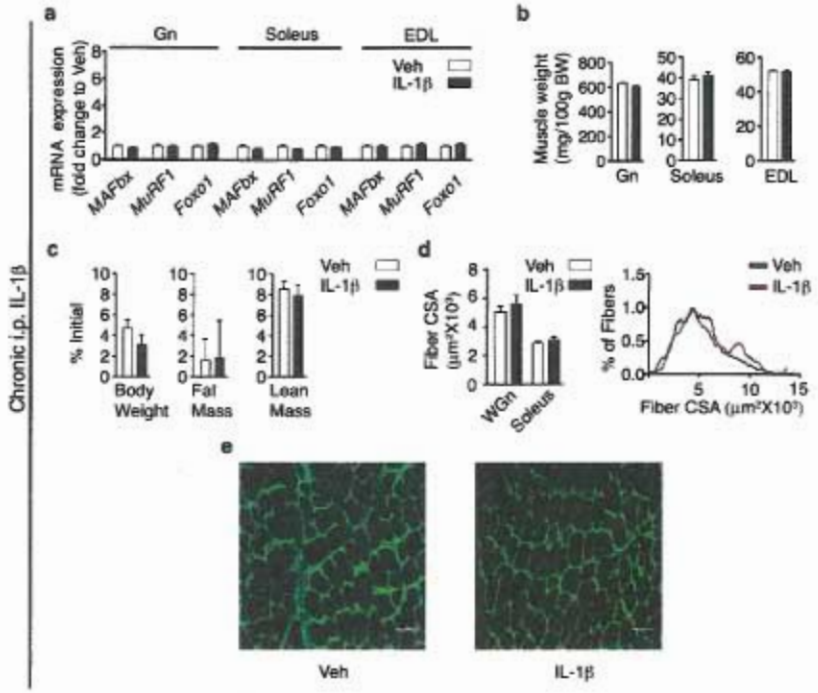

Figure 4. Peripheral infusion of low dose IL-1β does not cause atrophy

Rats were i.p. infused (10 ng/h, n=7-8/group) for 3 days with IL-1β or vehicle (Veh) solution. (**a**) Atrophy gene expression in rat muscle (Gastrocnemius [Gn], Soleus, and extensor digitorum longus [EDL]) after 3-day i.p. IL-1β infusion was measured by real time PCR. Reported values are relative to GAPDH. (**b**) Muscle weight normalized to initial body weight (BW). (**c**) Body composition after 3-day IL-1β infusion. (**d**) Average fiber cross sectional area (CSA) in white Gn (WGn) and soleus and frequency distribution in Gn. (**e**) WGn immunostained for laminin (green) delineating fiber area. Scale bar =100 μm. Data represented as mean ± s.e.m. Reprinted with permission from Rockefeller University Press, Braun TP et al. *J Exp Med.* 2011;208(12):2449–2463.

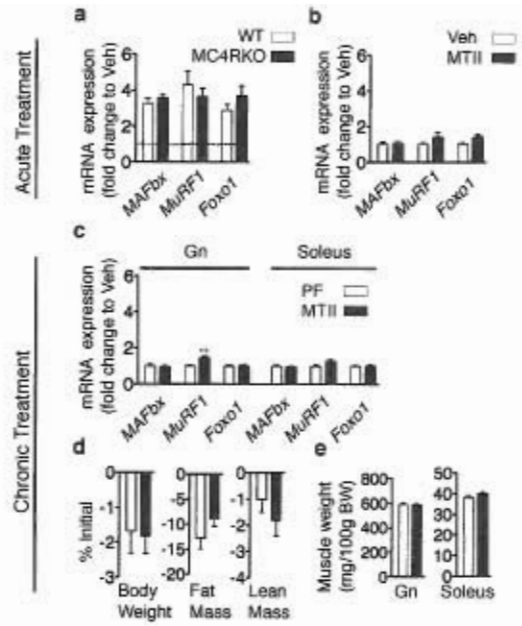

Figure 5. Signaling through the type 4 melanocortin receptor is not a major contributor to the muscle catabolism independent of food intake

(**a**) Atrophy gene expression in WT and MC4RKO mouse gastrocnemius (Gn) 8 h after acute intracerebroventricular (i.c.v.) IL-1β injection (10 ng, n=8-9/group)) and in (**b**) rat Gn 6 h after acute i.c.v. melanotan II (MTII, 1 nmol, n=6-9/group) or vehicle (Veh) injection was measured by real-time PCR. (**c-e**) Rats were treated for 36 h (chronic) with MTII or Veh (1 nmol/12 hX4, n=7-8/group). Veh treated animals were pair fed (PF) to the MTII treatment group. (**c**) Gene expression in rat Gn and soleus after chronic MTII treatment was measured by real-time PCR. Reported values are relative to GAPDH. (**d**) Body composition after chronic MTII treatment. (**e**) Muscle weight normalized to initial body weight (BW). Dotted line in (**a**) represents Veh treated controls at a relative quantity of 1. Data represented as mean ± s.e.m. **=P<0.01, as calculated by unpaired t-test. (**a**) Analyzed by two-way ANOVA with Bonferroni corrected t-test and no significant effect of genotype was found. (**b, d, e**) Analyzed by unpaired t-test, with no comparisons reaching p<0.05. Reprinted with permission from Rockefeller University Press, Braun TP et al. *J Exp Med*. 2011;208(12):2449–2463.

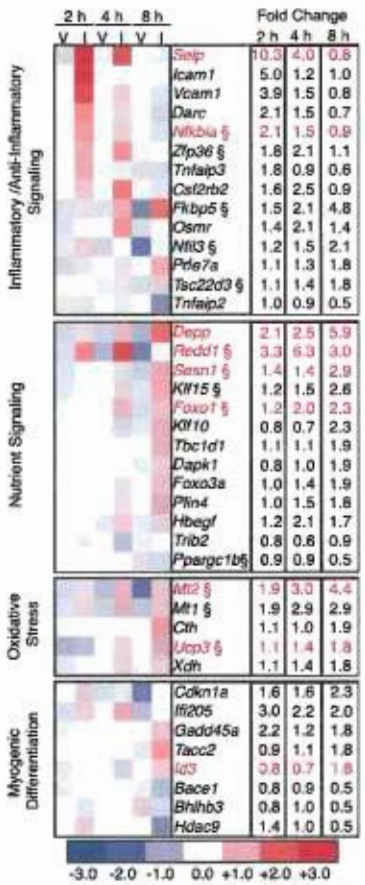

Figure 6. Central IL-1β treatment induces rapid and dynamic changes in skeletal muscle gene expression

Wild type mice received lateral ventricle injections of IL-1β (I) or vehicle (V). Food was removed from the cages at the time of injection, and animals were sacrificed at 2, 4 and 8 h after the injection (n=3-5/group). Skeletal muscle RNA was hybridized to Affymetrix Exon 1.0 ST arrays. Data was analyzed for a false discovery rate of 0.01. Genes that were greater than 1.75-fold up-or down-regulated at any time point were categorized based on their annotated and published functions. Heat map values are $\log_2$ normalized array intensities. Genes with differential expression confirmed by real-time PCR are indicated in red. § Indicates genes that are annotated as glucocorticoid responsive, or are regulated in muscle by glucocorticoids in published array data sets. Reprinted with permission from Rockefeller University Press, Braun TP et al. *J Exp Med.* 2011;208(12):2449–2463.

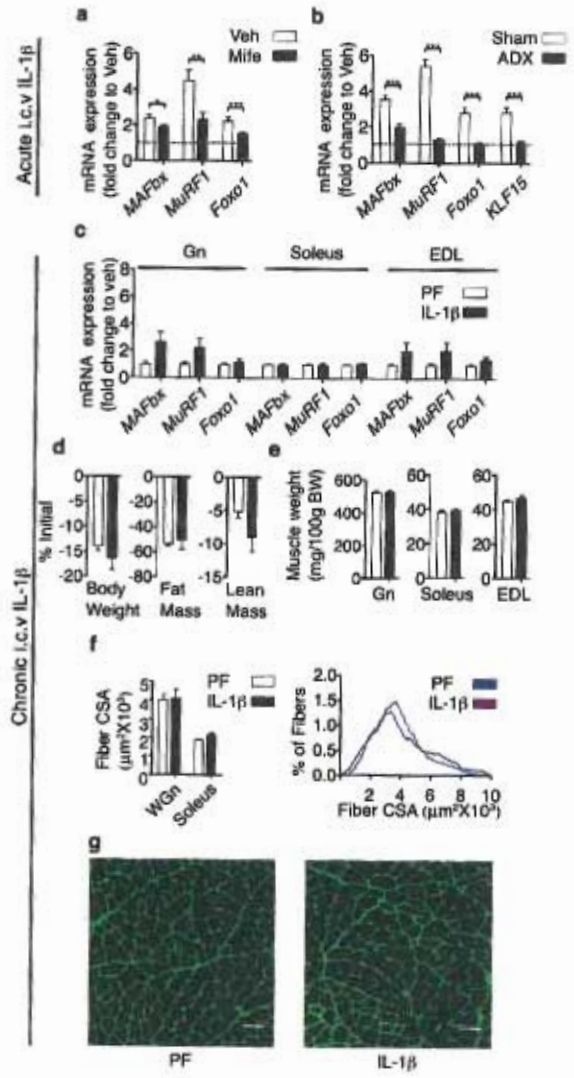

Figure 7. HPA axis activation is necessary for i.c.v. IL-1β-induced muscle catabolism

(**a**) Muscle atrophy gene expression in mifepristone (Mife) or vehicle (Veh) treated (n=6-8/group) and (**b**) ADX or sham (n=7-8/group) mouse gastrocnemius (Gn) 8 h after acute intracerebroventricular (i.c.v.) IL-1β injection (10 ng) was measured by real-time PCR. (**c-g**) ADX rats were treated for 3 days with chronic i.c.v. IL-1β or Veh (10 ng/h, n=8-9/group). Veh treated animals were pair fed (PF) to the IL-1β treated group. (**c**) Atrophy gene expression in ADX rat muscle after 3-day chronic i.c.v. IL-1β infusion was measured by real-time PCR. Reported values are relative to GAPDH. (**d**) Body composition. (**e**) Muscle weight normalized

to initial body weight (BW). (**f**) Average fiber cross sectional area (CSA) in white gastrocnemius (WGn) and soleus, and frequency distribution in WGn. (**g**) WGn immunostained for laminin (green) delineating fiber area. Dotted line in (**a**, **b**) represents Veh treated controls at a relative quantity of 1. Scale bar =100 μm. Data represented as mean ± s.e.m. *=p<0.05, **=p<0.01, ***=p<0.001 by (**a**, **b**) two-way ANOVA with Bonferroni corrected t-test (raw data in Supplementary Table 1). (**d-g**) analyzed by unpaired t-test, with no comparisons reaching p<0.05. Reprinted with permission from Rockefeller University Press, Braun TP et al. *J Exp Med.* 2011;208(12):2449–2463.

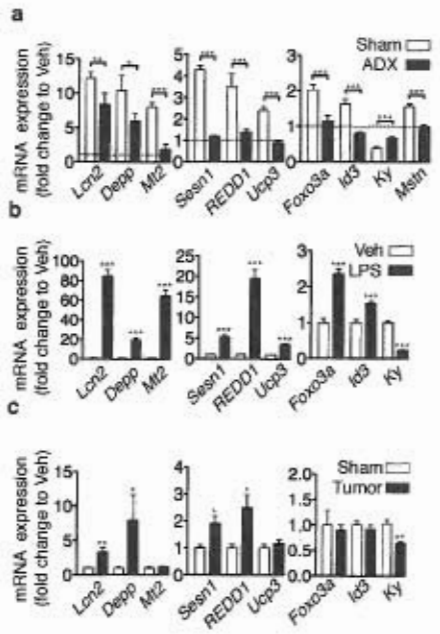

Figure 8. Glucocorticoid-driven gene expression signatures are present in skeletal muscle during central and peripheral inflammation

(**a**) Gene expression in ADX mouse gastrocnemius muscle (Gn) 8 h after acute intracerebroventricular (i.c.v.) IL-1β injection (10 ng) or vehicle (Veh) was measured by real-time PCR (n=6-8/group). (**b**) Muscle gene expression in mouse Gn 8 h after i.p. LPS (250 μg/kg) or Veh was measured by real-time PCR (n=5-7/group). (**c**) Gene expression in Gn in mice bearing LLC tumors (or sham) was measured by real-time PCR (n=5-9/group). Reported values are relative to GAPDH. Data represented as mean ± s.e.m. Dotted line in (**a**) represents Veh treated controls at a relative quantity of 1. *=p<0.05, **=p<0.01, ***=p<0.001 by (**b**, **c**) unpaired t-test or (**a**) two-way ANOVA with Bonferroni corrected t-test (raw data in Table 3). Reprinted with permission from Rockefeller University Press, Braun TP et al. *J Exp Med.* 2011;208(12):2449–2463.

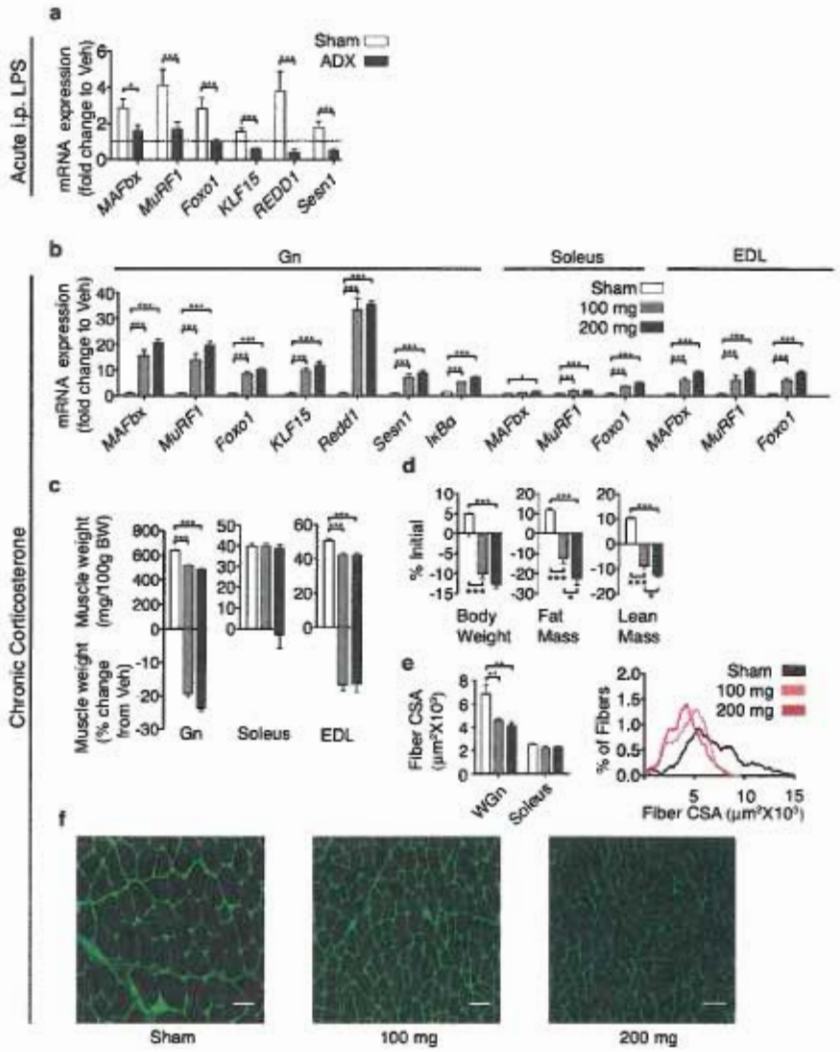

Figure 9. Glucocorticoid signaling contributes to atrophy due to systemic inflammation

(**a**) Gene expression in ADX mouse gastrocnemius muscle (Gn) 8 h after i.p. LPS (250 μg/kg) or vehicle (Veh) was measured by real-time PCR (n-6-8/group). (**b-f**) Rats were treated for 3 days with corticosterone (100 or 200 mg) (n=6-7/group). (**b**) Gene expression in rat muscle (Gn, soleus and extensor digitorum longus [EDL]). Reported values are relative to GAPDH. (**c**) Muscle weight normalized to initial body weight (BW) and weight change relative to vehicle. (**d**) Body composition after 3-day corticosterone treatment. (**e**) Average fiber cross sectional area (CSA) in white Gn (WGn) and soleus and frequency distribution in Gn. (**f**) WGn immunostained for laminin (green) delineating fiber area. Dotted line in (**a**) represents Veh

treated controls at a relative quantity of 1. Scale bar =100 μm. Data represented as mean ± s.e.m. *=P<0.05, **=P<0.01, ***=P<0.001 calculated by one-way (**b-f**) or two-way (**a**) ANOVA with Bonferroni corrected t-test (raw data in Table 3). Reprinted with permission from Rockefeller University Press, Braun TP et al. *J Exp Med.* 2011;208(12):2449–2463.

Table 1

Treatment	IL-6 (pg/mL)	IL-1β (pg/mL)	IGF-1 (ng/mL)	Corticosterone (ng/mL)
2-hr Vehicle	13 ± 3	22 ± 6	225 ± 11	104 ± 16
2-hr 10 ng IL-1β	298 ± 35 ***	25 ± 6	216 ± 18	397 ± 30 ***
4-hr Vehicle	21 ± 6	16 ± 3	200 ± 8	103 ± 14
4-hr 10 ng IL-1β	69 ± 14	28 ± 6	168 ± 9	258 ± 35 ***
8-hr Vehicle	13 ± 6	46 ± 15	173 ± 4	115 ± 34
8-hr 10 ng IL-1β	8 ± 2	32 ± 5	205 ± 6	72 ± 10

Table 1. Circulating cytokines, growth factors and hormones in acute IL-1β treated mice

Wild type mice received i.c.v. injections of IL-1β. Animals were sacrificed at 2, 4 and 8 h after the injection (n=6-9/group). Plasma IL-6, IL-1β and IGF-1 levels were measured by ELISA and Corticosterone was measured by RIA. (***=P<0.001 vs corresponding vehicle injected control as calculated by 2-way ANOVA with Bonferroni post-test). Reprinted with permission from Rockefeller University Press, Braun TP et al. *J Exp Med.* 2011;208(12):2449–2463.

Table 2

Treatment	IL-6 (pg/mL)	IGF-1 (ng/mL)	Corticosterone (ng/mL)
Ad Lib	106 ± 44	1075 ± 63	48 ± 29
Pair Fed	Undetectable (LOD= 62.5)	851 ± 41 *	70 ± 27
IL-1β	102 ± 26	1013 ± 46	183 ± 40 *

Table 2. Circulating cytokines, growth factors and hormones in 3 day IL-1β treated rats

Rats were infused for 3 days with IL-1β into the lateral ventricle using an osmotic minipump. Control animals were infused over the same time period with a vehicle solution and were fed *ad lib*, or pair fed with IL-1β treated animals (n=8-11/group). Plasma IL-6 and IGF-1 were measured by ELISA, corticosterone was measured by RIA. Data represented as mean ± SEM. (*=P<0.05 vs *ad lib* control as calculated by one-way ANOVA and Bonferroni post-test or Kruskal-Wallis test and Dunn's multiple comparison post-test where appropriate). Reprinted with permission from Rockefeller University Press, Braun TP et al. *J Exp Med.* 2011;208(12):2449–2463.

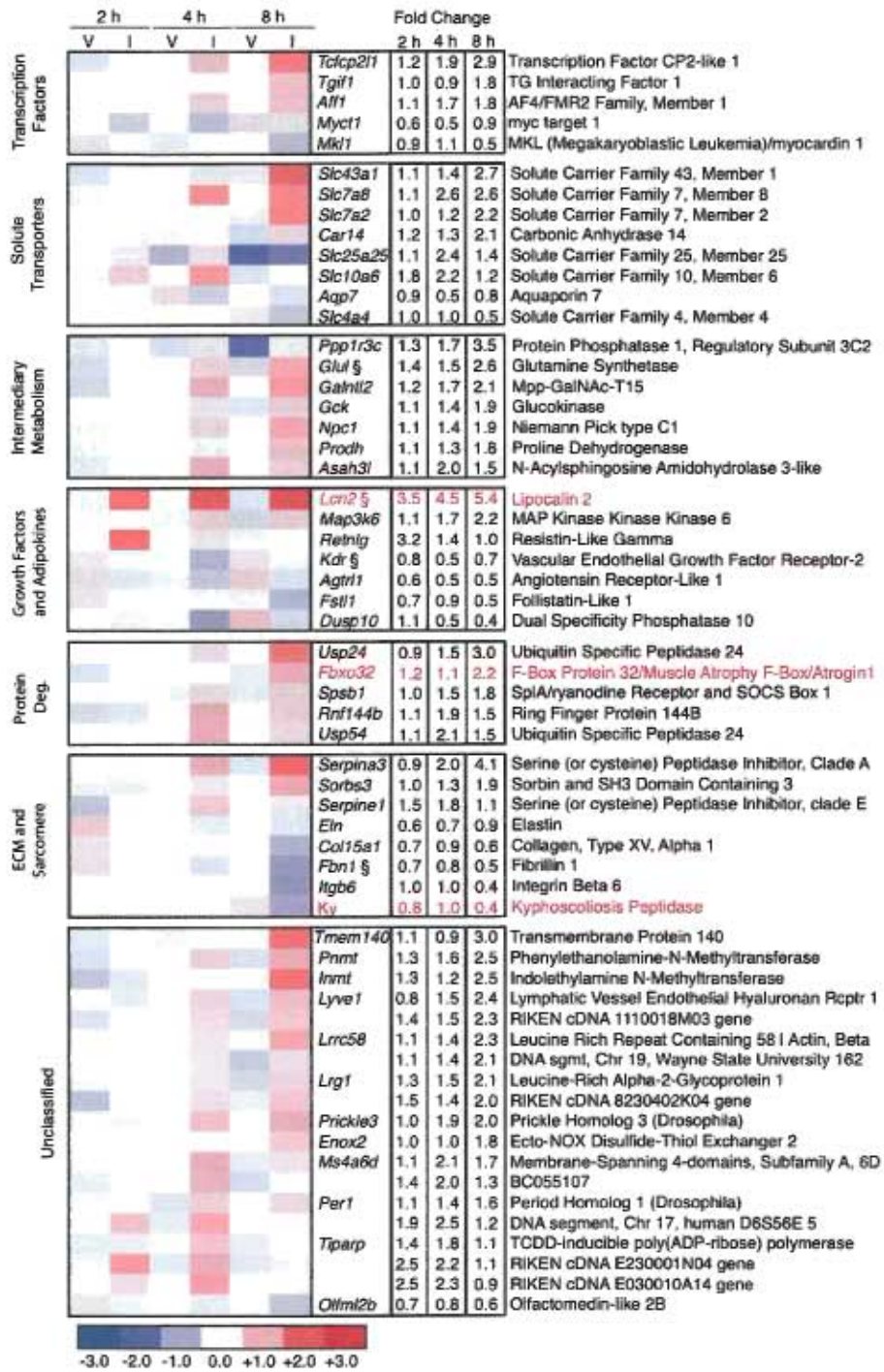

Figure 10. Central IL-1β treatment induces rapid and dynamic changes in muscle gene expression.

Wild type mice received i.c.v. injections of IL-1β. Food was removed from the cages at the time of injection, and animals were sacrificed at 2, 4 and 8 h after the injection (n=3-5/group).

Gn RNA was hybridized to Affymetrix Exon 1.0 ST arrays. Data was analyzed by analysis of variance with a Benjamini Hochberg correction for a false discovery rate of 0.01. Genes found to have significant differential expression that were greater than 1.75-fold up or down regulated at any time point were categorized based on their annotated and published functions. Genes with differential expression confirmed by real-time PCR are indicated in red. § Indicates glucocorticoid responsive gene. Heat map values are $\log_2$ normalized array intensities. V=vehicle, I=IL-1β. Reprinted with permission from Rockefeller University Press, Braun TP et al. *J Exp Med.* 2011;208(12):2449–2463.

Table 3

dCT values relative to GAPDH					IL-1β/LPS		ADX/MIFE		Interaction	
Gene	**Sham/ Veh**	**Sham/ IL-1β**	**ADX/ Veh**	**ADX/ IL-1β**	**% Total Variation**	**p Value**	**% Total Variation**	**p Value**	**% Total Variation**	**p Value**
MAFbx	6.971± 0.134 (8)	5.135± 0.094 (8)	7.132± 0.176 (7)	6.164± 0.167 (7)	62.79	<0.0001	11.3	0.0003	6.02	0.0054
MuRF1	6.308± 0.078 (8)	3.895± 0.107 (8)	6.337± 0.163 (7)	5.972± 0.147 (7)	41.1	<0.0001	23.63	<0.0001	22.35	<0.0001
FOXO1	11.723± 0.144 (8)	10.259± 0.176 (8)	11.969± 0.099 (7)	11.991± 0.106 (7)	34.4	<0.0001	34.75	<0.0001	18.92	<0.0001
Lcn2	13.526± 0.130 (8)	9.908± 0.111 (8)	13.693± 0.192 (6)	10.764± 0.314 (7)	86.94	<0.0001	2.31	0.0152	0.97	0.0911
Mt2	13.934± 0.168 (8)	10.909± 0.139 (8)	14.652± 0.263 (6)	13.978± 0.354 (7)	33.45	<0.0001	35.09	<0.0001	13.51	<0.0001
Sesn1	10.677± 0.065 (8)	8.577± 0.072 (8)	10.995± 0.125 (6)	10.626± 0.060 (7)	35.72	<0.0001	32.70	<0.0001	21.36	<0.0001
Depp	10.323± 0.190 (8)	7.039± 0.267 (8)	10.784± 0.371 (6)	8.111± 0.243 (7)	77.35	<0.0001	5.12	0.0080	0.82	0.2605
Foxo3a	11.429± 0.101 (8)	10.411± 0.104 (8)	11.829± 0.122 (6)	11.674± 0.196 (7)	19.91	0.0002	40.03	<0.0001	10.75	0.0037
Ky	6.874± 0.131 (8)	8.299± 0.170 (7)	7.061± 0.088 (7)	7.635± 0.085 (7)	61.20	<0.0001	3.38	0.0720	10.96	0.0024
Id3	9.108± 0.121 (8)	8.397± 0.0131(7)	9.289± 0.170 (6)	9.565± 0.073 (7)	4.20	0.0965	40.34	<0.0001	21.62	0.0006
Ucp3	5.939± 0.090 (8)	4.673± 0.110 (7)	5.915± 0.173 (6)	6.162± 0.192 (7)	13.85	0.0016	28.61	<0.0001	30.49	<0.0001
Ddit4	8.882± 0.265 (8)	7.022± 0.225 (7)	10.140±0 .437 (6)	9.391± 0.155 (7)	24.46	<0.0001	47.30	<0.0001	4.43	0.0567
Mstn	8.362± 0.055 (8)	7.725±0. 078 (8)	8.691±0. 142 (7)	8.847±(0. 125 (7)	5.43	0.0291	50.91	<0.0001	15.82	0.0005
KLF15	9.469± 0.075 (8)	7.961± 0.083 (7)	10.041± 0.131 (6)	9.795± 0.071 (7)	28.29	<0.0001	51.72	<0.0001	15.26	<0.0001
	Veh/ Veh	**Veh/ IL-1β**	**Mife/ Veh**	**Mife/ IL-1β**						
MAFbx	5.415± 0.290 (5)	4.100± 0.141 (7)	5.598± 0.144 (6)	4.651± 0.080 (8)	63.58	<0.0001	6.69	0.0304	1.68	0.2590
MuRF1	6.021± 0.269 (5)	3.835± 0.192 (7)	6.190± 0.250 (6)	4.998± 0.229 (8)	59.21	<0.0001	9.21	0.0102	5.12	0.0479
FOXO1	10.119± 0.119 (5)	8.972± 0.138 (7)	10.585± 0.064 (6)	9.878± 0.065 (8)	51.83	<0.0001	28.43	<0.0001	2.92	0.0422
	Sham/ Veh	**Sham/ LPS**	**ADX/ Veh**	**ADX/ LPS**						
MAFbx	7.061± 0.218 (7)	5.588± 0.273 (7)	7.277± 0.240 (7)	6.700± 0.361 (8)	28.44	0.0015	11.92	0.0292	5.43	0.1309
MuRF1	6.824± 0.186 (7)	7.355± 0.157 (7)	4.960± 0.375 (7)	6.831± 0.351 (8)	26.71	0.0004	26.99	0.0004	8.41	0.0296
FOXO1	10.464± 0.164 (7)	9.135± 0.378 (7)	10.825± 0.173 (7)	10.891± 0.221 (8)	11.31	0.0175	31.81	0.0002	13.81	0.0094
KLF15	8.802± 0.157 (7)	7.740± 0.189 (7)	9.373± 0.073 (7)	9.721± 0.175 (8)	4.40	0.0323	56.34	<0.0001	17.21	0.0001
REDD1	10.587± 0.393 (7)	8.235± 0.406 (7)	11.639± 0.164 (7)	12.613± 0.353 (8)	3.46	0.0570	53.77	<0.0001	20.17	<0.0001
Sesn1	11.725± 0.172 (7)	10.559± 0.311 (7)	12.378± 0.087 (7)	12.881± 0.130 (8)	2.76	0.0947	55.82	<0.0001	17.55	0.0002

Table 3. Raw data from two-way ANOVA analysis of gene expression

All statistical analysis of differential gene expression was performed on dCT values relative to the GAPDH endogenous control, as RQ values have non-normal distribution. Two-way ANOVA analysis derived p values and % variation are indicated here. Reprinted with permission from Rockefeller University Press, Braun TP et al. *J Exp Med*. 2011;208(12):2449–2463.

Table 4

Gene Symbol	Refseq	p
Slc7a8	NM_016972	1.14E-12
Foxo1	NM_019739	2.59E-12
Aff1	NM_001080798|NM_133919	1.15E-11
Tcfcp2l1	NM_023755	2.12E-11
Usp54	NM_030180	4.04E-11
Slc39a14	NM_144808	4.19E-11
Slc7a2	NM_007514|NM_001044740	6.50E-11
Ppp1r3c	NM_016854	8.32E-11
Lrrc58|Actb	NM_177093	1.43E-10
Itgb6	NM_021359	1.45E-10
Slc43a1	NM_001081349|NM_001083809|NM_024497	1.74E-10
Cdkn1a	NM_007669|NM_001111099	2.67E-10
Galntl2	NM_030166	2.85E-10
Npc1	NM_008720	3.67E-10
Asah3l	NM_139306	3.77E-10
Rnf144b	NM_146042	6.27E-10
Csf2rb2	NM_007781	6.74E-10
Nfil3|LOC100046232	NM_017373	7.64E-10
Pde7a	NM_001122759|NM_008802	8.08E-10
Slc25a25	NM_146118	8.97E-10
6430548M08Rik|Usp24		1.04E-09
Fkbp5	NM_010220	1.73E-09
Prickle3	NM_175097	2.04E-09
Ppargc1b	NM_133249	2.20E-09
Dusp10	NM_022019	5.13E-09
Ucp3	NM_009464	7.54E-09
8430408G22Rik-DEPP		8.39E-09
Cth|EG621697	NM_145953|NM_001101561	8.49E-09
Klf10	NM_013692	1.69E-08
Lcn2	NM_008491	1.70E-08
Prodh	NM_011172	1.76E-08
Slc10a6	NM_029415	1.81E-08
Ky	NM_024291	1.92E-08
Tnfaip2	NM_009396	2.72E-08
D19Wsu162e		2.73E-08
Foxo3a	NM_019740	2.94E-08
Map3k6	NM_016693	2.96E-08
Tacc2	NM_001004468|NM_206856|NM_021314	3.79E-08
Trib2	NM_144551	4.18E-08
Kdr	NM_010612	5.27E-08
Sorbs3	NM_011366	7.29E-08
Bace1	NM_011792	7.69E-08
Tnfaip3	NM_009397	9.96E-08
1110018M03Rik	NM_026271	1.05E-07
S3-12	NM_020568	1.18E-07
Ddit4	NM_029083	1.42E-07
Xdh	NM_011723	1.45E-07
Klf15	NM_023184	1.53E-07
Id3	NM_008321	1.61E-07

Mt2	NM_008630	1.95E-07
Mt1	NM_013602	2.10E-07
Tiparp	NM_178892	2.28E-07
Agtrl1	NM_011784	2.51E-07
Myct1	NM_026793	2.92E-07
Serpine1	NM_008871	3.02E-07
Tmem140	NM_197986	3.54E-07
E030010A14Rik	NM_183160	4.03E-07
Osmr	NM_011019	4.49E-07
Mkl1	NM_001082536INM_153049	5.13E-07
Pnmt	NM_008890	5.24E-07
Sesn1	NM_001013370	5.82E-07
BC055107	NM_183187	6.30E-07
Zfp36	NM_011756	6.92E-07
Inmt	NM_009349	8.82E-07
Hbegf	NM_010415	9.20E-07
Ifi205	NM_172648	9.53E-07
Icam1	NM_010493	9.60E-07
E230001N04Rik		1.05E-06
Selp	NM_011347	1.29E-06
Nfkbia	NM_010907	1.73E-06
Fbxo32	NM_026346	1.92E-06
Serpina3n	NM_009252	2.20E-06
Dapk1	NM_029653INM_134062	2.30E-06
Tgif1	NM_009372	2.32E-06
8230402K04Rik	NM_177755	2.74E-06
Enox2	NM_145951	2.95E-06
Hdac9	NM_024124	3.99E-06
Glul	NM_008131	4.17E-06
Tsc22d3	NM_001077364INM_010286	4.86E-06
Ms4a6d	NM_026835	5.50E-06
Lrg1	NM_029796	5.75E-06
Slc4a4	NM_018760	5.80E-06
Bhlhb3	NM_024469	6.39E-06
Darc	NM_010045	7.41E-06
Car14	NM_011797	8.09E-06
Tbc1d1	NM_019636	8.21E-06
Vcam1	NM_011693	8.61E-06
Lyve1	NM_053247	8.72E-06
Per1	NM_011065	8.80E-06
Fstl1	NM_008047	9.69E-06
Olfml2b	NM_177068	1.03E-05
Retnlg	NM_181596	1.15E-05
Aqp7	NM_007473	1.18E-05
Fbn1	NM_007993	1.24E-05
Gadd45a	NM_007836	1.25E-05
Col15a1	NM_009928	1.27E-05
Spsb1	NM_029035	1.37E-05
Gck	NM_010292	1.46E-05
Eln	NM_007925	2.53E-05

Table 4. Significantly regulated genes from microarray analysis

Wild type mice received i.c.v. injections of IL-1β. Animals were sacrificed at 2, 4 and 8 h after the injection (n=3-5/group). Skeletal muscle RNA was hybridized to Affymetrix Exon 1.0 ST arrays. Data were analyzed by analysis of variance with a Benjamini Hochberg correction for a false discovery rate of 1% ($P<2.8X10^{-5}$). Genes found to have significant differential expression that were greater than 1.75-fold up or down regulated at any time point were considered. Reprinted with permission from Rockefeller University Press, Braun TP et al. *J Exp Med.* 2011;208(12):2449–2463.

CHAPTER 3

Manuscript #2

Glucocorticoid but not MyD88 Signaling in Skeletal Muscle is Required for Atrophy in Response to Systemic Inflammation

Theodore P. Braun[1,2], Peter R. Levasseur[1], Aaron J. Grossberg[1,2], Marek Szumowski[1], Anthony P. Barnes[1] and Daniel L. Marks[1]

Papé Family Pediatric Research Institute[1], MD/PhD Program[2], Oregon Health & Science University, Portland, Oregon, 97239, USA.

Chapter 3 is a manuscript in preparation for submission to *The Journal of Experimental Medicine* as a Brief Definitive Report.

Introduction

Muscle atrophy in response to systemic inflammation is a common co-morbidity of multiple diseases. While the mobilization of skeletal muscle protein is likely beneficial to the immune response in acute infection, the loss of muscle mass that occurs in sustained inflammation has a negative effect on disease survival. Patients suffering from cancer, heart failure, renal failure, and sepsis all experience increased mortality when muscle atrophy is present (10, 277, 278), yet treatment options for this co-morbidity are limited.

Inflammatory cytokines are critical mediators of muscle atrophy. When administered to experimental animals, inflammatory cytokines produce a rapid loss of skeletal muscle. The activation of the ubiquitin-proteasome system is critical to this process. The muscle specific E3 ubiquitin ligases muscle atrophy F box (MAFbx/atrogin-1) and muscle ring finger protein 1 (MuRF1), are highly induced in catabolic muscle and are critical for normal muscle atrophy in response to a variety of stimuli (58, 59). These two genes are under the transcriptional regulation of the forkhead box (Foxo) family of transcription factors (70). Multiple *in vitro* studies have demonstrated that the direct action of inflammatory cytokines is sufficient to produce the cardinal molecular signs of muscle atrophy, and induce myofibrillar protein loss. This process is dependent on both activation of nuclear factor kappa B (NFκB) and p38 mitogen activated protein kinase (p38 MAPK) (104-106).

However, the picture *in vivo* is more complicated. NFκB and upstream signaling proteins such as tumor necrosis factor receptor associated factor 6 (TRAF6) are clearly requisite for atrophy in response to systemic inflammation (104, 267). Despite this, there is ample evidence that cytokines mediate muscle atrophy by acting at alternate sites. Inflammation in the central nervous system alone is sufficient to induce muscle atrophy (279), an effect dependent on increases in circulating

glucocorticoids. Inflammatory conditions including cancer, metabolic acidosis, angiotensin treatment, endotoxemia, cytokine infusion and sepsis, all result in increased levels of glucocorticoids (52, 76, 93, 96, 115, 222, 231). Many of these conditions show an attenuation of the atrophy response when glucocorticoid signaling is blocked (76, 93, 96). When glucocorticoid levels are increased to levels similar to those occurring in the aforementioned inflammatory conditions, significant muscle atrophy is observed (279).

Direct cytokine action and glucocorticoid signaling may represent independent and additive or synergistic components of the atrophy process. This possibility is somewhat contradictory given the fundamentally opposed nature of inflammatory and glucocorticoid (anti-inflammatory) signaling. Alternately, one of these mechanisms may be the dominant mediator in inflammation-induced muscle atrophy *in vivo*. To explore these possibilities, we generated mice with targeted loss of function of the glucocorticoid receptor (GR) or the inflammatory adaptor protein myeloid differentiation factor 88 (MyD88) in skeletal muscle, and subjected them to a systemic inflammatory challenge known to evoke muscle atrophy.

Results

Generation of muscle specific GR and MyD88KO mice.

To examine the isolated impact of glucocorticoid signaling in skeletal muscle, we generated muscle specific glucocorticoid receptor knockout mice (mGRKO) by crossing mice expressing Cre recombinase under the muscle creatine kinase (MCK-Cre) promoter with $GR^{Lox/Lox}$ mice. The resultant mice have been independently generated and are resistant to atrophy in response to acute diabetes and starvation (95). To functionally examine whether the glucocorticoid receptor had been deleted from skeletal muscle, mGRKO mice were treated for 3 days with dexamethasone (5

mg/kg). Dexamethasone-induced muscle atrophy was markedly attenuated in mGRKO mice which exhibited a 61% sparing of muscle mass (Figure 11 c, d). Furthermore, dexamethasone treatment failed to induce MAFbx, MuRF1 and Foxo1 gene expression in mGRKO mice (Figure 11 e). However, other responses to glucocorticoid treatment such as increased adiposity and increases in food intake were intact in mGRKO mice (Figure 11 a, b). These results collectively demonstrate specific deletion of GR in muscle. MyD88 is an essential signaling protein downstream of both toll-like receptors (toll like receptors) and the type 1 IL-1 receptor (IL-1R1). Both IL-1β and LPS (via TLR4) have been shown to myocyte atrophy *in vitro*. To explore the role of the direct action of inflammatory mediators in muscle atrophy we generated muscle-specific MyD88KO mice (mMyD88KO).

GR but not MyD88 Signaling Is Required for the Acute Induction of Catabolic Genes in Response to LPS

Circulating levels glucocorticoids and IL-1β are both increased in response to systemic inflammation (280). We therefore examined the ability of LPS to induce atrophy genes in the skeletal muscle of mGRKO and mMyD88KO mice. As LPS decreases food intake, and starvation alone can result in atrophy, mice were treated with LPS (250 μg/kg) during the light cycle (when feeding does not normally occur) and food was removed from cages at the time of injection. After 8 hours, LPS significantly induced MAFbx, MuRF1 and Foxo1 mRNA in the skeletal muscle of littermate control Lox/Lox mice of both genotypes (Figure 12 a, b). In mMyD88KO mice LPS induced MAFbx, MuRF1 and Foxo1 normally, while in mGRKO mice, this effect was completely blocked (Figure 12 a, b). The expression of the mTOR regulators Krüpple like factor 15 (KLF15) and regulated in DNA damage responses 1 (REDD1) are both increased by LPS treatment, which would be expected to exert a

negative effect on the protein synthetic rate (Figure 12 a, b) (81, 260). Both genes were again normally induced by LPS in mMyD88KO mice, but not in mGRKO mice. Myostatin has been proposed to play a critical role in mediating glucocorticoid-induced muscle atrophy (114). Consistent with this, myostatin expression in muscle is increased in response to LPS in mMyD88KO but not in mGRKO animals (Figure 12 a, b). Activation of the autophagy-lysosome system also plays an important role in the atrophy process (123, 126). Expression of the autophagy genes BCL-2/adenovirus E1B-19kDA-interacting protein 3 (Bnip3), and GABA(A) receptor-associated protein like 1 (Gabarapl1) were induced by LPS along with the lysosomal protease Cathepsin L (CstL). This effect is attenuated in mGRKO mice, where LPS failed to induce Bnip3, and induced Gabarapl1 to a lesser degree (Figure 12 a, b). In mMyD88KO mice however, LPS-induced all three markers of autophagy normally relative to littermate controls. Collectively these data demonstrate that glucocorticoid signaling in skeletal muscle is necessary for the activation of the atrophy process by systemic inflammation. MyD88 signaling however, is dispensable for induction of the catabolic program by systemic inflammation.

MyD88 Reexpression in Skeletal Muscle Fails to Rescue LPS Mediated Regulation of the MAFbx Gene

LPS has been proposed to act directly on skeletal muscle increasing MAFbx expression via activation of p38 MAPK resulting in atrophy (106). MAFbx was slightly induced in the mGRKO mice, which may represent the effect of direct inflammatory signaling on skeletal muscle. To explore this possibility, we re-expressed MyD88 selectively in the skeletal muscle of whole body MyD88KO mice by electroporation. Transfected fibers were identified by expression of GFP via an internal ribosome entry site (IRES) in the expression plasmid. To control for the effects of electroporation, the

contralateral limb was electroporated with a plasmid containing mCherry-IRES-GFP. In wild type mice, LPS (250 µg/kg) significantly induced MAFbx expression in skeletal muscle as measured by in situ hybridization 8 h after injection (Figure 13 a). Importantly, this increase in signal was seen equally in fibers transfected with mCherry and MyD88, as well as in surrounding untransfected fibers. Furthermore, over expression of mCherry or MyD88 did not significantly induce MAFbx in muscle in the absence of LPS treatment. In MyD88KO mice, LPS failed to induce MAFbx mRNA in skeletal muscle. Re-expression of MyD88 by electroporation failed to rescue LPS mediated induction of MAFbx, demonstrating that the MyD88 pathway is not sufficient for LPS-induced activation of MAFbx gene expression. To confirm successful re-expression of MyD88 in skeletal muscle, we examined MyD88 protein levels by western blot (Figure 13 b). Electroporation of MyD88 resulted in a significant over expression of the protein by western blot.

Muscle Atrophy in Response to Systemic Inflammation Depends on Glucocorticoid not MyD88 Signaling

LPS failed to significantly induce gene expression changes consistent with the atrophy process in mGRKO mice. To investigate whether this also results in significant protection from skeletal muscle atrophy, mGRKO mice were treated with a higher dose of LPS (1 mg/kg) immediately before the onset of the dark cycle and sacrificed 18 h later. LPS treatment resulted in a significant decrease in food intake in both mGRKO mice and $GR^{Lox/Lox}$ mice (Figure 14 a). The effects of food intake were controlled for by pair feeding a subset of vehicle treated animals the LPS injected animals. LPS treatment resulted in a similar decrease in body weight in both mGRKO mice and $GR^{lox/lox}$ mice, while pair feeding resulted in a lesser degree of weight loss (Figure 14 b). When the mass of the gastrocnemius muscle was examined, significant

differences in the response to LPS emerged between genotypes. $GR^{Lox/Lox}$ mice lost ~10% of their muscle mass in response to LPS treatment relative to vehicle treated controls, while mGRKO mice lost only ~3% of their gastrocnemius weight relative to vehicle treated controls of the same genotype (Figure 14 c, d). When skeletal muscle gene expression was measured, results were consistent with the observed differences in muscle mass (Figure 14 e). The induction of MAFbx, MuRF1 and Foxo1 gene expression by LPS was markedly attenuated in mGRKO mice when compared with $GR^{Lox/Lox}$ mice. KLF15, REDD1 and myostatin gene expression was significantly induced by LPS in $GR^{Lox/Lox}$ mice. However, this effect was almost completely absent in mGRKO mice, where LPS produced small inductions of KLF15 and REDD1 but no change in myostatin expression. The induction of autophagy genes by LPS treatment was also blunted in mGRKO mice. LPS produced a significant induction in Bnip3, CstL, and Gabarapl1 in the muscle of $GR^{Lox/Lox}$ mice. In mGRKO mice, LPS failed to induce Bnip3 and induced CstL and Gabarapl1 to a lesser extent than in $GR^{Lox/lox}$ littermates. Cross sections of tibialis anterior muscle were also examined for signs of myofibrillar atrophy in response to LPS. Glycolytic type IIb fibers make up the vast majority of mouse tibialis muscle. Type IIb fiber area was significantly reduced by LPS in $GR^{Lox/Lox}$ mice but was reduced to a much lesser extent by LPS in mGRKO mice (Figure f, g). The intermediate type IIa and type IId/x fibers were unaffected by LPS treatment in $GR^{Lox/Lox}$ animals. At baseline, type IIa fibers in mGRKO animals were larger. With LPS treatment however, IIa fiber area returned to the levels seen in $GR^{Lox/Lox}$ animals.

The atrophy response to high dose LPS was also examined in mMyD88KO mice. LPS produced a normal suppression of food intake and body weight loss in mMyD88KO animals (Figure 14 h, i). In contrast with mGRKO mice, mMyD88KO mice exhibited normal LPS-induced loss of muscle mass relative to $MyD88^{Lox/Lox}$

littermates (Figure 14 j, k). Similar to the results seen with lower doses of LPS and shorter time points, 18h LPS treatment in mMyD88KO mice also produced equivalent induction of atrophy and autophagy genes relative to their littermate controls (Figure 14 l). To confirm specific recombination of the MyD88 locus in mMyD88KO mice, genomic DNA from various tissues was subjected to PCR amplification with primers surrounding the site of recombination. Consistent with the known sites of cre expression in the MCK-Cre mouse, exon 3 of the MyD88 gene was recombined in skeletal and cardiac muscle but no other tissues examined (Figure 14 m). Collectively, these results demonstrate that glucocorticoid but not MyD88 signaling is required for atrophy in response to LPS administration.

Discussion

Experimentally inducing inflammation through a variety of methods rapidly brings about muscle atrophy. Further, anti-inflammatory interventions have proven successful in attenuating muscle atrophy in experimental models of cachexia (101, 104, 106). Numerous cell culture studies demonstrate that cytokines can act directly on skeletal muscle to potentiate catabolism. However, the *in vivo* response to inflammation results in numerous neuroendocrine changes that are not recapitulated in cultured myocytes exposed to cytokines. Principal among these systemic changes is a significant increase in the level of circulating glucocorticoids, which also negatively impact skeletal muscle mass. While glucocorticoids are frequently listed as potential mediators of muscle atrophy, their contribution to inflammation-induced atrophy is incompletely described. Here we demonstrate that glucocorticoid signaling in skeletal muscle is requisite for atrophy in response to systemic inflammation. We further present evidence that direct cytokine signaling in muscle via MyD88 dependent pathways is dispensable for the atrophy response to inflammation *in vivo*.

Cell culture experiments show that both IL-1β and LPS act directly on skeletal muscle to evoke atrophy (99, 106). MyD88 plays a fundamental role in transducing inflammatory signals as MyD88KO mice are unresponsive to IL-1β (281). In addition, many of the effects of LPS (and other toll-like receptor agonists) require MyD88 as well (282). MyD88KO mice fail to demonstrate increased levels of inflammatory cytokines after IL-1β or LPS treatment, demonstrating the critical nature of this pathway. While somewhat surprising, there are multiple possible explanations for the failure of muscle specific knockout of MyD88 to alter LPS-induced atrophy. One possibility comes in the overlapping and redundant properties of cytokines. Multiple cytokines are capable of eliciting atrophy *in vitro* or *in vivo* (45, 105, 283), and LPS treatment increases circulating levels of many cytokines including IL-1β, IL-6, and TNF (280, 282). Both TNF and IL-6 signal via pathways that do not involve MyD88. Therefore, despite the fact that both IL-1β and LPS signaling on myocytes are sufficient to induce atrophy, they may be dispensable components for the induction of wasting by systemic inflammation. Alternately, it is possible that MyD88-independent pathways play a role in mediating the atrophy process. It has been suggested, based on evidence from cultured immune cells, that p38 MAPK mediated activation of the MAFbx gene via TLR4 signaling occurs in a MyD88-independent manner (106). However, our finding that whole body MyD88KO mice fail to induce MAFbx mRNA in response to LPS shows that this is not the case. Therefore, while MyD88 is requisite in some cell type for muscle wasting in response to LPS, it is not necessary in skeletal muscle for normal atrophy in response to systemic inflammation.

Glucocorticoids are appreciated to play a role in acute changes in protein turnover resulting from a variety of conditions. Using adrenalectomized animals, or pharmacologic antagonism of the glucocorticoid receptor, it has been shown that atrophy in response to acute sepsis, starvation, metabolic acidosis and diabetes

depend to some degree on glucocorticoid signaling (53, 93, 95, 96). However, this approach is complicated in the setting of inflammation. Adrenalectomized mice display a 1000 fold decrease in the LD_{50} of endotoxin (284), likely due to a combination of cardiovascular instability and a loss of anti-inflammatory feedback from glucocorticoids. Early studies examining the mechanisms of cytokine-induced protein degradation found that concurrent cytokine administration and glucocorticoid antagonism resulted in significant mortality (285). Therefore, the study of inflammation-induced muscle atrophy in animals with systemic glucocorticoid blockade/insufficiency is confounded by the essential role of glucocorticoid signaling in non-muscle tissue. As a result of this, such experiments have produced conflicting results (285, 286). Deleting the glucocorticoid receptor specifically from skeletal muscle allows for the clarification of the contribution of glucocorticoid signaling to inflammation-induced muscle atrophy without the complication of complete adrenal insufficiency. While it is clear that glucocorticoids are integral to inflammatory atrophy, this may occur in synergy with the direct action of inflammatory cytokines. However, recent data suggests that the levels of circulating glucocorticoids evoked by inflammatory challenge are sufficient to produce substantial atrophy in isolation (279). Future studies will likely expand on the interaction between the catabolic effects of glucocorticoids and cytokines on skeletal muscle.

Materials and Methods:

Animals

Wild type C57BL/6J mice, MCK-Cre (Stock# 006405), MyD88 Flox (Stock# 008888) and My88KO mice (Stock# 009088) were obtained from The Jackson

Laboratories (Bar Harbor, ME). GR Flox mice were provided by L. Muglia (Washington University, St. Louis, Missouri, USA). All animals were maintained on a normal 12:12 hr light/dark cycle and provided *ad libitum* access to water and food (Purina rodent diet 5001; Purina Mills, St. Louis, MO), except in the case of pair fed animals in which food intake was restricted to that consumed by the indicated group. Mice were injected with 250 µg/kg or 1 mg/kg LPS (Sigma, St Louis, MO) dissolved in normal saline/0.5% BSA, and sacrificed 8 or 18 h later. Dexamethasone (Sigma, St Louis, MO) was dissolved in peanut oil, and injected i.p at 5mg/kg daily for 3 days. Mice were sacrificed by decapitation under anesthesia from a ketamine cocktail. Both male and female mice were utilized for electroporation experiments, and were equally represented in all experimental groups. No difference in any measures of atrophy was observed as a result of animal sex. Experiments were conducted in accordance with the National Institutes of Health Guide for the Care and Use of Laboratory Animals, and approved by the Institutional Animal Care and Use Committee of Oregon Health & Science University.

Expression Vectors

The complete MyD88 cDNA was purchase from Origene (Rockville, MD). The coding region of MyD88 was then amplified with the following PCR primers containing a XhoI restriction site and Kozak sequence on the 5' primer and an EcoRI restriction site on the 3' primer: 5'-AAAACTCGAGCGCCACCATGTCTGCGGGAGACCCC-3' and 5'-TTTTGAATTCTCAGGGCAGGGACAAAGC-3'. MyD88 was then ligated into the pCAG plasmid containing a CAG promoter and an IRES-GFP. For *in vivo* electroporation, plasmids were prepared by EndoFree Giga kit (Qiagen, Valencia, CA).

Electroporation of Skeletal Muscle

Under isoflurane anesthesia, the region overlying the tibialis anterior muscle was shaved, and the muscle was injected percutaneously with 25 µL of 0.4U/µL bovine haluronidase (Sigma, St Louis, MO). After 2 hours, the tibialis was exposed and 100 µg of expression plasmid in 50 µL normal saline was injected. The muscle was then electroporated using stainless steel needle electrodes and an ECM 830 square wave pulse generator (Harvard Apparatus Inc, Holliston, MA). The following parameters were used for electroporations: 50 V/cm, 5X50 ms pulses with an interpulse interval of 200 ms. The incision was closed, and animals were allowed to recover for 2 weeks prior to LPS treatment

Real Time PCR

Total muscle RNA was extracted using the RNeasy fibrous tissue mini kit (Qiagen, Valencia, CA) and hypothalamic RNA was extracted using an RNeasy mini kit according to the manufacturer's instructions. cDNA was transcribed using Taqman reverse transcription reagents and random hexamers according to the manufacturers instructions. PCR reactions were run on an ABI 7300, using Taqman universal PCR master mix, using Taqman gene expression assays: mouse GAPDH (Mm99999915_g1), mouse MAFbx (Mm00499518_m1), mouse MuRF1 (Mm01185221_m1), mouse Foxo1 (Mm00490672_m1), Mouse REDD1 (Mm00512504_g1), Mouse KLF15 (Mm00517792_m1), Mouse Myostatin (Mm01254559_m1), Mouse Bnip3 (Mm01275600_g1), Mouse CstL (Mm00515597_m1), Mouse Gabarapl1 (Mm00457880_m1) (Applied Biosystems, Carlsbad, CA). Relative expression was calculated using the delta-delta Ct method, and was normalized to vehicle treated control. Statistical analysis was performed on the normally distributed delta-Ct values.

PCR Analysis of MyD88 Recombination

Genomic DNA was isolated from a variety of tissues using a DNeasy tissue minikit (Qiagen, Valencia, CA). PCR primers were utilized which flank the LoxP sites surrounding Exon 3 of the MyD88 gene. 5'-TGGACCTGGGACCTTGGGCA-3', 5'-TACCCAGGCGGGACAGAGCC-3'. The following thermocycling program was utilized: 95°C for 45 s, 70°C for 30 s, 72°C for 60 s for 35 cycles.

Immunohistochemistry

Cryosections of the tibialis anterior were cut in cross section at 10μm. Unfixed cryosections were blocked for 1 hour in PBS (10 mM NaPO4, 150 mM NaCl) /1% BSA/10% goat serum, and then incubated overnight in primary antibodies diluted 1:250 in PBS/1% BSA/10% goat serum. The following mouse primary antibodies were used: SC-71 for myosin IIa, BF-F3 for myosin IIb, BA-D5 for myosin I (Developmental Studies Hybridoma Bank, University of Iowa, Iowa City, Iowa). Basement membrane was identified by staining with a rabbit anti-laminin antibody (Sigma, St Louis, MO). Sections were washed in PBS, and incubated with the secondary antibodies diluted 1:500 in 1%BSA/10% goat serum. The following secondary antibodies were used: goat anti rabbit Alexafluor 405, goat anti mouse IgM Alexafluor 488, goat anti mouse IgG2b Alexafluor 555, and goat anti mouse IgG1 Alexafluor 633 (Invitrogen, Carlsbad, CA). Sections were washed in PBS and mounted with aqua-poly mount (Polysciences, Warrington, PA). Images were acquired on a Nikon Eclipse Ti confocal fluorescence microscope (Nikon Instruments Inc., Melville, NY). Tiled images of entire sections were captured at ambient temperature and at 200X. Images were processed using Image J. An evenly spaced grid was placed over the section. Fiber area was measured in fibers expressing Myosin IIb, Myosin IIa, or in fibers lacking expression

of Myosin IIb, IIa and Myosin I (type IId/x fibers) Fibers at grid crossing points were measured along with all adjacent fibers of the same type. Grid size was adjusted for a given fiber type such that ~100 fibers were counted per section. Representative images were selected from the same anatomic region of the TA from animals representative of the group mean fiber area.

Western Blotting

Muscles were homogenized in cell lysis buffer (Cell Signaling, Danvers, MA): 20mM Tris pH 7.5, 150mM NaCl, 1mM EDTA, 1mM EGTA 1% Triton X, 2.5 mM sodium pyrophosphate, 1mM beta-glycerophosphate, 1mM Sodium Orthovanadate, 1ug/mL leupeptin, and supplemented with Complete protease inhibitors (Roche, Indianapolis, IN), 1 mM PMSF (Sigma, St Louis, MO), and 5 µL/mL phosphatase inibitor cocktail II (Sigma, St Louis, MO). Samples were homogenized for 30 s minutes using a Polytron homogenizer (Kinematica, Bohemia, NY), then were sonicated 2x10s. Samples were and centrifuged at 13,000 RPM for 10 minutes at 4C. 100 ug of total protein per lane was run on Criterion 4-15% gradient polyacrylamide gels (Biorad, Hercules, CA), and transferred to Immobilon PVDF membranes (Millipore, Billerica, MA). Proteins were detected using a Lumi-Imager (Roche, Indianapolis, IN) and SuperSignal West Pico Chemiluminescent Substrate (Thermo, Rockford, IL). The following antibodies were used: Rabbit anti MyD88(Cell Signaling, Danvers, MA), Anti Rabbit HRP conjugate (Promega, Madison, WI).

In Situ Hybridization

Cryosections were cut at 20 µM for ISH analysis. Serial sections were cut and immediately immersed in LN_2 for GFP visualization. Antisense 33P-labeled rat MAFbx riboprobe (corresponding to bases 68-413 of mouse MAFbx) (0.12 pmol/ml) was

denatured, dissolved in hybridization buffer along with tRNA (1.7 mg/ ml), and applied to slides. Slides were covered with glass coverslips, placed in a humid chamber, and incubated overnight at 55 °C. The following day, slides were treated with RNase A and washed under conditions of increasing stringency. Slides were dipped in 100% ethanol, air dried, and then dipped in NTB-2 liquid emulsion (Eastman Kodak Co., Rochester, NY). Slides were developed 3 d later and cover slipped. Images were acquired on a Leica DM4000 B microscope, using a Leica DFC340 FX camera at ambient temperature at 50X magnification using Leica Applications Suit 3.6 software (Leica, Buffalo Grove, IL). For visualization of GFP/mCherry in serial sections, slides were fixed in a vapor chamber with filter paper soaked in 37% formaldehyde at -20°C overnight. Slides were then post fixed in 4% PFA/PBS for 15 min, washed in PBS and mounted with aqua-poly mount (Polysciences, Warrington, PA). Fluorescent images were acquired on a Nikon Eclipse Ti confocal fluorescence microscope (Nikon Instruments Inc., Melville, NY). Tiled images of entire sections were captured at ambient temperature and at 200X. Images were processed using Image J.

Statistical Analysis

Data are expressed as mean ±SEM. Statistical analysis was performed using Prism software (Version 4.0, Prism Software Corp., Irvine, CA). All data were analyzed with a two-way ANOVA followed with post hoc analysis using a Bonferroni post-test. For all analyses, significance was assigned at the level of $P<0.05$.

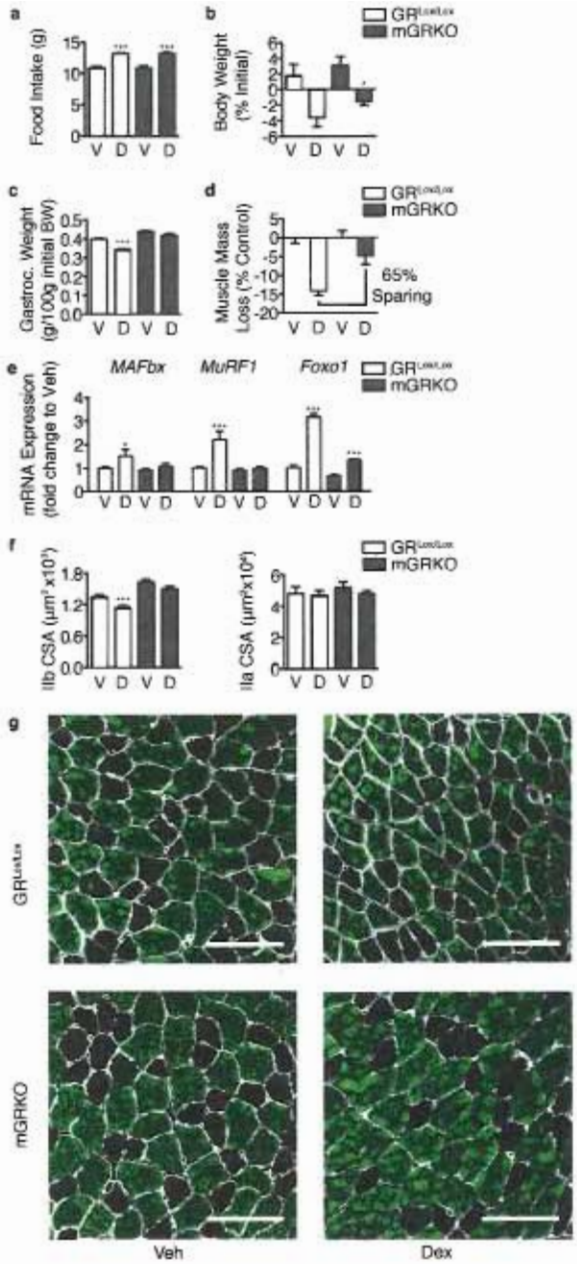

Figure 11. Muscle-specific deletion of the glucocorticoid receptor protects against dexamethasone-induced muscle atrophy

$GR^{Lox/Lox}$ and mGRKO mice (n=5-6/group) were treated for 3 days with Dexamethasone (5 mg/kg). (**a**) Food weight and (**b**) Body weight were measured daily. (**c**) Gastrocnemius muscle was weighed after 3 days and normalized to pre treatment body weight. (**d**) Muscle mass loss as a percentage of vehicle treated controls. (**e**) Gastrocnemius muscle gene expression

measured by real time PCR with GAPDH as an endogenous control. (**f**) Tibialis anterior muscles were cut in cross section and immunostained with antibodies against laminin, myosin IIb, myosin IIa, and myosin I. Type IIb and IIa fiber area was measured. (**g**) Representative images of tibialis muscle in a region of type IIb fibers (Laminin=white, Myosin IIb=green). ***= $P<0.001$, **=$P<0.01$, *= $P<0.05$ as measured by two-way ANOVA with Bonferroni post-test. Scale bar represents 100 μm. V=Vehicle, D=Dexamethasone.

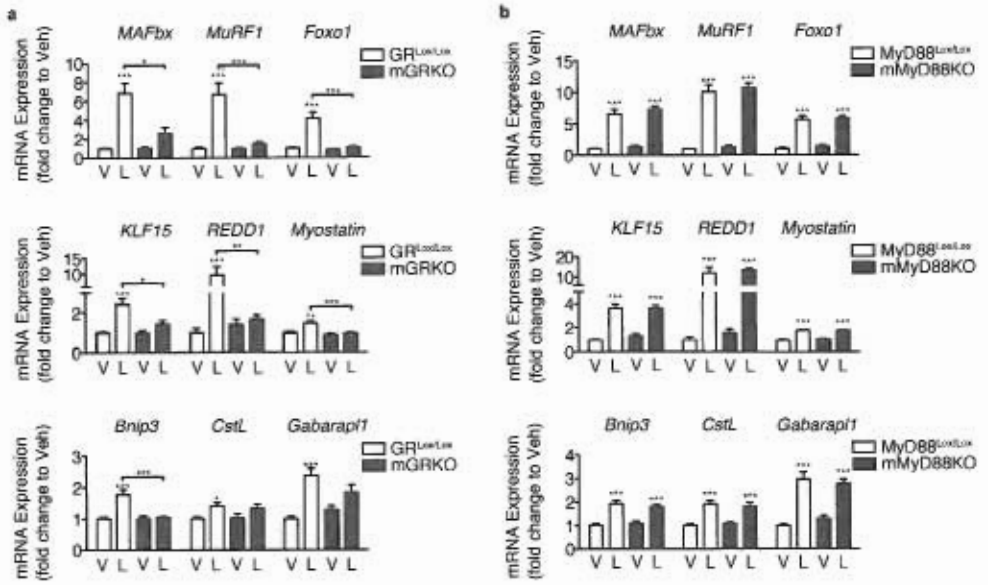

Figure 12. Muscle-specific deletion of the glucocorticoid receptor but not MyD88 prevents atrophy gene induction by LPS

Gene expression in the gastrocnemius muscle of female (**a**) mGRKO (n=6-9/group) and (**b**) mMyD88KO mice (n=6-10/group) 8 h after i.p. LPS injection (250 µg/kg) measured by real time PCR using GAPDH as an endogenous control. ***= P<0.001, **=P<0.01, *= P<0.05 as measured by two-way ANOVA with Bonferroni post-test. V=Vehicle, L=LPS.

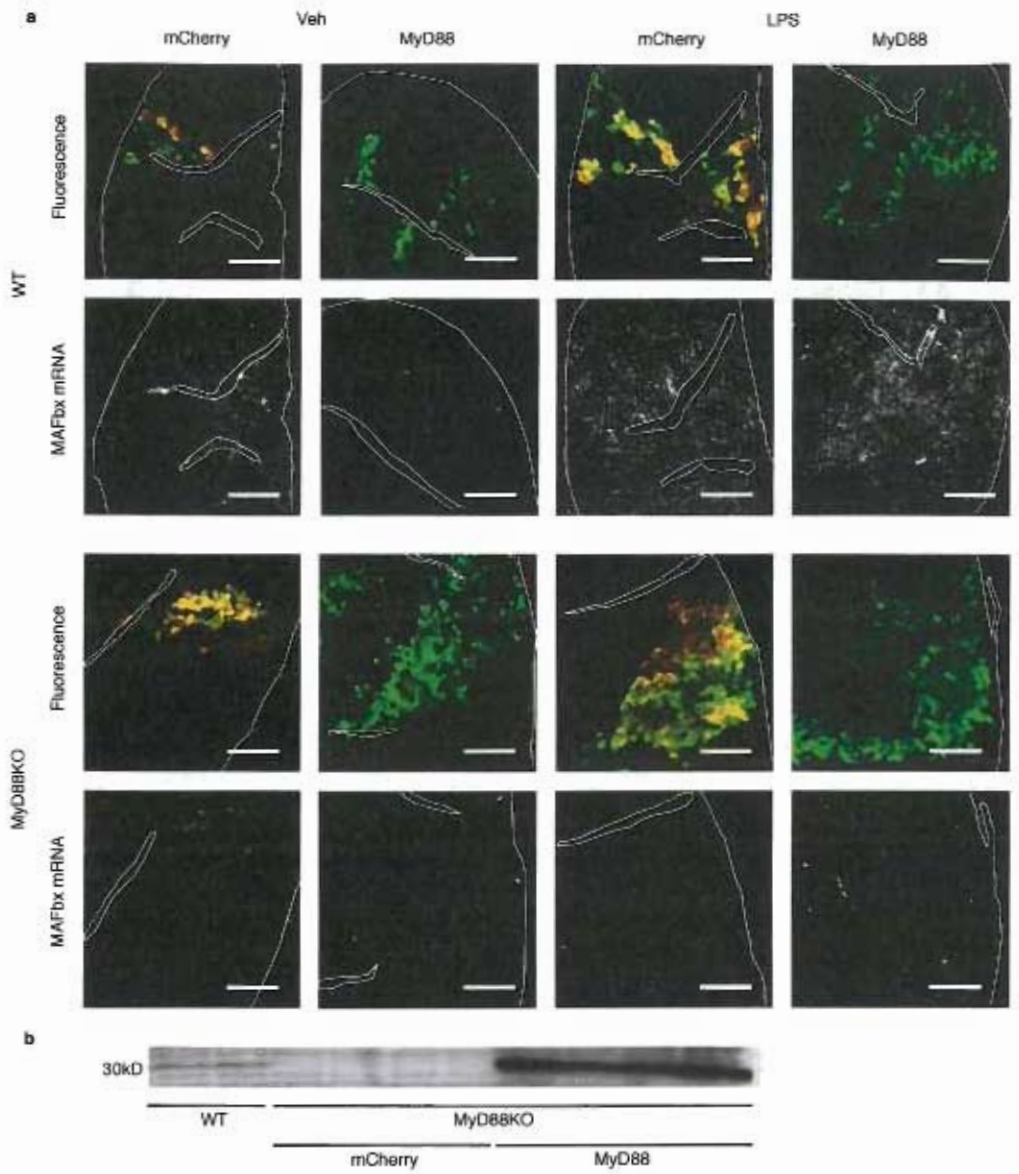

Figure 13. MyD88 signaling in muscle is not sufficient for LPS-induced atrophy

Wild type (n=2/group) and MyD88KO (n=4/group) mice were electroporated in the tibialis anterior muscle with plasmid containing mCherry-IRES-GFP or MyD88-IRES-GFP then treated with LPS (250 µg/kg). (**a**) MAFbx mRNA levels were examined by in situ hybridization in regions expressing GFP in serial sections 8 h after LPS treatment. For ease of comparison between GFP and ISH sections, connective tissue boundaries and section edges have been outlined (**b**) MyD88 expression examined by western blot in WT and MyD88KO muscle electroporated with mCherry and MyD88. Scale bar represents 400 µm.

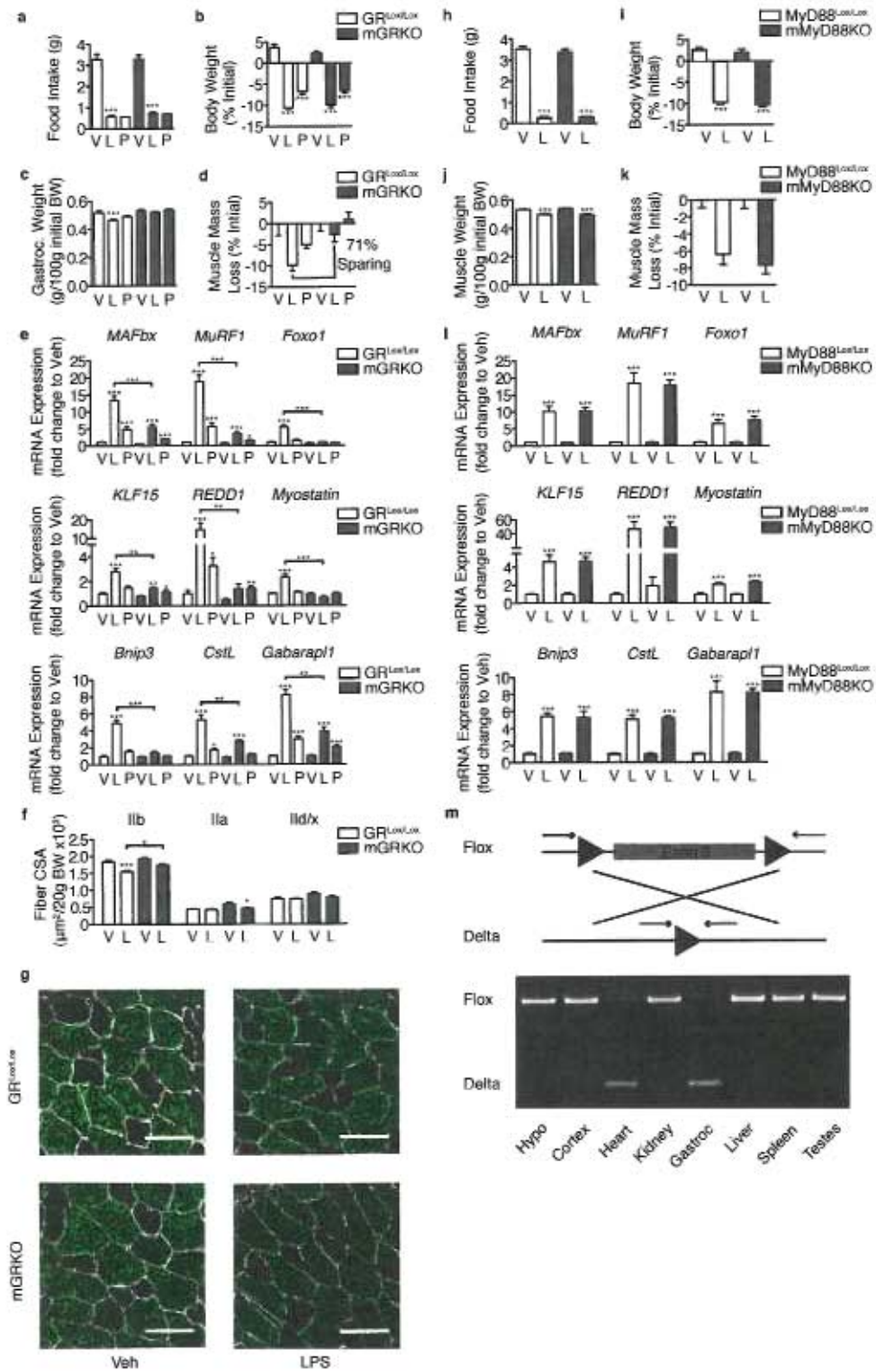
a
Food Intake (g)
V L P V L P
b
Body Weight (% Initial)
GR Lox/Lox
mGRKO
c
Gastroc. Weight (g/100g initial BW)
d
Muscle Mass Loss (% Initial)
71% Sparing
h
i
MyD88 Lox/Lox
mMyD88KO
j
Muscle Weight (g/100g initial BW)
k
e
MAFbx
MuRF1
Foxo1
KLF15
REDD1
Myostatin
Bnip3
CstL
Gabarapl1
mRNA Expression (fold change to Veh)
l
f
IIb
IIa
IId/x
Fiber CSA (μm²/20g BW x10³)
m
Flox
Delta
Hypo
Cortex
Heart
Kidney
Gastroc
Liver
Spleen
Testes
g
GR Lox/Lox
mGRKO
Veh
LPS

Figure 14. Muscle-specific deletion of the glucocorticoid receptor but not MyD88 muscle atrophy in response to LPS

Male mGRKO (n=6-9/group) and MyD88KO mice (n=7-11/group) were treated with LPS (1 mg/kg) and examined for signs of atrophy 18 h later. A subset of vehicle treated animals was pair fed to the LPS treatment group. (**a**, **h**) Food weight and (**b**, **i**) Body weight were measured. (**c**, **j**) Gastrocnemius muscle was weighed after 3 days and normalized to pre treatment body weight. (**d**, **k**) Muscle mass loss as a percentage of vehicle treated controls. (**e**, **l**) Muscle gene expression measured by real time PCR with GAPDH as an endogenous control. (**f**) Tibialis anterior muscles were cut in cross section and immunostained with antibodies against laminin, myosin IIb, myosin IIa, and myosin I. Type IIb, IId/x (absent IIb, IIa, or I staining), and IIa fiber area was measured. (**g**) Representative images of tibialis muscle in a region of type IIb fibers (Laminin=white, Myosin IIb=green). (**m**) Recombination mapping for the MyD88 locus using PCR with primers outside the LoxP sites. ***= P<0.001, **=P<0.01, *= P<0.05 as measured by two-way ANOVA with Bonferroni post-test. Scale bar represents 50μm. V=Vehicle, L=LPS.

CHAPTER 4

Manuscript #3

Myeloid Differentiation Factor 88 is Not Requisite in Neurons for the Induction of Sickness Behavior by Interleukin-1β

Theodore P. Braun[1,2*], Aaron J. Grossberg[1,2*], Marek Szumowski[1], and Daniel L. Marks[1]
* These authors contributed equally to this work.

Papé Family Pediatric Research Institute[1], MD/PhD Program[2], Oregon Health & Science University, Portland, Oregon, 97239, USA.

Chapter 4 is a manuscript in preparation as a short report for the Journal of Neuroinflammation.

Introduction

Systemic inflammation elicits an evolutionarily conserved behavioral response, including anorexia, lethargy, anhedonia, and hyperalgesia (287). Collectively known as sickness behavior, this response is likely adaptive in the acute setting as it reduces energy expenditure associated with foraging. However, it becomes pathological when present for longer periods of time. Individuals suffering from chronic inflammatory illnesses such as cancer, chronic renal failure, congestive heart failure and many others exhibit decreased appetite and reduced ability to complete activities in the course of daily living (254). Diminished nutritional intake consequent to decreased appetite contributes to ongoing weight loss in such individuals. Both weight loss and reduced activity not only negatively impact quality of life, but also are tightly correlated with mortality (10, 14). Despite this, there are currently no effective therapeutic interventions that alter the impact of sickness behavior.

One common feature of diseases associated with sickness behavior is an increase in circulating inflammatory cytokines. Administration of inflammatory cytokines to experimental animals recapitulates the major behavioral features of sickness, and cytokine antagonism has shown some efficacy in reversing these behaviors in models of inflammation and disease (136, 141). However, the mechanism by which inflammatory cytokines mediate behavioral changes remains incompletely described. Myeloid differentiation factor 88 (MyD88) is a signaling protein downstream from toll-like receptor 4 (TLR4) and the type I interleukin 1 receptor (IL-1R1). MyD88 is a critical mediator of anorexia in response to the bacterial cell wall product lipopolysaccharide, and the prototypical inflammatory cytokine interleukin-1β (IL-1β) (127). Furthermore, MyD88 is required in a non-hematopoietic derived cell population for LPS-induced sickness behavior, suggesting that MyD88 within the central nervous system is requisite for the behavioral response to these

inflammatory stimuli (128). Cytokine receptors are expressed on neurons known to regulate feeding and other behavioral responses (131, 186, 187). However, others have provided evidence that cerebrovascular endothelial cells and perivascular macrophages are the targets of inflammatory cytokines in mediating the behavioral response to disease (163, 168, 230, 288).

To explore these distinct mechanisms of cytokine action and to establish the necessity of CNS MyD88 expression, we performed intracerebroventricular (i.c.v.) injections of IL-1β in MyD88 knockout mice (MyD88KO) and mice with a targeted deletion of MyD88 in the CNS only ($MyD88^{\Delta CNS}$). Our work here describes the behavioral response to CNS inflammation, and the role of MyD88 in mediating this response.

Methods

Animals

Male C57BL/6J wild type and MyD88KO (Stock# 009088) mice were purchased from The Jackson Labs (Bar Harbor, ME). Nestin-cre mice (Stock# 003771), MyD88 Flox mice (Stock# 008888) and MyD88KO mice (Stock# 009088) were obtained from The Jackson Labs (Bar Harbor, ME), and crossed to obtained Nes-$cre^{+/-}$ /MyD88 $Flox^{+/+}$ mice. These mice were then crossed back to the original MyD88 $Flox^{+/+}$ line to obtain $MyD88^{\Delta CNS}$ and $MyD88^{Flox}$ littermate controls. Nestin-Cre mice were also bred to mice harboring a Flox-Stop-Flox tdTomato behind a CAG promoter knocked into the ROSA locus (The Jackson Labs, Bar Harbor, ME, Stock# 007908) to examine the cellular specificity of cre-mediated recombination. All mice were genotyped using standard protocols from The Jackson Labs. Animals were maintained on a normal 12:12 hr light/dark cycle and provided *ad libitum* access to water and food (Purina rodent diet 5001; Purina Mills, St. Louis, MO). Mice were used

for experiments between 6 and 10 weeks of age. Experiments were conducted in accordance with the National Institutes of Health Guide for the Care and Use of Laboratory Animals, and approved by the Animal Care and Use Committee of Oregon Health & Science University.

Immunohistochemistry

For histology experiments, mice were deeply anesthetized using ketamine cocktail and sacrificed by transcardial perfusion fixation with 15 mL ice cold 0.01 M PBS + heparin sodium (15,000 U/L) followed by 25 mL 4% paraformadehyde (PFA) in 0.01 M PBS. Brains were post-fixed in 4% PFA overnight at 4°C and cryoprotected in 20% sucrose for 24 h at 4°C before being stored at -80°C until use for IHC. Free-floating sections were cut at 30 µm from perfused brains using a sliding microtome (Leica SM2000R; Leica Microsystems, Bannockburn, IL). Hypothalamic sections were collected from the division of the optic chiasm (bregma -1.0 mm) caudally through the mammillary bodies (bregma -3.0 mm). The sections were incubated for 1 h at room temperature in blocking reagent (5% normal donkey serum in 0.01 M PBS and 0.1% Triton X-100). After the initial blocking step, the sections were incubated in mouse anti-NeuN (1:1000, Millipore, Billerica, MA), rabbit anti-GFAP (1:500, DAKO, Carpinteria, CA), rabbit anti-Iba1 (1:500, DAKO, Carpinteria, CA), rat anti-CD31 (1:100, BD Pharmingen, Sparks, MD) in blocking reagent for 72 h at 4°C, followed by incubation in donkey anti-rabbit Alexa 488 (1:500), donkey anti-mouse Alexa 647 (1:500), goat anti-rat 633 Alexa (1:500, Invitrogen, Carlsbad, CA) for 2 h at room temperature. Between each stage, the sections were washed thoroughly with 0.01 M PBS. Incubating the sections in the absence of primary antisera was used to ensure specificity of the secondary antibodies. Sections were mounted onto gelatin-coated slides and coverslipped using Vectashield mounting media (Vector Laboratories,

Burlingame, CA). Images were acquired using a Nikon Eclipse Ti confocal fluorescence microscope (Nikon Instruments Inc., Melville, NY).

Intracerebroventricular Injection

26-gauge lateral ventricle cannulas (PlasticsOne, Roanoke VA) were placed under isoflurane anesthesia, using a stereotactic alignment instrument (Kopf, Tujunga, CA) at the following coordinates relative to bregma: -1.0 mm X, -0.5 mm Y, and -2.25 mm Z. 10 ng mouse IL-1β or 500 ng TNF (R&D, Minneapolis, MN). Injections were given in 1 µL total volume. IL-1β and TNF were dissolved in artificial cerebrospinal fluid (aCSF, 150 mM NaCl, 3 mM KCl, 1.4 mM $CaCl_2$, 0.8mM $MgCl_2$, 1.0 mM $NaPO_4$) with 0.1% endotoxin free BSA.

LPS Injection

LPS (Sigma, St. Louis, MO) was dissolved at 62.5 µg/mL in 0.9% Saline/ 0.5% endotoxin free BSA, and injected intraperitoneally at 4 µL/g body weight (250 µg/kg).

Locomotor Activity Measurement

Voluntary home cage locomotor activity (LMA) was measured using implantable telemetric transponders (MiniMitter, Bend, OR). Animals were anesthetized using 2% isoflurane, a small incision was made in the abdominal wall, and transponders were implanted adjacent to the abdominal aorta in the retroperitoneal space. The incision was then closed with 4/0 silk suture. Transponders were implanted during the lateral ventricle cannulation surgery. Mice were individually housed and allowed to acclimate for at least 5 days before temperature and net movement in *x*-, *y*-, and *z*-axes was recorded in 1 min intervals (Vital View, MiniMitter, Bend, OR).

Overnight Feeding Studies

Animals were transferred to clean cages and injected i.c.v. with IL-1β (10 ng) , TNF (500 ng) or LPS (250 μg) 1 h prior to lights off. At 2, 6, 13, 24, 37 and 48 h after the onset of the dark cycle, food was weighed and returned to the cage. Body weight was recorded at 13, 24 and 48 h.

Fast-Refeed Studies

At lights out, food was removed from the cages and animals were fasted for 12h. At the start of the light cycle, animals were injected i.c.v with IL-1β (10 ng) and food was returned to the cages 15 min later. Food intake was measured at 1, 2, 5, 8, 12 and 24 h after the return of food to the cages.

Results

MyD88 is Requisite for Sickness Behavior in Response to Centrally Administered IL-1β

MyD88 is an essential signaling molecule for conveying the anorectic signal in response to peripheral inflammation. Despite this, it has been proposed that IL-1β signaling on neurons is dependent on PI3K, not MyD88 (289). Peripherally administered IL-1β may not directly reach neurons as it has been suggested that cytokines are too large to cross the blood brain barrier (228). However, i.c.v injection of IL-1β results in significant amounts of cytokine in the brain parenchyma via mass action (265). To examine whether MyD88 is requisite for the behavioral response to cytokines administered directly into the brain, we examined the response of MyD88KO mice to i.c.v injection of IL-1β. Injections of IL-1β (10 ng) were performed in the hour before lights off at Zeitgaber time (ZT) 11-12. While wild type (WT) mice

showed a significant suppression of dark-phase food intake in response to IL-1β (Figure 15 a), My88KO mice showed no anorectic response to IL-1β. WT mice lost BW in response to IL-1β treatment, while MyD88 mice were undistinguishable from Veh treated controls (Figure 15 b). WT mice treated with IL-1β showed a significant suppression of home cage LMA for the first 8 h of the dark cycle, while MyD88KO mice treated with IL-1β showed normal LMA (Figure 15 c, d). This result demonstrates that MyD88 is required for sickness behavior in response to IL-1β applied directly into the brain.

MyD88 Knockout Mice Display Sickness Behavior in Response to MyD88 Independent Inflammatory Signaling

MyD88KO mice demonstrate normal sickness behavior in response to peripheral tumor necrosis factor (TNF) administration, consistent with the MyD88-independent canonical signaling pathway downstream from the TNF receptor. To examine whether this is also the case with centrally administered TNF, we performed i.c.v. injections of TNF (500 ng) in MyD88KO mice before the onset of the dark cycle (ZT 11-12). TNF significantly attenuated nighttime feeding during the first 6 hours of the dark cycle in both WT and MyD88KO mice (Figure 16 a). After 6 hours, the rate of food intake in WT animals injected with TNF paralleled Veh treated animals. However, MyD88KO mice treated with TNF showed a significant increase in food intake during the second half of the dark cycle, such that 13 hours after treatment, their cumulative food intake was roughly equivalent to Veh treated mice. TNF injection resulted in decreased body weight relative to Veh treatment in both genotypes, although this difference was only statistically significant in WT mice (Figure 16 b). Central TNF treatment also significantly reduced LMA activity during the first 8h of the dark cycle relative to Veh treated animals for both WT and MyD88KO mice (Figure 16

c, d). These data demonstrate that MyD88KO mice display normal acute sickness behavior in response to an inflammatory challenge that does not require MyD88. However, MyD88 is essential for the maintenance of some aspects of sickness behavior during the later phases of the dark cycle, irrespective of the signaling mechanism of the initial inflammatory stimulus.

Generation of Mice Lacking MyD88 Exclusively in the CNS

To explore the identity of the cells requiring MyD88 to respond to inflammation, we generated mice lacking MyD88 exclusively in the central nervous system ($MyD88^{\Delta CNS}$) by crossing mice expressing Cre recombinase under the control of the rat nestin promoter with mice harboring an allele of MyD88 where exon 3 is flanked by LoxP sites. This mouse has no overt phenotype until challenge with a high fat diet, despite displaying appropriate recombination (290). While the nestin-Cre mouse has been utilized extensively and characterized in a variety of ways, reports vary as to the precise identity of cells in the CNS expressing recombinase activity. To clarify this issue, we crossed the Nestin-Cre mouse to a reporter line in which the tdTomato fluorescent protein is present in cells that have expressed cre recombinase at any point during their development. Both neurons (marked by NeuN) and astrocytes (marked by GFAP) co-express tdTomato, demonstrating that Cre recombinase activity is present in both these cell types (Figure 17). To confirm co localization of GFAP and tdTomato, high magnification images are also provided. Cre recombinase activity is not present in microglia (marked by Iba1) or endothelium (marked by CD31). While the images shown in Figure 17 focus on the hypothalamic arcuate nucleus (ARC), due to its known fundamental role in feeding, and expression of cytokine receptors, these results are representative of all regions of the brain examined (186, 187).

Deletion of MyD88 From Neurons and Astrocytes Does Not Alter Sickness Behavior in Response to IL-1β

As MyD88 is absolutely requisite for the behavioral response to IL-1β, and neurons can respond to cytokines, we assessed the behavioral response of $MyD88^{\Delta CNS}$ mice to IL-1β administered prior to the onset of the dark cycle (ZT 11-12). $MyD88^{\Delta CNS}$ mice displayed a normal suppression of overnight feeding in response to i.c.v. IL-1β (Figure 18 a, b). Spontaneous home cage activity was suppressed by i.c.v. IL-1β equally in $MyD88^{\Delta CNS}$ and $MyD88^{lox/lox}$ mice (Figure 18 c, d). These data show that the despite being essential for sickness behavior, MyD88 is not required in neurons or astrocytes for this response.

MyD88 in Neurons and Astrocytes Is Not Required for the Suppression of Refeeding by IL-1β

Multiple cytokines are rapidly induced in the CNS after injection of IL-1β, many of which produce anorexia, and do not signal via MyD88 (131, 291). Therefore, it is possible that population of cells not expressing Cre, such as microglia, responds rapidly to IL-1β injected i.c.v. and produces other cytokines which are sufficient for the anorectic response. While some cell types are believed to store inflammatory cytokines, releasing them upon stimulation, this does not appear to be the case for macrophages/microglia (292). Therefore, it is possible that the behavioral response to injected IL-1β acting directly on neurons would only be observable at early time-points prior to amplification of this signal into a redundant cytokine response in other cell types. To assess this possibility we examined the ability of IL-1β to suppress the refeeding response after an overnight fast in $MyD88^{\Delta CNS}$ mice. Fasting overnight increases food intake in the first several hours after food reintroduction, increasing the

precision of food intake measurements at early time points. Animals were fasted for 12 h at the start of the dark cycle, and then injected with IL-1β immediately prior to the return of food to the cages. IL-1β suppressed food intake equally in both MyD88$^{\Delta CNS}$ and MyD88$^{Lox/Lox}$ littermates at early time points during refeeding with the suppression of food intake becoming statistically significant in both groups 2h after IL-1β injection (Figure 19 a, b). At later time points MyD88 $^{\Delta CNS}$ mice exhibited a subtle defect in refeeding. MyD88$^{Lox/Lox}$ littermates fed at an accelerated rate between 12-24 h after IL-1β injection such that they had caught up with Veh treated animals by 24 h (Figure 19 c). MyD88 $^{\Delta CNS}$ mice however continued to feed at the same rate, maintaining a ~1 g deficit in cumulative food intake (Figure 19 d).

MyD88 is Not Required in Neurons or Astrocytes for LPS-Induced Sickness Behavior

MyD88 is also an integral component of the signaling pathway downstream of TLR4. While inflammatory signaling pathways downstream of TLR4 can be activated independent of MyD88, MyD88KO mice fail to mount a cytokine response to LPS injection (282). Therefore, we examined whether MyD88$^{\Delta CNS}$ mice would display altered behavioral responses to peripheral LPS injection. One hour prior to the onset of the dark cycle, MyD88$^{\Delta CNS}$ mice were injected i.p. with LPS (250 µg/kg). This treatment resulted in a suppression of nighttime food intake in both MyD88$^{Lox/lLox}$ and MyD88$^{\Delta CNS}$ mice (Figure 20 a). LPS treatment produced a significant suppression of food intake starting 2 h after the injection, however no differences were observed between genotypes (Figure 20 b). LPS resulted in a significant loss of body weight without any differences evident between genotypes (Figure 20 c). Home cage activity was also equally suppressed by LPS administration in MyD88$^{\Delta CNS}$ and MyD88$^{Lox/Lox}$ mice for the entire duration of the dark cycle (Figure 20 d). Cumulative dark cycle LMA was significantly decreased in both genotypes without significant differences

being evident between genotypes (Figure 20 e). These results demonstrate that expression of MyD88 is not required in neurons or glia for LPS-induced sickness behavior.

Discussion

Sickness behavior represents an important component of the adaptive metabolic response to infection. In chronically ill patients this response becomes maladaptive significantly worsening quality of life and potentially contributing to mortality. Despite numerous mechanistic inroads into the pathogenesis of sickness behavior, the neuroanatomic substrate upon which inflammation acts to produce this behavior has remained elusive. In this work, we describe studies that localize the target of inflammation-induced sickness behavior to specific cell types within the brain. Despite the fact that MyD88 is required for the behavioral response to IL-1β (128), we found that MyD88 in both neurons and astrocytes is completely dispensable for the behavioral response to IL-1β.

The receptor for IL-1β is expressed in multiple locations within the CNS (228), many of which are known to regulate food intake. In particular, the type I IL-1 receptor (IL-1R1) is expressed in the ARC on anorectic proopiomelanocortin (POMC) and orexigenic Agouti Related Peptide (AgRP) neurons (186, 187). IL-1β increases the firing of POMC neurons and increases the release of alpha-melanocyte stimulating hormone (α-MSH) the natural ligand of the type 4 melanocortin receptor (MC4R) from hypothalamic explants. IL-1β simultaneously decreases the release of AgRP, the endogenous antagonist of the MC4R. Consistent with this, blockade of the MC4R prevents IL-1β and LPS-induced anorexia, demonstrating that alterations in melanocortin signaling underlie changes in feeding in response to IL-1β (35, 129).

However, despite clear recombination in ARC, MyD88$^{\Delta CNS}$ mice respond normally to IL-1β. There are several possible explanations to resolve these apparently conflicting results. It is possible that Cre mediated recombination of the MyD88 allele was incomplete, and a sufficient number of neurons remain responsive to IL-1β in the MyD88$^{\Delta CNS}$ mouse for a normal anorectic response. Indeed, POMC neurons maintain their anorectic activity even after ablation of 90% of ARC POMC neurons (Malcolm Low, personal communication). Alternately, it is possible that IL-1β produces anorexia in a pathway that is dependent on the IL-1RI, but independent from MyD88. There is some precedence for this, as it has been proposed that IL-1β signals via a PI3K dependent mechanism in neurons, similar to the mechanism by which leptin mediates electrophysiologic changes in neurons (289, 293). However, the MyD88KO mouse fails to respond to IL-1β, even when it is delivered intracerebroventricularly and would be expected to reach neurons. An additional possibility is that the signal from injected cytokine has an obligate amplification step in a cell type that does not undergo recombination in the MyD88$^{\Delta CNS}$ mouse, leading to the paracrine release of a second messenger, which ultimately conveys the anorectic signal to the neurons regulating sickness behavior.

One possible target for inflammatory signaling is cerebrovascular endothelial cells. Endothelial knockdown of the IL-1RI prevents the activation of neurons in the paraventricular nucleus (PVN) of the hypothalamus and blocks the suppression of home cage LMA activity in response to i.c.v. IL-1β injection (230). Furthermore, brain endothelial specific knockout of transforming growth factor β-activated kinase (TAK1) attenuates the depression in LMA seen after IL-1β administration (288). Perivascular macrophages have also been implicated as key intermediaries in the central response to inflammation. Selective depletion of perivascular macrophages decreases the activation PVN neurons in response to peripheral IL-1β but does not alter the

depression of locomoter activity observed with this treatment (168). Therefore, it is likely that endothelium and the associated perivascular macrophages represent components of the cell population in which MyD88 is required for sickness behavior.

Prostaglandins are one of the key signaling intermediates that transmit inflammatory signals from endothelium to neurons in mediating the sickness response (163, 230, 288). While this is clearly the case for fever where genetic or pharmacologic inhibition of prostaglandin signaling can completely attenuate the febrile response (294), results are less impressive for other aspects of sickness behavior. COX inhibition fails to substantially alter the changes in volitional activity observed after i.p. LPS injection (291) and decreases but does not block the anorectic response to peripheral and central inflammatory challenges (131, 169, 171). Therefore, while prostaglandins play a role in mediating some of the behavioral response to systemic inflammation, other second messengers also serve as a relay between inflammatory cytokines and the neurons regulating behavior.

IL-1β itself has the potential to be the ultimate mediator of inflammation-induced anorexia. The message for IL-β increases during inflammatory challenge specifically in the parenchyma of the arcuate nucleus of the hypothalamus (279). It is possible that IL-1β does not reach sufficient concentration after i.c.v. injection to engage the IL-1RI on feeding center neurons, yet is produced in sufficient concentration locally. There is some experimental evidence to support this mechanism. When IL-1 receptor antagonist (IL-1Ra) is administered centrally at a high dose during peripheral endotoxemia, anorexia is prevented, demonstrating that endogenous brain IL-1 signaling is integral to the anorectic response. Furthermore, endogenous IL-1 signaling also plays a role in mediating protein catabolism in sepsis, as i.c.v. infusion of IL-1Ra attenuates the loss of muscle mass during experimental sepsis (258). However, in order for this mechanism to be consistent with the

presented data, the induction of hypothalamic IL-1β would have to be dependent on MyD88, yet its ultimate action on neurons independent from MyD88. As evidence exists from other cell types that cytokine production is dependent on MyD88 (281), and IL-1β signaling on neurons is MyD88 independent (289), this remains a possible explanation for the data presented here.

The concept that neurons are the substrate upon which cytokines act to produce sickness behavior is suggested by many studies (136, 186, 295). Leptin, a cytokine hormone extensively studied with regards to behavior effects is widely accepted to produce many of its physiologic actions via direct action on neurons (185, 296). However, others have suggested that the induction of sickness behavior requires an intermediary cell type such as endothelium (163, 228, 230, 288). The results here demonstrate that the induction of sickness behavior by IL-1β requires MyD88 in a non-neuronal cell type. While direct IL-1β action on neurons may participate in the behavioral response to this inflammatory insult, MyD88 signaling in at least one other cell population is also required as an obligate step.

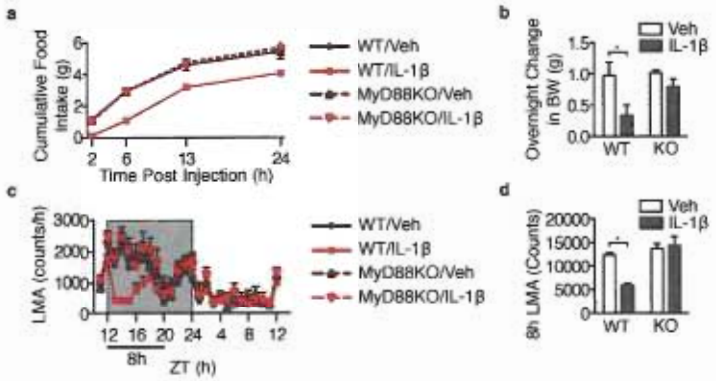

Figure 15. MyD88 is required for sickness behavior in response to central IL-1β injection

WT and MyD88KO mice received i.c.v. injections of IL-1β (10 ng) 1 h before the onset of the dark cycle (n=5-6/group). (**a**) Cumulative food intake. (**b**) Overnight change in body weight. (**c**) Hourly locomotor activity. (**d**) Cumulative locomotor activity over 8 h post injection. KO=MyD88KO, ZT= Zeitgeber Time. *= P<0.05 as measured by two-way ANOVA with Bonferroni post-test.

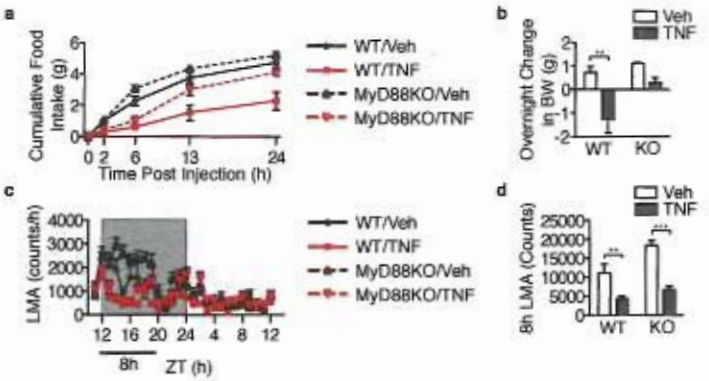

Figure 16. MyD88 is not required for sickness behavior in response to central TNF injection

WT and MyD88KO mice received i.c.v. injections of TNF (500 ng) 1 h before the onset of the dark cycle (n=5-6/group). (**a**) Cumulative food intake. (**b**) Overnight change in body weight. (**c**) Hourly locomotor activity. (**d**) Cumulative locomotor activity over 8 h post injection. KO=MyD88KO, ZT= Zeitgeber Time. ***= P<0.001, **= P<0.01 as measured by two-way ANOVA with Bonferroni post-test.

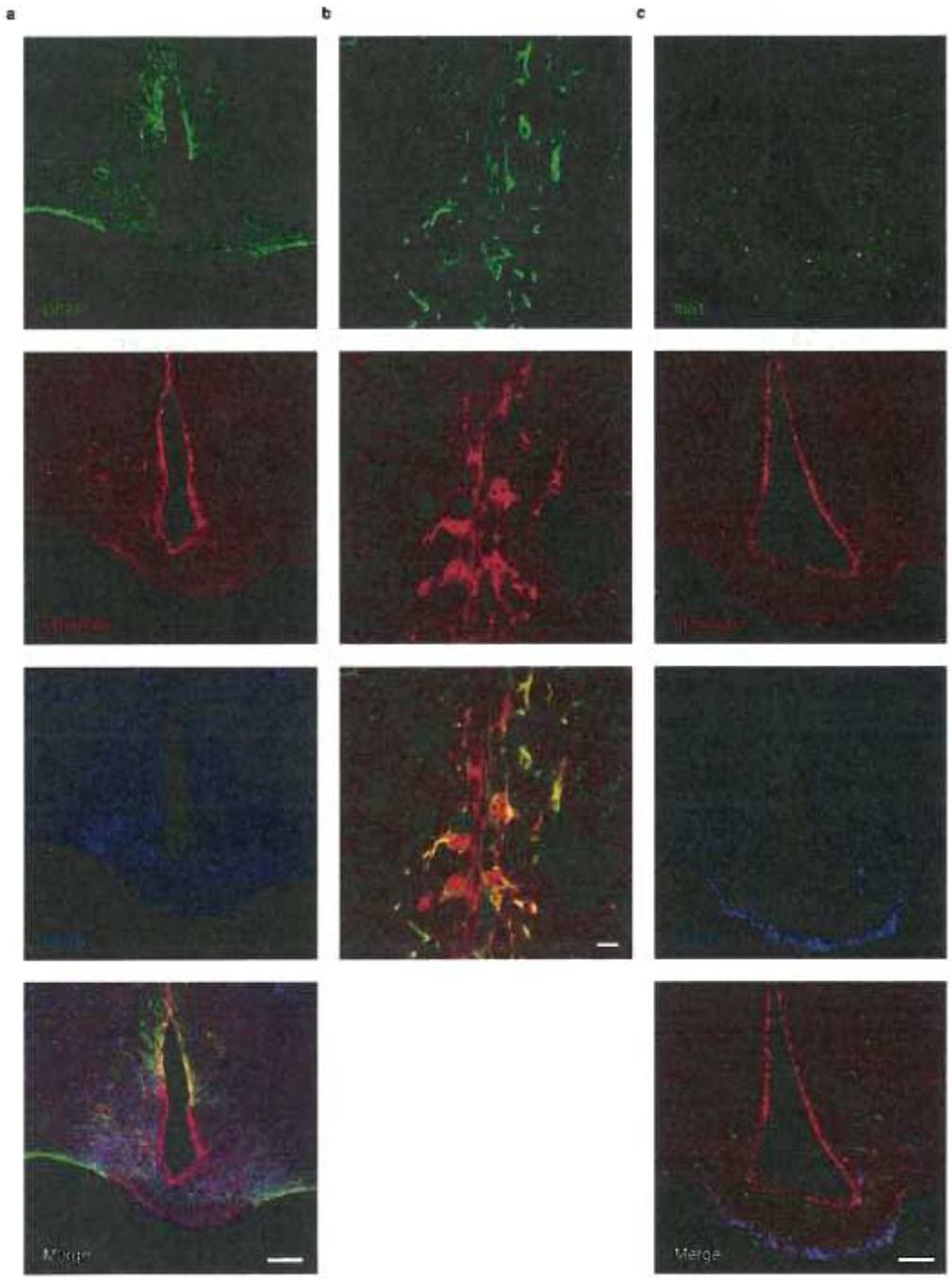
a
b
c
Merge
Merge

Figure 17. Nestin Cre drives recombination in neurons and astrocytes but not endothelium or microglia

Nes-Cre tdTomato reporter mice were immunostained with antibodies against (**a**) GFAP marking astrocytes and NeuN labeling neuronal nuclei or (**c**) Iba1 labeling microglia and CD31 labeling endothelium. Images seen in (**b**) show high magnification of GFAP and tdTomato to examine co-expression in astrocytes. Representative images of the ARC at -1.46 to -1.70 mm relative to bregma respectively. Scale bar in (**a**) and (**c**) represents 100 µm, and in (**b**) represents 10 µm.

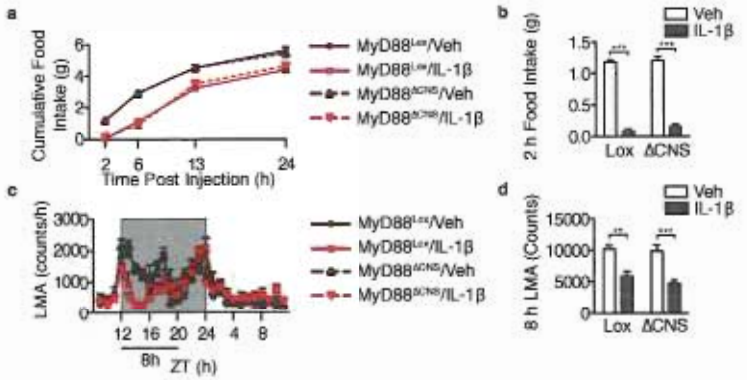

Figure 18. MyD88 expression in the CNS is not required for IL-1β-induced sickness behavior

WT and MyD88$^{\Delta CNS}$ mice received i.c.v. injections of IL-1β (10 ng) 1 h before the onset of the dark cycle (n=4-9/group). (**a**) Cumulative food intake. (**b**) Cumulative food intake at 2 h post injection. (**c**) Hourly locomotor activity. (**d**) Cumulative locomotor activity over 8 h post injection. Lox= MyD88$^{Lox/lox}$, ΔCNS=MyD88$^{\Delta CNS}$, ZT= Zeitgeber Time. ***= P<0.001, **= P<0.01, *= P<0.05 as measured by two-way ANOVA with Bonferroni post-test.

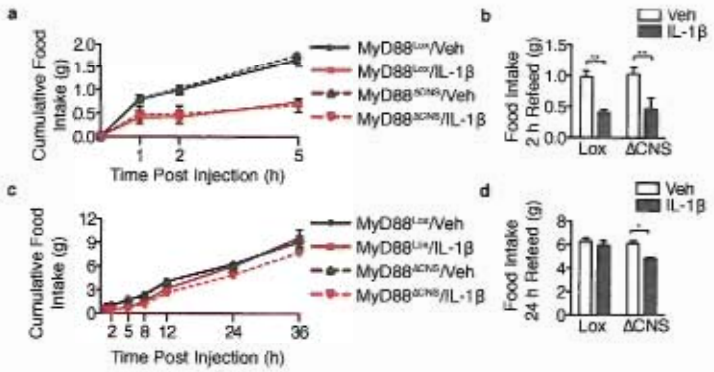

Figure 19. MyD88 expression in the CNS is not required for IL-1β-induced suppression of refeeding

WT and MyD88$^{\Delta CNS}$ mice were fasted for 12 h and then received i.c.v. injections of IL-1β (10 ng) 15 minutes prior to food being returned to the cages (n=4-5/group). (**a**) Cumulative food intake 0-5 h. (**b**) Cumulative food intake at 2 h. (**c**) Cumulative food intake 0-36 h. (**d**) Cumulative food intake at 24 h. ΔCNS=MyD88$^{\Delta CNS}$. ***= P<0.001, **= P<0.01, *= P<0.05 as measured by two-way ANOVA with Bonferroni post-test.

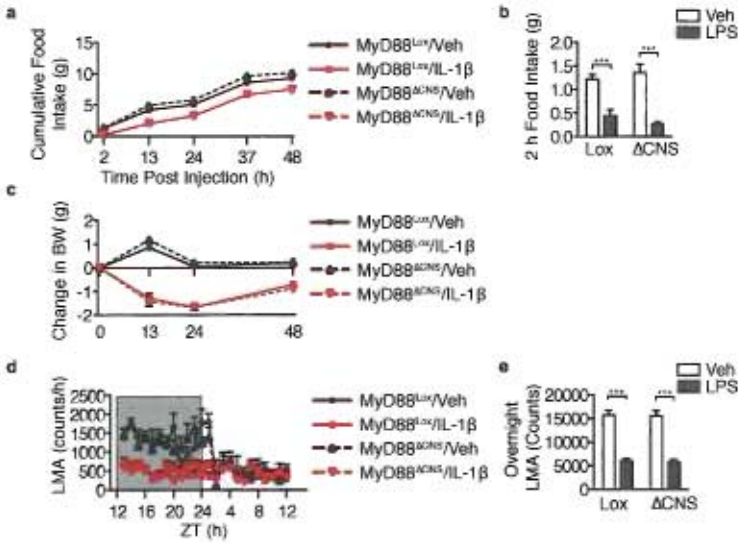

Figure 20. MyD88 expression in the CNS is not required for LPS-induced sickness behavior

WT and MyD88$^{\Delta CNS}$ mice received i.p. injections of LPS (250 µg/kg) 1 h before the onset of the dark cycle (n=4-9/group). (**a**) Cumulative food intake. (**b**) Cumulative food intake at 2 h post injection. (**c**) Change in body weight. (**d**) Hourly locomotor activity. (**e**) Cumulative locomotor activity over the dark cycle. Lox= MyD88$^{Lox/lox}$, ΔCNS=MyD88$^{\Delta CNS}$, ZT= Zeitgeber Time. ***= P<0.001 as measured by two-way ANOVA with Bonferroni post-test.

CHAPTER 5

Manuscript #4

Regulation of lean mass, bone mass and exercise tolerance by the central melanocortin system

Theodore P. Braun[1,2*], Benjamin Orwoll[4*], Xinxia Zhu[1], My Linh T. Nguyen[1], Mary L. Bouxsein[5], Robert F. Klein[3], Daniel L. Marks[1]
* These authors contributed equally to this work.

Author Affiliations:
Papé Family Pediatric Research Institute[1], MD/PhD Program[2], Bone and Mineral Unit, Division of Endocrinology, Diabetes and Clinical Nutrition[3], Oregon Health & Science University, Portland, Oregon, 97239, USA.
Department of Pediatrics, Loma Linda University, Loma Linda, California, 92350, USA[4].
Center for Advanced Orthopedic Studies, Beth Israel Deaconess Medical Center and Harvard Medical School, Boston, Massachusetts, 02215, USA[5].

Chapter 5 is modified from the original paper submitted to *The Journal of Endocrinology* Mar 7th, 2011.

Abstract

Signaling via the type 4-melanocortin receptor (MC4R) is an important determinant of body weight in mice and humans, where loss-of function mutations lead to significant obesity. In addition to dramatically increased adipose mass, a significant increase in lean body mass is also observed. This increase in lean mass is independent from increased body weight, as MC4R knockout (MC4RKO) mice display increased fat free mass relative to diet-induced obese mice with equivalent body weight. However, skeletal muscle mass is not increased in MC4RKO mice. Bone mass and strength do increase with age in MC4RKO mice, which likely contributes to increases in lean body mass. MC4R deficiency also results in an increase in grip strength and a dramatic decrease in exercise performance. No changes in the ratio of oxidative to glycolytic fibers were seen, however MC4RKO mice demonstrate a significantly reduced heart rate, which may underlie their deficient exercise performance. This work demonstrates that although lean mass and muscle mass are often equated, this is not true in the MC4RKO mouse. The impaired exercise performance we report in the MC4RKO mouse has potential clinical ramifications, as efforts to control body weight in humans with melanocortin deficiency may be ineffective due to poor tolerance for physical activity.

Keywords: Melanocortin, Muscle, Bone, Exercise

Introduction

The type 4-melanocortin receptor (MC4R) is a known regulator of somatic growth. Genetic blockade (297) or loss of function of the MC4R results in increased linear growth in rodents (275) and humans (298). Interestingly, humans with MC4R deficiency have a lower body fat content, and therefore higher lean mass when compared to leptin-deficient individuals with similar body mass index (BMI). MC4RKO mice resist lean mass loss due to tumor growth (35) and chronic renal failure (150). Furthermore, pharmacologic blockade of the MC4R attenuates lean mass loss in a multitude of catabolic conditions (35, 36, 150, 299, 300). This regulation of lean mass has often been attributed to skeletal muscle (189, 301), however no studies to date have examined whether skeletal muscle or some other component of lean mass is increased in response to a loss of signaling at the MC4R.

Despite the significant contribution of skeletal muscle to overall lean mass, many other lean tissues also contribute to fat-free body weight and are under the regulation of the central melanocortin system. Increased bone mineral density has also been reported in humans (298) and animals (302) with MC4R deficiency, demonstrating that increases in bone mass accounts for some of the lean mass phenotype seen in these cases. Further complicating the interpretation of increased lean mass with melanocortin deficiency is the compensatory muscle hypertrophy and bone mineralization that occur in parallel with increasing fat mass. As body weight increases, muscle and bone mass increase, presumably in response to increased mechanical loading. To address this complex issue, we examined skeletal muscle and bone in MC4RKO mice at a series of developmental time-points.

Our results show that young MC4RKO mice initially have an increase in fat mass without changes in lean mass relative to WT mice. However, increased lean mass rapidly develops relative to WT mice with diet-induced obesity (DIO).

Paradoxically, muscle weight is decreased in the MC4RKO mice. Additionally, MC4RKO mice have a late onset increase in bone mass and strength. These results challenge the notion that increased lean mass in MC4R deficiency is associated with increased skeletal muscle mass, and point to other lean tissues as contributors to this effect.

Materials and Methods

Animals

Wild type C57BL/6J mice (20-25g) were obtained from The Jackson Laboratory (Bar Harbor, ME). MC4RKO mice were used as previously reported (275). MC4RKO mice were backcrossed at least 10 generations into the C57BL/6J strain. All animals were maintained on a normal 12:12 hr light/dark cycle and provided *ad libitum* access to water and food (Purina rodent diet 5001; Purina Mills, St. Louis, MO). The high fat diet (HFD) (D12492, Research Diets, Inc.) contains 60% fat (5.24 kcal/g). Mice were sacrificed by decapitation under anesthesia from a ketamine cocktail. Experiments were conducted in accordance with the National Institutes of Health Guide for the Care and Use of Laboratory Animals, and approved by the Animal Care and Use Committee of Oregon Health & Science University.

Body composition

Mouse body composition analysis was performed using a 4-in-1 small animal MRI (Echo Medical Systems, Houston, TX).

Treadmill

Exercise performance was measured with an Exer-3/6 treadmill (Columbus Instruments, Columbus, OH). Animals were conditioned in the treadmill chamber

every other day for one week prior to the experiment. At the start of training sessions, animals were acclimatized to the treadmill chamber for ten minutes with the treadmill off. The speed of the treadmill was started at 6 m/min was increased by 1 m/min every min. Once 10 m/min was reached, the animals were run for 5 minutes. On the day of the experiment, the treadmill was started at 6m/min, and the speed was increased by 1 m/min every 10 minutes until 15 m/min was reached. Animals were run at 15 m/min until exhaustion.

Fiber type analysis

For analysis of muscle fiber type, 9 µm unfixed cryosections of gastrocnemius were blocked for 1 hour in PBS/1% BSA/10% goat serum, and then incubated overnight in primary antibody diluted 1:250 in PBS/1% BSA/10% goat serum. The following primary antibodies were used: SC-71 for myosin IIa, BF-F3 for myosin IIb (Developmental Studies Hybridoma Bank, University of Iowa, Iowa City, IA), and anti Myosin I (Vector Labs, Burlingame, CA). Sections were washed in PBS/0.025% triton-X-100, and incubated with a goat anti-mouse Alexafluor-488 nm labeled secondary antibody (Invitrogen, Carlsbad, CA) diluted 1:500 in PBS/10% BSA. Sections were mounted with Vectashield fluorescent mounting media (Vector Labs, Burlingame, CA). Images were acquired on a Leica DM4000 B microscope, using a Leica DFC340 FX camera at ambient temperature at 100X magnification using Leica Applications Suite 3.6 software (Leica, Buffalo Grove, IL).

Grip Strength

Grip strength was measured using a Grip Strength Meter (Columbus Instruments, Columbus, OH). Five measurements were collected per animal. The high and low value for each animal were discarded, and the middle three values

averaged.

Heart rate

Mouse heart rate was measured using a Vivo770 (Visualsonics, Toronto, ON) under isoflurane anesthesia. Mice were maintained under anesthesia for one hour prior to heart rate measurement to establish a stable baseline.

Bone Phenotype

Female mice from the wild type (WT, C57BL/6) and MCR4KO strains were bred under identical conditions. All procedures were approved by the VA Institutional Animal Care and Use Committee and performed in accordance with National Institutes of Health guidelines for the care and use of animals in research.
At 5 and 10 months of age, both WT and MCR4KO mice were euthanized by CO_2 inhalation and weighed to the nearest 0.1 g. Lumbar vertebrae and femora were immediately harvested, wrapped in sterile gauze soaked in PBS, and stored frozen at -20°C for subsequent biomechanical analyses. Prior to sacrifice, *in vivo* whole body composition and BMD measurements were carried out on anesthetized mice using dual-energy X-ray absorptiometry (pixiMus®, GE Medical Systems, Waukesha, WI) after an overnight fast. Analysis was performed using the mouse whole body software provided by the manufacturer. BMD of isolated femoral and L_5 vertebral specimens were determined as well.

Cortical femoral shaft bone geometry was assessed with a desktop x-ray microtomographic scanner (SkyScan Model 1074, Aartselaar, Belgium). Images were analyzed with Optimas software (version 6.2; Media Cybernetics, Silver Spring, MD). To determine femoral structural properties, the left femur was tested to failure by three-point bending on a high-resolution materials test apparatus (Model 4442,

Instron Corp., Canton, MA). Load and displacement data were recorded and failure load was determined using system software. Vertebrae were evaluated using a desktop μCT imaging system (μCT40; Scanco Medical AG, Bassersdorf, Switzerland) equipped with a 10-mm focal spot microfocus X-ray tube and images acquired with a 12 μm isotropic voxel size, as previously described (303). Morphometric variables describing bone microstructure were computed using direct 3D methods, including bone volume fraction (BV/TV, %), trabecular number (Tb.N, mm^{-1}), trabecular thickness (Tb.Th, μm), trabecular separation (Tb.Sp, μm), connectivity density (ConnD, mm^{-3}), and the structure model index (SMI), a measure of the plate- versus-rod-like nature of the trabecular structure. All microCT analyses adhere to published guidelines (304).

Statistics

Data are expressed as mean ± SEM. Statistical analysis was performed using Prism software (Version 4.0, Prism Software Corp., Irvine, CA). All data were analyzed with an unpaired t test, or Pearson correlation. For all analyses, significance was assigned at the level of $P<0.05$.

Results

Young MC4RKO Mice Have Normal Lean Mass, but Poor Exercise Endurance.

To examine the time course of the increased lean mass phenotype in MC4RKO mice, we examined young WT and KO mice at 8 weeks of age. At this age, MC4RKO mice were not significantly heavier than WT mice (21.7±0.5 g for KO vs 20.6±0.3 g for WT, p=0.09) (Figure 21 a). Interestingly, at this time point, MC4RKO mice had increased fat mass relative to WT mice (2.2±0.1 g for KO vs 1.8±0.1g for WT), but equivalent lean mass (18.8±0.4 g for KO vs 18.1±0.3 g for WT) (Figure 21 b, c). This

results in an increased fat mass percentage and a decreased lean body mass percentage in KO mice relative to WT mice (Figure 21 d, e). To examine the endurance capacity of the muscle in MC4RKO mice, they were subjected to treadmill running. Despite only mild differences in body composition, MC4RKO mice showed a dramatic reduction in treadmill running time, and distance covered (Figure 22 a, b). MC4RKO mice ran for less than half the time and covered only one third of the distance achieved by WT mice. There was no significant correlation between body weight and either run time or distance covered in WT or MC4RKO mice (Figure 22 c, d).

MC4RKO Mice Rapidly Develop an Increased Lean Mass While Maintaining Poor Endurance

To determine whether an increased lean mass phenotype would occur with aging in the MC4RKO mice, we examined MC4RKO mice one month later at 12 weeks of age. To control for the effects of increasing body weight and fat mass, we placed WT control mice on a high fat diet (HFD) to generate DIO. Despite DIO mice gaining significant weight over the month of high fat feeding, chow-fed MC4RKO mice gained more weight and were significantly heavier than DIO WT mice at 12 weeks of age (34.9±0.9 g for KO vs 31.5±0.4 g for DIO-WT) (Figure 23 a). Remarkably, WT mice fed a HFD mice gained an equivalent amount of fat mass compared with chow-fed MC4RKO mice over the 4-week period, such that there was no significant difference in fat mass between the two groups at 12 weeks of age (8.9±0.5 g for KO vs 9.1±0.5 g for WT) (Figure 23 b, d). In contrast, MC4RKO mice gained nearly double the lean mass over the one-month period (6.2±0.5 g for KO vs 3.5±0.4 g for WT) (Figure 23 c, e). This resulted in a significantly increased lean mass (25.0±0.4 g for KO vs 21.6±0.3 g for WT) and percent lean body mass in MC4RKO mice relative

to DIO WT mice (Figure 23 f, g). When controlling for body weight by only considering the 5 heaviest DIO WT mice and the 5 lightest MC4RKO mice (32.4±0.3 g for KO vs 32.4±0.3 g for WT), the differences in body composition become even more pronounced (Figure 23 h). MC4RKO mice show an increased lean mass (23.9±0.2 g for KO vs 21.5±0.4 g for WT) and decreased fat mass (7.5±0.4 g for KO vs 10.2±0.7 g for WT) relative to weight-matched DIO WT mice (Figure 23 i, j). The endurance performance of MC4RKO mice was examined again at 12 weeks and again a significantly reduced run time and total distance traveled was observed in MC4RKO mice (Figure 24 a, b). BW was not a determining factor in the running performance of MC4RKO mice as it showed no significant correlation with run time or total distance covered for either WT or MC4RKO mice (Figure 24 c, d). When only weight matched mice were considered, there was a trend toward decreased exercise performance in the MC4RKO mice, but due to the inherent variability of treadmill performance and the reduced sample size, the differences in run time did not rise to the level of statistical significance ($p=0.07$ for time and $p=0.08$ for distance) (Figure 24 e, f).

MC4RKO Mice Have Decreased Muscle Weight and a Low Resting Heart Rate

To examine the possible causes for the reduced running performance in the MC4RKO mouse, we examined 11-week-old MC4RKO mice relative to chow fed WT controls. Although the MC4RKO mice were heavier at this time point, an increase in lean mass was not evident in MC4RKO mice relative to WT mice (22.6±0.5 g for KO vs 21.8±0.4 g for WT) (Figure 25 a, c). However, MC4RKO mice did show an increase in fat mass relative to controls (4.7±0.5 g for KO vs 1.5±0.1 g for WT), resulting in a significantly increased fat mass and a decreased percent lean body mass relative to non-obese controls (Figure 25 b, d, e). Gastrocnemius muscle weight was surprisingly reduced in MC4RKO mice, despite having normal total lean body

mass (Figure 25 f). To determine if a functional deficit in skeletal muscle might be responsible for the poor exercise endurance phenotype of MC4RKO mice, we measured grip strength and found that it was slightly increased in MC4RKO mice relative to WT mice (Figure 25 g). We also examined the fiber composition of the gastrocnemius and soleus muscles, as alterations in the relative abundance of glycolytic versus oxidative fibers could potentially explain the poor exercise endurance phenotype in the MC4RKO mouse. The mouse gastrocnemius is composed of predominantly type IIb glycolytic fibers, with scattered centrally located type IIa intermediate fibers. In contrast the mouse soleus is made up of predominantly type IIa fibers at approximately a 2:1 ratio with type I oxidative fibers. We saw no differences in the number of type IIa immunoreactive fibers in the gastrocnemius or soleus, and also saw no differences in the number of type I immunoreactive fibers in the soleus between genotypes (Figure 25 i-q). This suggests that alterations in fiber composition are not responsible for the reduced exercise performance in MC4RKO mice. We also measured resting heart rate in MC4RKO mice and found a dramatic reduction relative to WT controls, suggesting that impaired cardiac performance may underlie the endurance deficit in these animals (Figure 25 h).

Aged MC4RKO Mice Have Increased Bone Mass and Strength

Bone mass is known to be elevated in MC4RKO mice, and skeletal mass is a major contributor to non-muscle, whole body lean mass. Therefore, we examined the skeletal phenotype in middle aged (20 weeks) and old (40 weeks) MC4RKO mice. Despite the significant discrepancy in overall body size between the MC4RKO and WT mice, there were no observed differences in femoral length at either 20 or 40 weeks of age (Tables 5 and 6). In 20-week-old MC4RKO mice, whole body and femoral bone mineral density (BMD) were significantly increased (by 6% and 11%,

respectively) as compared to WT mice. By 10 months of age the markedly increased body size of the MC4RKO mice precluded assessment by the pixiMus® densitometer, but femoral and L5 vertebral BMD were significantly increased (by 11% and 13%, respectively) as compared to WT mice.

Although trends existed in bone strength and geometry, there were no statistical differences in femoral geometry or strength at 20 weeks of age (Table 5). However, by 40 weeks of age MC4RKO mice exhibited 19% greater femoral cortical area, 13% greater cortical thickness and 45% greater moment of inertia than WT mice (Table 6). These differences in femoral geometry were accompanied by a 29% increase in ultimate failure load and 21% increase in stiffness (Table 6). In addition to the femoral morphological differences, the vertebral BV/TV and trabecular number of 10-month-old MC4R-KO L_5 vertebrae compared to WT were 13% and 28% greater, respectively. Consistent with the increased vertebral bone volume and trabecular number, MC4R-KO mice exhibited a 57% increase in trabecular connectivity density compared to WT mice. Representative two-dimensional frontal planar μCT images illustrating the differences in bone integrity of the fifth lumbar vertebral body between WT and MC4RKO mice are presented in Figure 26. These data demonstrate that MC4RKO mice have increased bone mass that evolves in concert with the development of severe obesity.

Discussion

Increased lean mass has been associated with MC4R mutations in humans (298, 305) and melanocortin blockade protects against lean mass loss in experimental cachexia in rodents (36, 188, 192). Furthermore, MC4RKO mice exhibit increased body length, suggesting a role for signaling at the MC4R in restraining somatic growth (275). Obesity results in an increase in both fat and lean body mass,

although fat mass increases to a larger extent, increasing the fat:lean ratio. While MC4RKO loss of function has been associated with increased lean mass for a given BMI, a thorough characterization of body composition has yet to be performed to allow for the deconvolution of increasing adiposity from alterations in lean mass (35, 193, 194, 299). Furthermore, while it has been suggested that an increase in lean mass associated with MC4R blockade is the result of increased muscle mass, the function of skeletal muscle in this setting has not been examined. This work demonstrates that MC4RKO mice accumulate lean mass at an accelerated rate, independent from the accumulation of fat mass. While MC4R deficiency in humans is associated with increased lean mass relative to leptin deficient individuals, we confirm the association between MC4R loss-of-function and increased lean mass in MC4RKO mice relative to DIO mice.

As skeletal muscle is a major contributor to whole body lean mass, we examined skeletal muscle mass and function in MC4RKO mice. MC4RKO mice demonstrated significantly reduced limb muscle mass. Multiple lines of evidence suggest that signaling via the MC4R can influence metabolic pathways in peripheral tissues via the autonomic nervous system (232, 306). Furthermore, both insulin and circulating IGF-1 levels are elevated in humans with MC4R mutations, which would be expected to exert powerful trophic effects on muscle (307). In total, these features of MC4R deficiency would be expected to promote the accrual of muscle mass. Importantly, while lean mass and skeletal muscle mass are often equated, these results demonstrate dissociation between these parameters. This implies that the increase in fat free mass in the setting of MC4R deficiency results from increases in a non-muscle lean tissue. MC4RKO mice also demonstrate decreased locomotor activity, which may play a role in mediating the decrease in muscle mass associated with MC4R deficiency (304).

Bone mass represents another significant component of total lean mass. Elevated bone mass was found in multiple cohorts of MC4R deficient humans, and in MC4RKO mice (302). Furthermore, MC4R deficient humans display isolated decreases in circulating markers of bone resorption, without alterations in markers of bone formation (302). Consistent with these findings, we found significant elevations in bone mineral density in 5-month and 10-month-old MC4RKO mice. At both time points examined, significant elevations in body weight were already present in MC4RKO mice. Some controversy exists as to whether obesity is associated with increased bone mass (308). Obese individuals demonstrate increased bone mass. However, when the effects of mechanical loading due to increased body weight are accounted for, this association is no longer present. As the MC4RKO mice used in our study were already obese when bone parameters were measured, it is difficult to assess the role of decreased melanocortin signaling in regulating bone mass independent from increases in body weight. It has been suggested that the elevated bone mass in MC4RKO mice arises from elevated cocaine and amphetamine regulated transcript (CART) levels (302). Indeed, mice lacking the prohormone convertase carboxypeptidase E are obese with low bone mass and are unable to produce mature α-melanocyte stimulating hormone (the primary MC4R ligand) or CART (309). This suggests that CART signaling lies downstream of the MC4R in the regulation of bone mass. Additionally, there is some evidence to suggest that melanocortin signaling has direct influences on bone. The MC4R is expressed both on osteoblasts and osteoclasts (310, 311), demonstrating the potential for melanocortin peptides to directly influence bone metabolism. While increased bone mass has been previously described in the MC4RKO mouse, our study is the first to show that bone strength is also increased by MC4R deficiency. Importantly, this demonstrates that in addition to regulating bone mass, melanocortin signaling is also

an important determinant of bone quality.

To further evaluate the function of skeletal muscle in MC4RKO mice, we assessed treadmill run time as a measure of endurance. MC4RKO mice were markedly deficient in their exercise capacity. Furthermore, increased body weight does not appear to be responsible for this effect, as there was no relationship between body weight and treadmill run times. We also found that grip strength is slightly increased in MC4RKO mice, suggesting a shift in the balance of muscle fiber types. However, there were no differences in fiber type distribution in MC4RKO mice, demonstrating that an overt change in the balance of oxidative and glycolytic fibers is not responsible for the exercise phenotype of these animals. Interestingly, MC4RKO mice have a dramatically decreased resting heart rate, consistent with previous findings in MC4R deficient mice and humans (312, 313). It is possible that an inability to achieve peak exercise-induced cardiac output underlies the exercise phenotype of the MC4RKO mouse. The central melanocortin system is also a regulator of glucose uptake by skeletal muscle. Central administration of melanocortin agonists increases the activity of AMP-activated protein kinase (AMPK), which results in the translocation of the type 4 glucose transporter to the cell membrane (306). Another potential explanation for the reduced exercise performance of the MC4RKO mouse is impaired glucose uptake in skeletal muscle consequent to decreased AMPK activity.

Signaling via the MC4R controls multiple facets of growth and metabolism. While numerous studies have focused on the regulation of fat mass by the central melanocortin system, the regulation of lean mass has not been previously explored. While we demonstrate increased lean mass in the setting of MC4R deficiency, it appears that bone mass but not muscle mass contributes to this effect. Furthermore, MC4R deficiency results in impaired exercise performance. This result has important clinical ramifications for the care of patients with the melanocortin obesity syndrome,

where reduced ability to sustain physical activity may confound attempts to control body weight via exercise.

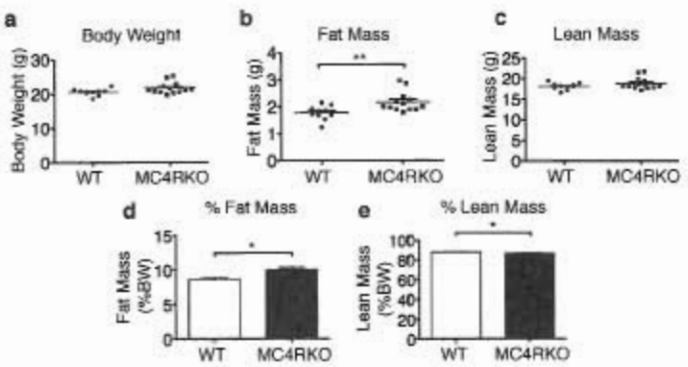

Figure 21. Fat Mass is increased in mice lacking the type-4 melanocortin receptor prior to total body weight or lean mass

(**a**) Body weights of 8-week-old male MC4RKO mice (n=13) were compared with age and weight matched WT mice (n=10). (**b**) MC4RKO mice have increased fat mass, (**c**) but normal lean mass. (**d**) Fat mass as a percentage of body weight (BW) is increased in MC4RKO mice. (**e**) Lean mass as a percentage of body weight is decreased in MC4RKO mice. Data represented as mean ± s.e.m. **=P<0.01, *=P<0.05 as calculated by unpaired t-test.

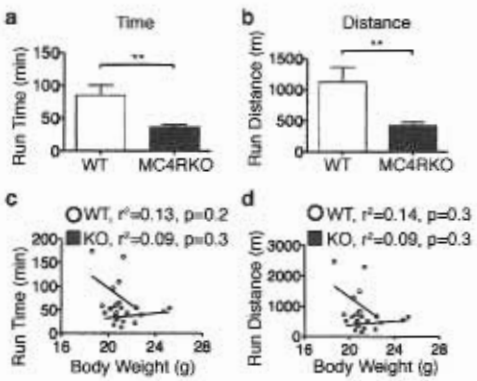

Figure 22. The type 4 melanocortin receptor is a critical regulator of exercise performance

8-week-old male MC4RKO mice (n=13) and age and weight matched WT controls (n=10) were subjected to treadmill running at escalating speed. (**a**) MC4RKO mice showed decreased total treadmill run time. (**b**) MC4RKO mice showed decreased treadmill run distance. (**c**) No correlation between run time or (**d**) run distance with body weight was observed. Data represented as mean ± s.e.m. **= P<0.01 as calculated by unpaired t-test.

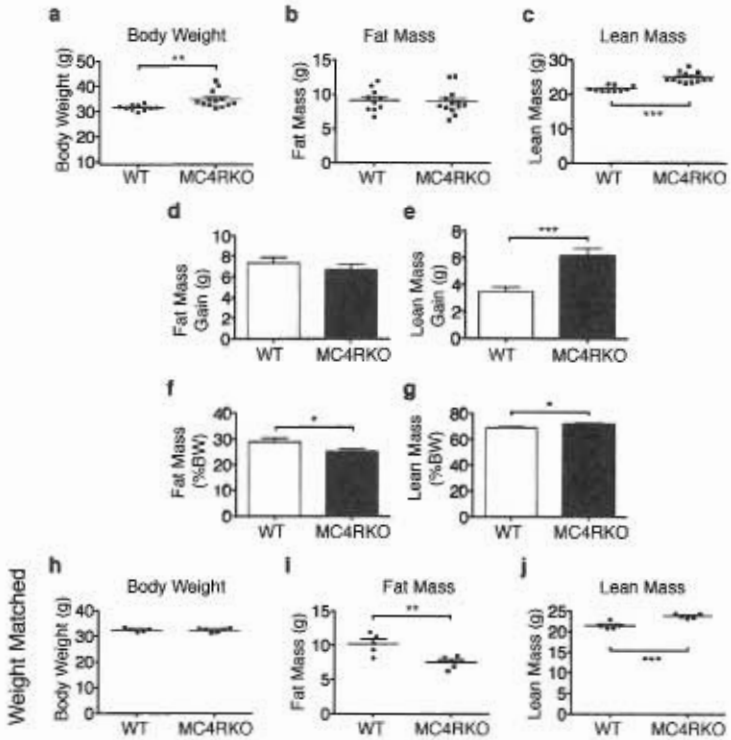

Figure 23. MC4RKO mice gain lean mass at a more rapid rate than diet-induced obese mice

8-week-old male WT mice (n= 10) age and weight matched to MC4RKO mice (n=13) were placed on high fat diet (HFD, 60% calories from fat) for 4 weeks until 12 weeks of age. MC4RKO mice were maintained on a low fat control diet during this time. (**a**) MC4RKO mice weighed more at 12 weeks of age than HFD fed mice. (**b**) MC4RKO mice have equivalent fat mass at 12 weeks of age compared with HFD fed mice. (**c**) MC4RKO mice have increased lean mass relative to HFD fed mice at 12 weeks of age. (**d**) Mice fed a HFD for 4 weeks gain an equivalent amount of fat mass as MC4RKO mice. (**e**) MC4RKO mice gain more lean mass than mice fed a HFD for 4 weeks. (**f**) After 4 weeks of HFD, WT mice have an increased % body fat, (**g**) and a decreased % lean mass compared with MC4RKO mice. (**h**) The 5 heaviest HFD fed mice and the 5 lightest MC4RKO mice were matched for body weight. (**i**) Weight matched MC4RKO mice have decreased fat mass (**j**) and increased lean mass. Data represented as mean ± s.e.m. *=P<0.05, **= P<0.01, ***=P<0.001 as calculated by unpaired t-test.

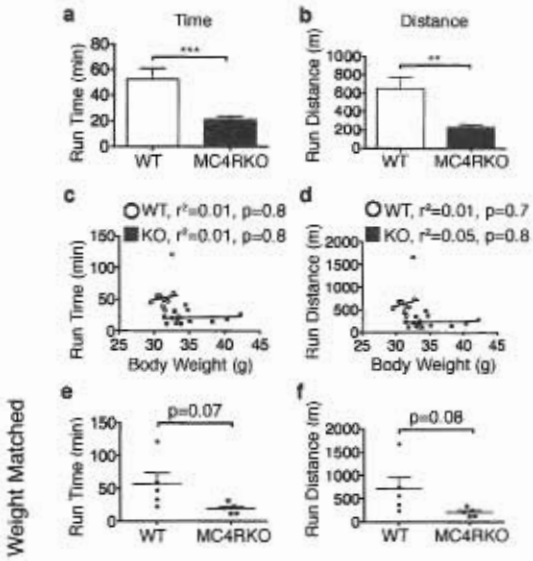

Figure 24. Deficiency of the type 4 melanocortin receptor results in impaired exercise performance despite increasing lean body mass

8-week-old male WT mice (n= 10) age and weight matched to MC4RKO mice (n=13) were placed on high fat diet (HFD, 60% calories from fat) for 4 weeks until 12 weeks of age. MC4RKO mice were maintained on a low fat control diet during this time. After 4 weeks, WT and MC4RKO mice were subjected to a treadmill endurance test. (**a**) MC4RKO showed a significantly attenuated run time (**b**) and run distance compared with WT mice. (**c**) There was no significant correlation between run time or (**d**) run distance and body weight. (**e**) Run time and (**f**) run distance for weight matched WT and MC4RKO mice. Data represented as mean ± s.e.m. **= P<0.01, ***=P<0.001 as calculated by unpaired t-test.

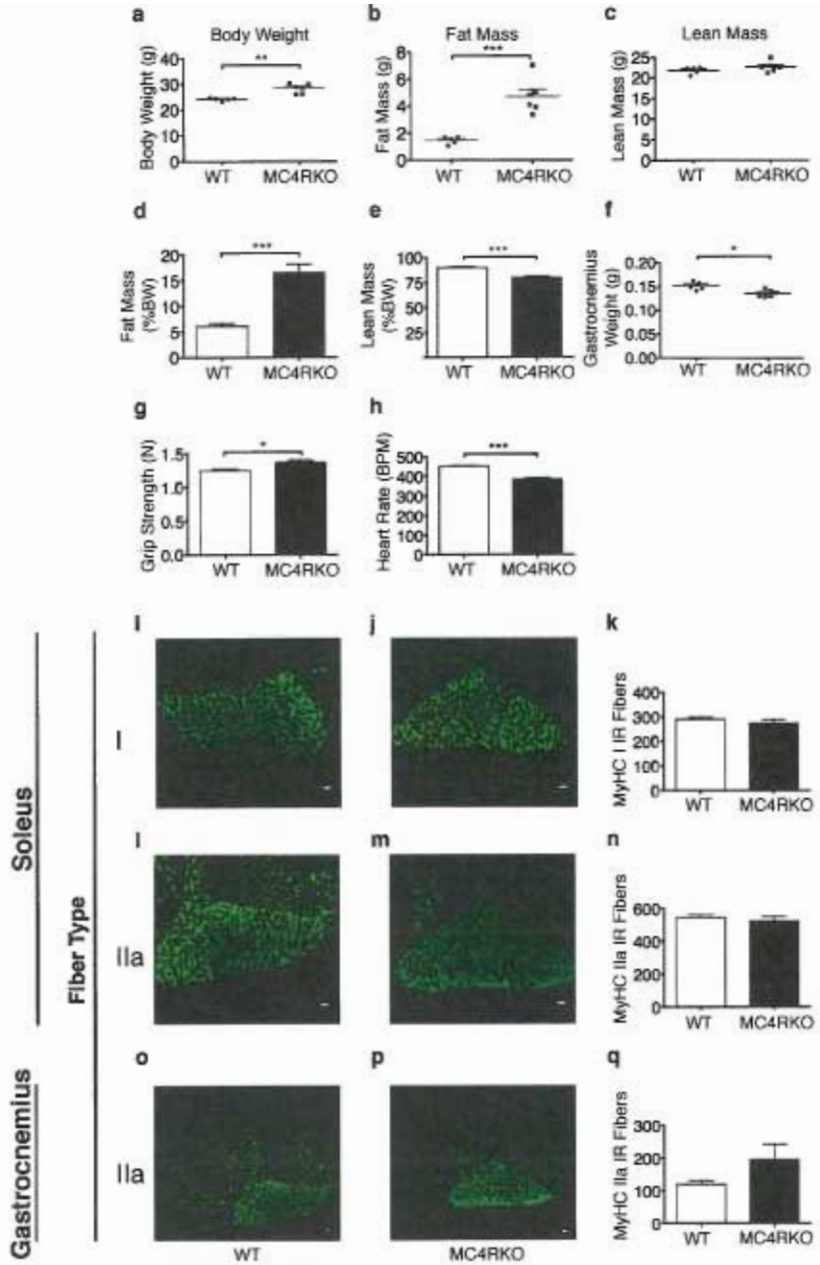

Figure 25. Mice lacking the type 4 melanocortin receptor have decreased muscle mass, increased grip strength and normal muscle fiber type distribution with a decreased resting heart rate

(**a**) Body weight in 11-week old male WT (n=5) and MC4RKO (n=6) mice. (**b**) Fat mass was significantly increased in MC4RKO mice without changes in (**c**) lean mass. (**d**) Fat mass as a percentage of total body weight was increased in the MC4RKO mice while (**e**) percent lean mass was decreased. (**f**) Gastrocnemius weight was decreased in MC4RKO mice. (**g**) Grip

strength was increased in MC4RKO mice. (**h**) Resting heart rate was decreased in MC4RKO mice. (**i-k**) No differences were seen in type I fiber number in the soleus, (**l-n**) type IIa fibers in the soleus or (**o-q**) type IIa fibers in the gastrocnemius.

Figure 26. Trabecular bone microarchitecture of WT and MC4RKO mice at 40 weeks. Two-dimensional frontal planar μCT images of the fifth vertebral body were obtained as described in the Methods sections

Table 5

Age = 20 Weeks		WT	MC4RKO	*p* value
Whole Body				
	Weight (g)	22.2 ± 0.3	31.5 ± 1.5	< 0.0001
	Length (cm)	9.51 ± 0.10	9.68 ± 0.09	NS
	BMD (mg/cm^2)	49.2 ± 0.4	52.0 ± 0.8	< 0.05
Femur				
	Length (mm)	15.5 ± 0.01	15.9 ± 0.01	NS
	BMD (mg/cm^2)	48.7 ± 0.5	54.1 ± 1.0	< 0.0005
	Ct. Ar. (mm^2)	0.68 ± 0.01	0.72 ± 0.03	NS
	Ct. Th. (mm)	0.16 ± 0.003	0.17 ± 0.006	NS
	Ixx (mm^4)	0.10 ± 0.004	0.11 ± 0.007	NS
	Ult. Force (N)	15.4 ± 0.6	17.6 ± 1.2	NS
	Stiffness (N/mm)	100.3 ± 2.4	105.9 ± 5.0	NS

Table 5: Skeletal phenotype of WT and MC4RKO mice at 20 weeks

The skeletal phenotype of twenty-week-old female WT (n=14) and MC4RKO mice (n=9) was examined by DEXA and microtomography. Bone strength was determined by 3 point bending to failure. Values are represented as mean ± SEM. Statistical significance was assessed by Students t-test, with significant differences assigned a p value <0.05.

Table 6

Age = 40 weeks		WT	MC4RKO	*p* value
Whole Body				
	Weight (g)	24.5 ± 0.4	61.4 ± 2.1	< 0.0001
	Length (cm)	9.44 ± 0.07	10.3 ± 0.05	< 0.0001
Femur				
	Length (mm)	16.1 ± 0.05	16.2 ± 0.05	NS
	BMD (mg/cm^2)	51.7 ± 0.8	57.6 ± 0.6	< 0.0001
	Ct. Ar. (mm^2)	0.76 ± 0.02	0.91 ± 0.02	< 0.0001
	Ct. Th. (mm)	0.18 ± 0.004	0.20 ± 0.004	< 0.0001
	Ixx (mm^4)	0.12 ± 0.004	0.18 ± 0.006	< 0.0001
	Ult. Force (N)	19.5 ± 0.6	25.0 ± 0.8	< 0.0001
	Stiffness (N/mm)	117.4 ± 4.5	142.5 ± 4.3	< 0.0001
L5 Vertebra				
	BMD (mg/cm^2)	43.1 ± 0.6	48.8 ± 0.7	< 0.0001
	BV/TV (%)	20.7 ± 0.8	25.7 ± 1.0	< 0.005
	Tb No	4.4 ± 0.1	3.4 ± 0.1	< 0.0001
	Tb Th	61.5 ± 0.7	60.8 ± 1.0	N.S.
	Conn Dens	135 ± 7	86 ± 7	< 0.0001

Table 6: Skeletal phenotype of WT and MC4RKO mice at 40 weeks

The skeletal phenotype of forty-week-old female WT (n=11) and MC4RKO mice (n=12) was examined by DEXA and microtomography. Bone strength was determined by 3 point bending to failure. Vertebral morphometric variables describing bone microstructure were computed using direct 3D methods. Values are represented as mean ± SEM. Statistical significance was assessed by Students t-test, with significant differences assigned a p value <0.05.

CHAPTER 6

SUMMARY AND CONCLUSIONS

Over the past 30 years the mechanisms of cachexia have been extensively investigated. One of the conclusions of this work is that inflammation is an integral component of cachexia. The various features of cachexia have been explained by the inflammatory cytokine action on distinct anatomic and cellular substrates. For example, muscle atrophy has been largely presumed to be dependent on the direct action of inflammatory cytokines on muscle. Sickness behavior too has been presumed to be the result of cytokines acting on distinct neuronal populations to control different facets of the behavioral response to inflammation. Completely dissociated control of the behavioral and metabolic responses to inflammation is not consistent however with growing evidence of an integrated, top-down control of behavior and metabolism by the brain. The hormone leptin (which based on its homology to inflammatory cytokines, would likely have been classified as an interleukin had it been discovered by an immunologist) regulates metabolism by acting predominantly in the brain. By analogy, it seems logical to assume that other cytokines similarly regulate metabolism via CNS action. The purpose of the experiments described in this thesis was twofold. The first was to describe pathway by which inflammation in the brain regulates lean body and muscle mass. The second was to begin to define the CNS substrates for cachexia both with regard to the regulation of skeletal muscle and sickness behavior.

The Central Melanocortin System as a Neural Substrate for Cachexia

At the outset of this work, one of our primary objectives was to understand the basis of lean mass preservation in cachectic animals treated with melanocortin antagonists. Our hypothesis was that inflammation resulted in increased melanocortin signaling, activating a neural pathway that increased the catabolism of skeletal muscle (potentially via the autonomic nervous system). Given that POMC and AgRP

neurons both express IL-1R1 (186, 187), they represented prime candidates as the neural substrate for inflammation-induced muscle wasting. This premise appeared to be on strong ground. Skeletal muscle constitutes a large component of lean mass, therefore protection of lean mass by melanocortin antagonism should be born out in a preservation of muscle mass. Mice lacking the MC4R have increased linear growth (275), and MC4R deficient humans have increased lean mass (298), suggesting that melanocortins tonically restrain skeletal muscle mass. We therefore undertook a series of studies to test this hypothesis, which are distributed throughout the chapters of this thesis. Although the melanocortin system clearly regulates food intake, the muscle mass in cachexia is lost independent from decreased food intake. Therefore, we expected that the process of melanocortin regulation of muscle mass would be independent to some degree from food intake. However, the melanocortin agonist MTII failed to increase MAFbx and MuRF1 when food intake was removed as a variable (Figure 5). Furthermore, no food intake independent loss of muscle mass was observed when MTII was administered chronically. Based on these data, we were forced to conclude that melanocortin signaling alone is not sufficient to induce muscle atrophy. These results are consistent published data in rats that underwent chronic MTII or melanocortin antagonist treatment. While MTII decreased lean mass, and melanocortin antagonism increased lean mass, both of these effects were shown to be dependent entirely on food intake (232).

Despite these data, it remained possible that melanocortin signaling still plays an integral role in mediating muscle catabolism. However, MC4RKO mice show an equal induction of atrophy genes in response to i.c.v. IL-1β, demonstrating that signaling at the MC4R is not required for the catabolic response to acute inflammation (Figure 5). To examine the role of melanocortin signaling in a model of chronic inflammation, we implanted rats with a syngenic sarcoma known to produce cachexia

and muscle atrophy. On the first day that anorexia was observable, we began daily i.c.v. treatment with the melanocortin antagonist AgRP. This treatment significantly increased food intake in tumor bearing animals on all experimental days except the day of sacrifice, when food intake dropped precipitously in all tumor-bearing animals (Figure 28, Appendix A). This is a common finding in experimental models of cancer cachexia, where progressive anemia and other non-specific factors can result in multisystem organ failure on the final days of experiments. Therefore, every effort is made to terminate the experiment prior to reaching this point, as it is generally believed that the results are not meaningful at this stage. However, despite this fact, review of this data does lead to some meaningful conclusions. In spite of the final day of the experiment, AgRP treated tumor-bearing animals showed a significant improvement in lean mass compared with Veh treated control animals. Muscle mass however, was equally reduced in both groups irrespective of AgRP treatment. MAFbx and MuRF1 were also equally induced in both AgRP and Veh treated tumor-bearing animals. The protection of lean mass by melanocortin antagonism reproduces previous work in our lab and others (35, 36). However, the muscle data would suggest that improvements in lean mass are not necessarily correlated with changes in muscle mass. These data suggest (but do not prove, given the experimental caveats) that melanocortin antagonism preserves lean mass but not muscle mass in cancer cachexia. In a separate experiment, chronic renal failure was induced in rats by 5/6th nephrectomy. These rats were then treated with ghrelin, a major function of which is to activate AgRP neurons, significantly improving food intake. Ghrelin treatment significantly improved body weight and lean mass in these animals (216). However, when ghrelin treated, nephrectomized animals were pair fed to saline treated controls, this protection of lean mass was lost. Furthermore, skeletal muscle mass was not improved by ghrelin independent from food intake (Figure 29, Appendix

A). This finding of food intake dependent changes in muscle mass was not included in the original publication, but further reinforces that the therapeutic properties of ghrelin rely on increased food intake.

Simultaneous to the studies described above, we undertook an effort to characterize the lean and skeletal muscle mass of MC4RKO mice, which is described in chapter 5. It is commonly stated in passing that MC4R deficiency leads to increased lean mass. Although no characterization of lean mass in these animals has been performed, they do display increased linear growth, which is the source of these claims (275). It is logical that a larger animal would have more lean mass, yet this does not implicate the MC4R in playing a specific role in restraining muscle mass. Consistent with the literature involving the MC4R and adipose tissue, the first difference that arises in MC4RKO mice as they grow is an increase in fat mass (Figure 21 and (232)). As they grow, they accumulate lean mass at an accelerated rate relative to wild type mice, and even DIO mice (Figure 23). Despite the frequently cited relationship between lean mass and muscle mass, MC4RKO mice do not demonstrate increased skeletal muscle mass. This finding, and the data discussed above showing divergence of lean mass and muscle mass in the setting of melanocortin blockade suggest that caution should be used when interpreting alterations in body composition in isolation.

Muscle wasting in cachexia has both nutritionally dependent and independent components. Since the discovery that parenteral nutrition does not completely reverse atrophy, the field has focused on disease mechanisms (and therapeutics) for food intake-independent muscle wasting. Activation of the central melanocortin system represented a promising mechanistic explanation for disease-related hypermetabolism. However, the data presented in this thesis do not support the concept that hyperactivity of the melanocortin system underlies food intake-

independent loss of muscle mass. On the other hand, the data do support a mechanism whereby melanocortin signaling underlies decreases in appetite in cachexia and in this way influences lean body mass. These revelations do not alter the enthusiasm for therapy aimed at decreasing melanocortin signaling in cachexia. Indeed, clinical trial data shows that ghrelin administration can significantly improve muscle strength in cachexia and will likely be widely useful to combat disease associated wasting (314, 315).

Cytokine Signaling on Neurons in the Generation of Sickness Behavior

Previous work from our lab has demonstrated that both POMC and AgRP neurons, which regulate signaling at the MC4R, express the IL-1RI, and modulate their activity in response to IL-1β (186, 187). It was somewhat surprising therefore, that deletion of MyD88 from all neurons did not prevent IL-1β-induced anorexia nor did it alter any other measure of sickness behavior. MyD88KO mice are completely resistant to the behavioral effects of IL-1β, even when IL-1β is applied directly into the brain, demonstrating the necessity of MyD88 for this response. This data is clearly in conflict with a model where cytokines act directly on neurons to mediate behavior. While the explanation that is most consistent with the data is presented in Chapter 3, several other potential explanations exist which need to be expanded upon. Firstly, it is possible that nestin-cre mediated recombination of the MyD88 allele was incomplete, and that residual MyD88 is present and sufficient to induce normal behavioral responses to inflammation. This is a difficult possibility to address, as MyD88 immunohistochemistry is not routinely performed. In situ hybridization represents another possible technique to detect MyD88 expression. However despite several attempts with multiple different riboprobes, we were also unable to detect MyD88 expression in a reliable or convincing manner. Data from the td tomato

reporter line however, shows that recombinase activity is present broadly across the CNS. In no case did we observe any evidence of cells labeling with the neuronal marker NeuN that did not also express the td tomato protein. While this is not definitive proof of recombination at the MyD88 locus in all neurons, it does provide evidence that nestin-cre does not have anatomically restricted expression. The nestin cre mouse has been previously reported to recombine with varied efficiency at different floxed alleles when assessed by western blot on tissue homogenates (316, 317). The MyD88$^{\Delta CNS}$ mouse has been previously reported and western blot showed an almost complete loss of MyD88 protein in brain homogenates that contain both cells derived from nestin positive and negative sources (290). Therefore, apparent differences in recombination with different floxed alleles are likely the result of the starting abundance of the targeted gene in nestin positive vs negative cells rather than actual differences in recombination efficiency. It is unclear what fraction of residual MyD88 is sufficient for IL-1β to induce behavioral changes and therefore it is impossible to rule out incomplete deletion of MyD88 as an explanation. However, the floxed MyD88 line we utilized has produced a phenotype when crossed to many other cre lines (318-320), and the nestin-cre driver has been successfully utilized to delete numerous floxed alleles sufficiently to produce a phenotype (316, 321). Finally, these lines have been previously intercrossed, producing a metabolic phenotype when the resulting mouse was challenged with a high fat diet (290). Therefore, while incomplete deletion remains a possibility, it is not among the most likely explanations for these data.

The second possible explanation for the failure of MyD88$^{\Delta CNS}$ mice to resist IL-1β-induced behavioral changes is developmental compensation. This is an argument that is often evoked when data from knockout mice fail to support the existing paradigm about the function of a gene. This term has become a catch-all for

adaptations that occur during the course of development that mask or alter the effect of gene loss of function. The clearest example of compensation is when a highly related member of a gene family takes over for the function of the lost gene. In hypothalamic neuroscience, one of the most commonly cited examples of this is the lack of a phenotype of the AgRP knockout mouse, which would be expected to be relatively lean (322). Despite this, ablation of AgRP neurons results in significant decreases in food intake and loss of body weight in adult animals (323). However, in early postnatal animals, AgRP neuron ablation was not accompanied by effects on ingestive behavior or body weight, suggesting that compensation can occur early in development. It has later become evident that AgRP neurons are also GABAergic, and that this property is likely more critical for the effects of AgRP neuronal ablation on feeding behavior, than the neuropeptide itself (324, 325). While this example makes it clear that neuronal networks can compensate for perturbations that occur early in life, the mechanisms by which this occurs are not as straight forward as one gene compensating for another. When we consider the case of nestin-cre mediated deletion of MyD88 only in the CNS, it is difficult to explain how developmental compensation could be responsible for the observed results. It is possible that MyD88 loss in neurons is compensated for by a MyD88 independent pathway for IL-1β signaling in neurons. Yet no evidence exists for such compensation in the whole body MyD88KO. As a result, in order to argue developmental compensation in the $MyD88^{\Delta CNS}$ mouse, one evokes a mechanism in which MyD88 loss in neurons can be compensated for only in the presence of MyD88 in other cell types. While this is certainly possible it is not a straightforward explanation and would require some form experimental proof to validate it.

Given the unsatisfactory nature of the above explanations, we are left with the original conclusion of the data. It appears that cytokines do not mediate sickness

behavior via direct action on neurons, or at least that a MyD88 dependent amplification step is required in another cell type. The only cell types that we found conclusively to not express cre recombinase within the CNS are endothelium and microglia. As a result, it appears likely that one of these two cell types is the target of MyD88 dependent cytokine action in mediating sickness behavior.

Understanding the Role of Glucocorticoids in Muscle Wasting

In papers describing the inflammatory basis of muscle atrophy, glucocorticoids are frequently mentioned as likely contributors to the loss of muscle mass. However, little effort has been made in the last decade to account for their contribution to inflammation-induced wasting. In the early 90s, several studies were performed that attempted to assess the contribution of glucocorticoids to cytokine-induced muscle wasting. It was discovered that pharmacologic glucocorticoid antagonism with mifepristone blocked the changes in protein turnover in response to TNF administration (285). However, the increase in skeletal muscle protein breakdown seen in response to IL-1α administration was not blocked by mifepristone or adrenalectomy (285, 286). These studies are confounded by the fact that both adrenalectomy and mifepristone result in systemic glucocorticoid insufficiency. This point is emphasized by the fact that 33% of animals treated with both mifepristone and IL-1α died during the course of the 18 h experiment, while no mortality was noted when either agent was given alone. Given that glucocorticoids are necessary for maintaining vasomotor tone during inflammation, it is likely this mortality was the result of cardiovascular collapse. The survivors were likely near death at the time this result was obtained; therefore it is difficult to attribute any significant meaning to these results. The same group subsequently went on to demonstrate a role for

glucocorticoids in mediating the changes in muscle protein turnover in sepsis (93). Interestingly, mortality was not reported in this study.

Simultaneous to the work on the role of glucocorticoids in inflammation-induced muscle atrophy, others were describing a role for glucocorticoids in mediating muscle atrophy in response to acute diabetes or metabolic acidosis (96, 326). One of the fundamental conclusions of this work was that elevated levels of glucocorticoids were necessary but not sufficient to explain muscle wasting. The experimental evidence for this concept was that adrenalectomy prevented muscle wasting in response to acidosis or acute diabetes. However, administration of low-dose dexamethasone restored wasting in both models. This dose of dexamethasone alone however, was insufficient to induce wasting in healthy animals. The authors argue that this dose of dexamethasone replicates endogenous levels of glucocorticoids present in stressed rodents. The basis for this is the work of Slusher and Roberts, who measured the production of corticosterone in anesthetized rats (327). This endogenous corticosterone production was then converted into a dexamethasone dose by accounting for a 265:1 relative potency of dexamethasone to corticosterone, normalized to rat body weight, and injected as a daily bolus dose in mice. However, they provided no evidence that this level of dexamethasone approximated the level seen in their disease models (i.e. measured ACTH levels). Therefore, the only conclusion that can be drawn is that acidosis and diabetes are states of increased sensitivity to the catabolic effects of low-dose dexamethasone. The results from these studies potentially shed some light on the lack of interest in glucocorticoids as mediators of inflammation-induced muscle wasting. While glucocorticoids appear to provide a component of the catabolic stimulus these papers argue that there are other factors that are required for the atrophy process to occur.

It should not be surprising therefore, that the catabolic effects of centrally administered IL-1β are also dependent on an intact HPA axis (Figure 7). Given the modest levels of glucocorticoids found after central IL-1β administration (Table 1, 2), and the precedent set in the literature, it seemed more likely that glucocorticoids were only a part of the mechanism behind central inflammation-induced muscle wasting. We therefore expected that central inflammation would also be a state of increased glucocorticoid sensitivity, mediated by some as-yet un-described factor. It was surprising therefore when we found that low-dose dexamethasone failed to restore the normal atrophy gene response to ADX mice treated i.c.v. with IL-1β, although subtle effects were seen (Figure 30, Appendix A). We therefore treated animals with sustained release corticosterone pellets allowing us to measure the resultant circulating levels and compare with those obtained during inflammation. We found that circulating levels of corticosterone equivalent to those seen after i.c.v. IL-1β infusion were sufficient to promote dramatic muscle wasting (Figure 9). These levels of corticosterone were also comparable to those found in many states associated with muscle wasting including endotoxemia, cancer and sepsis (115, 127, 328). This result suggests that glucocorticoids might not only be necessary but also sufficient to explain a large portion of muscle wasting in cachexia.

As was mentioned in the introduction, the generally held conclusion has been that glucocorticoids, despite being found at elevated levels, do not participate in muscle atrophy in cancer. However, the ramifications of our corticosterone treatment study suggest that the data excluding this possibility be examined in more detail. Both studies that examined this question utilized a rat model of cancer cachexia: the YAH130 ascites hepatoma, which grows aggressively in the peritoneal cavity. Death from this tumor will result within one week of inoculation, and food intake (in our hands, a very sensitive metric of the animals general well being) is significantly

suppressed (40% reduction on day 3, 60-70% reduction by day 7) starting within 1-2 days of inoculation. Furthermore, despite widespread use, the rapid intraperitoneal growth of this tumor complicates the interpretation of results due to direct interference with organ function. One of the studies implanted tumors in adrenalectomized (ADX) animals, and demonstrated a trend toward the protection muscle protein content by ADX (98). Adrenalectomy exerts powerful effects on body weight and body composition alone, yet ADX animals without tumors were not used as controls, nor were the appropriate sham-operated control animals. Furthermore, ADX animals demonstrate earlier mortality in response to starvation, presumably due to an inability to mobilize energy reserves. The maintenance of cardiovascular stability in response to inflammatory challenge is also compromised in ADX animals. Given all the confounding factors present in this study, the potential importance of glucocorticoids is highlighted by the marginal protection of muscle mass seen in ADX animals. The second study utilized the glucocorticoid/progesterone antagonist Mifepristone, and also used the YAH130 hepatoma tumor (97). In our hands, and in the hands of others, the effects of mifepristone are relatively subtle compared with adrenalectomy (76, 279). Mifepristone treatment never completely blocks the effects of increased endogenous glucocorticoids on muscle, but it does prevent muscle catabolism in response to exogenous dexamethasone administration (329). Furthermore, at the time that Llovera et al. published their study, it was assumed that the half life of mifepristone in rodents was similar to that in humans (~24 hours, (330)), and dosing was extrapolated from studies examining shorter time points (93). It was subsequently discovered that the half life of mifepristone is only 1-2 h in rodents (271) and as a result the once daily dosing in this study may have been sub-therapeutic. Finally, the authors of this study performed no measurement of glucocorticoid receptor

occupancy and no positive control for the success of their glucocorticoid blockade, even further complicating the interpretation of these studies.

While adrenalectomy prevents the acute changes atrophy gene expression associated with LPS treatment (Figure 9), the aforementioned limitations associated with adrenal insufficiency in inflammation prevent the study of longer time-points and therefore actual atrophy using adrenalectomized animals. Our muscle specific GR knockout mice provide just such an opportunity and allowed us to demonstrate that inflammation-induced myofibrillar atrophy requires glucocorticoid signaling to occur. Ultimately, the goal of generating the mGRKO mouse was to explore the contribution of glucocorticoids to muscle wasting in a more relevant model of human disease than LPS injection. While several attempts were made at models of both cancer cachexia and polymicrobial sepsis, the inherent difficulties of the model and time constraints prevented us from having a completed answer to this question at the time of the writing of this thesis. While the results from these experiments are included in Appendix B as a reference, at this time, no definitive statements can be made about the involvement of glucocorticoids in muscle wasting in either disease state.

A Role for Direct Cytokine Action on Skeletal Myocytes in Mediating Atrophy

It was somewhat surprising to find that MyD88 expression in muscle was neither necessary nor sufficient for LPS-induced muscle atrophy (Figure 14). While the lack of an LPS response in the MyD88 knockout mouse (Figure 13) is likely the result of impaired HPA axis activation, these findings must still be resolved with the *in vitro* data from other groups. Both IL-1β and LPS have been shown to directly promote atrophy in cell culture, and this has been shown to be dependent on NFκB and p38 MAPK activation of MuRF1 and MAFbx transcription respectively (99, 106). The direct action of LPS on skeletal muscle to alter myocyte metabolism is the subject

of an extensive number of reviews and primary research articles (80, 331). LPS accumulates at significant levels in muscle after parenteral administration demonstrating that sufficient ligand should be present to activate TLR4 signaling (332). Therefore, the MyD88 reexpression experiment was designed to simulate these *in vitro* conditions where the skeletal myocyte was the only possible signaling location for LPS. Our findings demonstrate that whatever metabolic actions LPS may have by direct signaling in skeletal muscle *in vivo*, activation of MAFbx gene expression and bulk atrophy are not the result of direct action.

An explanation for the lack of a discernible effect of the loss of MyD88 in skeletal muscle is that other cytokines such as TNF can activate p38 and NFκB independent of MyD88. Such cytokines are induced by LPS and may be able to compensate for a loss of IL-1/TLR signaling in muscle (100, 105). The simplest experiment would be to examine p38 and NFκB activation in the muscle of mMyD88KO mice after LPS treatment. However, NFκB activation seems to be inexorably linked to muscle atrophy. Every form of atrophy examined including denervation and disuse all involve NFκB signaling (104, 268, 269, 333). However, no evidence for classic inflammatory signaling has been found in muscle undergoing disuse atrophy (334). Because of this fundamental association between NFκB and atrophy, it is very likely that LPS increases NFκB activity in the muscle of mMyD88KO mice. Yet, such a finding would only reinforce this association and would do little to expand upon the mechanisms of inflammation-induced atrophy.

The E3 ligase TRAF6 is also part of the canonical TLR/IL-1R signaling pathway downstream of MyD88. Muscle specific TRAF6 knockout mice are completely resistant to tumor-induced muscle wasting (267), again supporting the notion of cytokines acting directly on skeletal muscle to mediate atrophy in cachexia. However, like skeletal muscle specific NFκB inhibition, muscle TRAF6KO mice resist

denervation-induced wasting as well, which again is not classically thought to depend on systemic inflammation. This finding makes the lack of an atrophy resistant phenotype in the mMyD88KO mouse even more remarkable. Furthermore, it suggests that atrophy, independent from its root cause, requires activation of the TLR/IL-1R signaling pathway upstream of TRAF6 but downstream of MyD88. However, the precise constituents of this pathway, or the mechanism by which they are activated remain unknown at this time.

One possible candidate is the generation of reactive oxygen species (ROS), which occurs in atrophy triggered by denervation, angiotensin II infusion or inflammatory cytokines (335-338). Importantly, ROS have the ability to activate both NFκB and Foxo signaling (337, 339) pointing to a potential causative role in atrophy. A plausible resolution to the conflict between our *in vivo* data with the *in vitro* cytokine data is that inflammatory signaling is required under both conditions, but the point of activation differs. While *in vitro* cytokines and LPS can activate inflammatory pathways, this may occur via alternate mechanisms *in vivo*. It is possible that culture conditions do not accurately reflect the tissue concentration of cytokines that are seen in animals undergoing inflammatory challenge, resulting in such experiments modeling pharmacology rather than physiology. Alternately, the immortalized cell lines (mouse C2C12 cells and rat L6 myoblasts) used for the vast majority of experiments may not be representative of mature skeletal muscle, even when differentiated. This potentially could result in alterations in cytokine/LPS sensitivity or altered receptor expression allowing for the activation of the TRAF6-NFκB pathway by direct engagement of cell surface inflammatory receptors. Indeed, cytokine application to adult muscles in explant culture fails to increase protein degradation, consistent with our data regarding direct cytokine action on muscle (340).

Interactions Between Inflammatory Glucocorticoids and Inflammatory Signaling Pathways

A fundamental contradiction arises from the finding that glucocorticoids are integral to the atrophy process in response to inflammation yet are generally regarded as antagonistic to inflammatory signaling. The classical view of GR signaling is that it transrepresses NFκB and AP-1 activity while simultaneously up regulating IκBα to shut off inflammatory gene expression (263, 341). However, both glucocorticoids and constitutive activation of NFκB signaling produce muscle atrophy (Figure 9 and (104)). Furthermore, dominant negative inhibition of NFκB signaling and deletion of the glucocorticoid receptor in skeletal muscle both prevent inflammation-induced atrophy (Figure 14 and (104)). Therefore, a full mechanistic description of the role of glucocorticoids in inflammatory muscle atrophy requires the resolution of this paradox.

There is some data to suggest that signaling in the TLR/IL-1R kinase cascade has effects independent from activation of NFκB. The transgenic methods that have demonstrated that NFκB activation is sufficient to produce muscle atrophy have relied on activating mutations of I kappa kinase-β (IKKβ) (104, 333). Interestingly, *in vitro* studies have shown that IKKβ mediates autophagy in response to nutrient deprivation independent from NFκB (125). Furthermore, liver specific deletion of IKKβ prevents starvation-induced autophagy in hepatocytes (124).

A second potentially more controversial possibility is that glucocorticoids activate NFκB in skeletal muscle. While certainly not consistent with the prevailing view, this idea has some merit. As the relationship between glucocorticoids and NFκB signaling has been largely worked out in immune cells, it is possible a distinct relationship exists in skeletal muscle. For some time it has been known that glucocorticoids also have the ability to stimulate the immune response (Reviewed in (342)) Glucocorticoids exhibit a U shaped curve with regard to concentration and

effect on inflammation. Low stress levels of glucocorticoids are pro-inflammatory while basal and high concentrations of glucocorticoids both exert restraining effects on the immune system. Part of this may be explained by the fact that cortisol and corticosterone bind both to the GR and to the mineralocorticoid receptor (MR). However, the MR has a 10 fold higher affinity for cortisol than does the GR. Given this difference in affinity the receptors are differentially occupied at lower concentrations of ligand. Once bound to cortisol, both the GR and MR bind the same consensus sequence in the promoters of target genes. Dramatically different transcriptional responses occur in response to GR vs. MR binding. While the GR transrepresses inflammatory genes, the MR is widely considered to be pro-inflammatory. While the inflammatory nature of MR signaling is less well described, there is abundant evidence from the heart failure literature showing that MR signaling is an important mediator of renal inflammation (343-346). Interestingly, MR signaling is proposed to activate NFκB via the generation of reactive oxygen species (346, 347). An alternate mechanism for NFκB activation is serum and glucocorticoid-inducible kinase-1 (SGK1), which activates NFκB signaling in response to aldosterone treatment in the renal tubular epithelium (343, 348). While best characterized with its role in regulating ion flux, SGK1 is expressed in a multitude of tissues and exerts diverse control over a multitude of processes (Reviewed in (349)). SGK1 phosphorylates IKKα, creating a potential mechanistic link between cortisol and NFκB activation (350). However, a purely MR dependent mechanism would not be consistent with the data obtained from the mGRKO mouse (Figure 12, 14). However, the GR and MR are known to heterodimerize, suggesting that some of the effects seen in the mGRKO mice may be dependent on the MR (351). Irrespective of the MR, the pure glucocorticoid agonist dexamethasone potently induces SGK1, and in certain situations promotes the generation of ROS and also induces muscle atrophy (352-354). At this time, no data

exists regarding the relationship between NFκB and glucocorticoids in skeletal muscle. The mGRKO mouse represents an ideal system to explore this relationship and studies are currently ongoing to investigate this potential interaction. To summarize the TLR4/IL-1R signaling pathways discussed throughout the last few sections and demonstrate the potential mechanisms for GR crosstalk with inflammatory pathways, a summary figure is presented below (Figure 27).

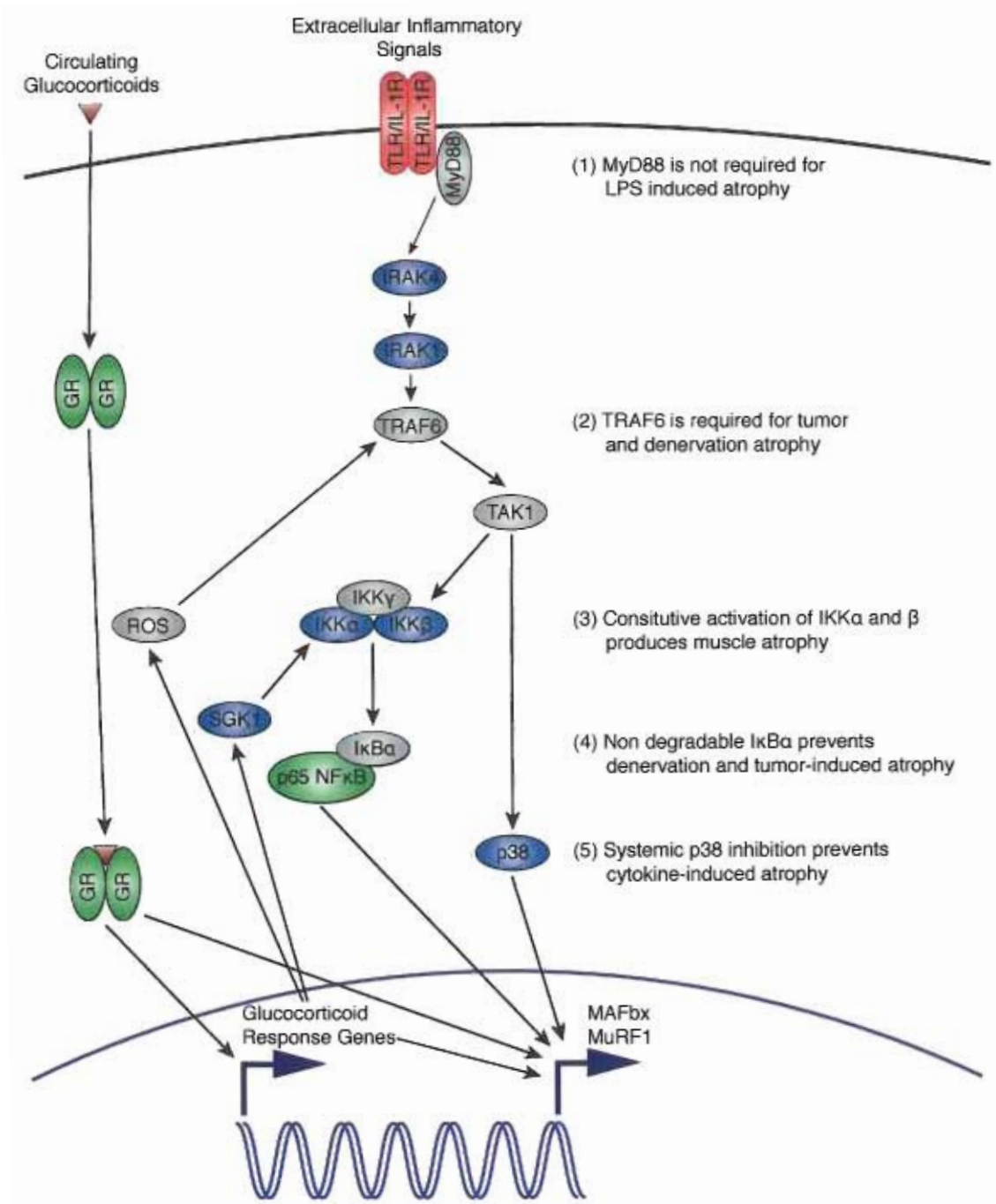
Extracellular Inflammatory Signals
Circulating Glucocorticoids
TLR/IL-1R
TLR/IL-1R
MyD88
(1) MyD88 is not required for LPS induced atrophy
IRAK4
IRAK1
GR
GR
TRAF6
(2) TRAF6 is required for tumor and denervation atrophy
TAK1
IKKγ
ROS
IKKα
IKKβ
(3) Consitutive activation of IKKα and β produces muscle atrophy
SGK1
IκBα
p65 NFκB
(4) Non degradable IκBα prevents denervation and tumor-induced atrophy
p38
(5) Systemic p38 inhibition prevents cytokine-induced atrophy
GR
GR
Glucocorticoid Response Genes
MAFbx
MuRF1

Figure 27. TLR/IL-1R signaling in muscle atrophy

In response to extracellular inflammatory signals, MyD88 is recruited to membrane bound IL-1 and Toll-like receptors. The resulting kinase cascade culminates in the activation of NFκB and p38 MAPK. (1) Muscle specific deletion of MyD88 does not prevent inflammation-induced atrophy (Figure 14). (2) Loss of TRAF6 in skeletal muscle prevents muscle atrophy in response to denervation and tumor growth (267). (3) Constitutive activation of the IKK complex produces atrophy (104, 333). (4) Dominant negative inhibition of IκBα prevents denervation and tumor-induced atrophy. (5) Systemic inhibition of p38 MAPK inhibits LPS-induced atrophy (106). Glucocorticoids mediate atrophy via direct transactivation of MuRF1 and glucocorticoid response genes such as KLF15 that have the ability to directly transactivate the E3 Ligases. In addition, a number of glucocorticoid response genes have the potential to enhance inflammatory signaling either via the direct activation of the IKK complex or via the production of ROS.

Therapeutic Potential of Targeting Glucocorticoids in Cachexia

As described in previous sections, systemic inhibition of glucocorticoid signaling would likely result in a significant number of untoward side effects in the setting of inflammation. However, agents are currently under development that have the potential to block only the catabolic effects of endogenous glucocorticoids. It was observed that a point mutation in GR that prevents homodimerization (GR*dim*) and the stimulation of the classical GRE, is still able to transrepress NFκB (355, 356). This lead to the hypothesis that the negative side effects of glucocorticoids are mediated by transactivation of the GR, while the anti-inflammatory properties are mediated by transrepression. Consistent with this, we observed that the majority of significantly regulated genes identified in our array analysis were increased rather than decreased in expression (Figure 6). It has become evident that this model is overly simplistic, as some anti-inflammatory genes are under the stimulatory control of glucocorticoids and the GR*dim* mouse still experiences some side effects from glucocorticoid treatment (357, 358). Regardless, the finding that the effects of glucocorticoids could be separated on the basis of transactivation and transrepression led to the development of a series of ligands for the glucocorticoid receptor known as selective glucocorticoid receptor modifiers (SERGMs) with the ability to differentially modify these parameters (359-362), (Recently reviewed in ((363)). The binding of each of these agents to the glucocorticoid receptor results in a distinct combination of DNA binding, dimerization and recruitment of cofactors to target gene promoters (362, 364-366).

The ability of such compounds to selectively maintain anti-inflammatory activity while minimizing negative side effects is exciting with regard to their use in the treatment of inflammatory muscle atrophy. While, systemic blockade of glucocorticoid receptors using the classic antagonist mifepristone leads to unfavorable side effects in the setting of inflammation, SERGMs have the potential to both be both anti-

inflammatory and anti-catabolic. By inhibiting inflammatory cytokine production, a SERGM would address the proximal cause of muscle wasting. By occupying the GR, a SERGM would also block access of endogenous glucocorticoids to the receptor, preventing glucocorticoid-mediated transactivation of atrophy genes. Despite the promise of such agents, caution must be used in this approach. While none of the agents described have been examined with regard to muscle wasting, at least one of these compounds still results in weight loss (367). The cause of weight loss in this report however was not described and may or may not be related to muscle atrophy. More concerning is a recent report demonstrating that dexamethasone treatment fails to induce MuRF1 gene expression in GR*dim* mice, but induces equal loss of muscle mass to that seen in WT mice (84). It is unclear how this situation relates to the effect of endogenous glucocorticoids on muscle owing to the innate differences between dexamethasone and corticosterone as well as the ever-confounding presence of the MR. Despite this, SERGMs represent an exciting class of novel therapeutic agents with the potential to reverse muscle wasting in response to endogenous glucocorticoids.

Summary

The work described in this thesis covers many aspects of the pathophysiology of cachexia. Its underlying goal however was to describe neural mechanism by which systemic inflammation is sensed by the brain using skeletal muscle as a physiologic readout. The major result of this work was something that had been understood for decades: inflammation elicits increases in circulating glucocorticoids. While this fact is not particularly novel, it led to a completely unexpected finding. The breakdown of skeletal muscle in response to inflammation appears to be driven primarily by glucocorticoids. There are two obvious ramifications of this finding. Firstly, while

muscle atrophy in response to inflammation has previously been considered to be a purely peripheral (outside the CNS) phenomenon, this can no longer be considered to be the case. It is clear that one of the major sites of cytokine action in mediating muscle atrophy is the CNS. Despite this, the precise neural target of cytokine signaling remains obscure, and is complicated by the overlapping nature of inflammatory cytokines. From a purely scientific standpoint an inflammatory loss-of-function experiment in a specific CNS cell type would be satisfying proof of the central regulation of muscle atrophy. Despite this, such an experiment may not ultimately prove possible owing to the redundant nature of inflammation. However, activation of the HPA axis appears to be a point of integration, leading to the second major ramification of these studies. If future work continues to support the mechanisms proposed here, glucocorticoids represent an exciting therapeutic target in cachexia.

REFERENCES

1. Tisdale MJ. Biology of cachexia. *J Natl Cancer Inst*. 1997;89(23):1763–1773.

2. Moley JF, Aamodt R, Rumble W, Kaye W, Norton JA. Body cell mass in cancer-bearing and anorexic patients. *JPEN J Parenter Enteral Nutr*. 1987;11(3):219–222.

3. Evans WJ et al. Cachexia: A new definition. *Clinical Nutrition*. 2008;27(6):793–799.

4. Bosaeus I, Daneryd P, Svanberg E, Lundholm K. Dietary intake and resting energy expenditure in relation to weight loss in unselected cancer patients. *Int J Cancer*. 2001;93(3):380–383.

5. DeWys WD. Weight loss and nutritional abnormalities in cancer patients: incidence, severity and significance. *Clinics in oncology*. 1986;5(2):251–261.

6. S J Wigmore CEPRARKCF. Changes in nutritional status associated with unresectable pancreatic cancer. *Br J Cancer*. 1997;75(1):106.

7. Anker SD et al. Wasting as independent risk factor for mortality in chronic heart failure. *Lancet*. 1997;349(9058):1050–1053.

8. Marinho LA, Rettori O, Vieira-Matos AN. Body weight loss as an indicator of breast cancer recurrence. *Acta Oncol*. 2001;40(7):832–837.

9. Tisdale MJ. Cachexia in cancer patients. *Nat Rev Cancer*. 2002;2(11):862–871.

10. Ross PJ et al. Do patients with weight loss have a worse outcome when undergoing chemotherapy for lung cancers? *Br J Cancer*. 2004;90(10):1905–1911.

11. Yee-Moon Wang A. Resting Energy Expenditure and Subsequent Mortality Risk in Peritoneal Dialysis Patients. *J Am Soc Nephrol*. 2004;15(12):3134–3143.

12. Kotler DP, Tierney AR, Wang J, Pierson RN. Magnitude of body-cell-mass depletion and the timing of death from wasting in AIDS. *Am J Clin Nutr*. 1989;50(3):444–447.

13. Inagaki J, Rodriguez V, Bodey GP. Proceedings: Causes of death in cancer patients. *Cancer*. 1974;33(2):568–573.

14. Zhou X et al. Reversal of cancer cachexia and muscle wasting by ActRIIB antagonism leads to prolonged survival. *Cell*. 2010;142(4):531–543.

15. Levine B, Kalman J, Mayer L, Fillit HM, Packer M. Elevated circulating levels of tumor necrosis factor in severe chronic heart failure. *N Engl J Med*. 1990;323(4):236–241.

16. Torre-Amione G et al. Proinflammatory cytokine levels in patients with depressed left ventricular ejection fraction: a report from the Studies of Left Ventricular Dysfunction (SOLVD). *J Am Coll Cardiol*. 1996;27(5):1201–1206.

17. Cicoira M et al. High tumour necrosis factor-alpha levels are associated with exercise intolerance and neurohormonal activation in chronic heart failure patients. *Cytokine*. 2001;15(2):80–86.

18. Kalantar-Zadeh K et al. Kidney insufficiency and nutrient-based modulation of inflammation. *Current opinion in clinical nutrition and metabolic care*. 2005;8(4):388–396.

19. Moradi MM et al. Serum and ascitic fluid levels of interleukin-1, interleukin-6, and tumor necrosis factor-alpha in patients with ovarian epithelial cancer. *Cancer*. 1993;72(8):2433–2440.

20. Scott HR, McMillan DC, Crilly A, McArdle CS, Milroy R. The relationship between weight loss and interleukin 6 in non-small-cell lung cancer. *Br J Cancer*. 1996;73(12):1560–1562.

21. Karayiannakis AJ et al. Serum levels of tumor necrosis factor-alpha and nutritional status in pancreatic cancer patients. *Anticancer Res*. 2001;21(2B):1355–1358.

22. Tas F et al. Serum levels of leptin and proinflammatory cytokines in advanced-stage non-small cell lung cancer. *Med Oncol*. 2005;22(4):353–358.

23. Gouin F et al. Increased levels of leukaemia inhibitory factor (LIF) in urine and tissue culture supernatant from human primary bone tumours. *Cytokine*. 1998;10(2):110–114.

24. Gascan H et al. Constitutive production of human interleukin for DA cells/leukemia inhibitory factor by human tumor cell lines derived from various tissues. *J Immunol*. 1990;144(7):2592–2598.

25. Villers D et al. Increased plasma levels of human interleukin for DA1.a cells/leukemia inhibitory factor in sepsis correlate with shock and poor prognosis. *J Infect Dis*. 1995;171(1):232–236.

26. Maltoni M et al. Serum levels of tumour necrosis factor alpha and other cytokines do not correlate with weight loss and anorexia in cancer patients. *Support Care Cancer*. 1997;5(2):130–135.

27. Hart BL. Biological basis of the behavior of sick animals. *Neurosci Biobehav Rev*. 1988;12(2):123–137.

28. Wing EJ, Young JB. Acute starvation protects mice against Listeria monocytogenes. *Infect Immun*. 1980;28(3):771–776.

29. Murray MJ, Murray AB. Anorexia of infection as a mechanism of host defense. *Am J Clin Nutr*. 1979;32(3):593–596.

30. Fong Y et al. Cachectin/TNF or IL-1 alpha induces cachexia with redistribution of body proteins. *Am J Physiol*. 1989;256(3 Pt 2):R659–65.

31. Fearon KC, Voss AC, Hustead DS, Cancer Cachexia Study Group. Definition of cancer cachexia: effect of weight loss, reduced food intake, and systemic inflammation on functional status and prognosis. *Am J Clin Nutr.* 2006;83(6):1345–1350.

32. Evans WK et al. Limited impact of total parenteral nutrition on nutritional status during treatment for small cell lung cancer. *Cancer Res.* 1985;45(7):3347–3353.

33. Tisdale MJ. Mechanisms of cancer cachexia. *Physiol Rev.* 2009;89(2):381–410.

34. Deboer MD et al. Ghrelin treatment causes increased food intake and retention of lean body mass in a rat model of cancer cachexia. *Endocrinology.* 2007;148(6):3004–3012.

35. Marks DL, Ling N, Cone RD. Role of the central melanocortin system in cachexia. *Cancer Res.* 2001;61(4):1432–1438.

36. Wisse BE, Frayo RS, Schwartz MW, Cummings DE. Reversal of cancer anorexia by blockade of central melanocortin receptors in rats. *Endocrinology.* 2001;142(8):3292–3301.

37. Cason J, Ainley CC, Wolstencroft RA, Norton KR, Thompson RP. Cell-mediated immunity in anorexia nervosa. *Clin Exp Immunol.* 1986;64(2):370–375.

38. Kluger MJ. The evolution and adaptive value of fever. *Am Sci.* 1978;66(1):38–43.

39. Beisel WR. Magnitude of the host nutritional responses to infection. *Am J Clin Nutr.* 1977;30(8):1236–1247.

40. Glass DJ. Skeletal muscle hypertrophy and atrophy signaling pathways. *Int J Biochem Cell Biol.* 2005;37(10):1974–1984.

41. Goldberg AL, Goodman HM. Relationship between cortisone and muscle work in determining muscle size. *J Physiol (Lond).* 1969;200(3):667–675.

42. Acharyya S et al. Cancer cachexia is regulated by selective targeting of skeletal muscle gene products. *J Clin Invest.* 2004;114(3):370–378.

43. Baracos VE, DeVivo C, Hoyle DH, Goldberg AL. Activation of the ATP-ubiquitin-proteasome pathway in skeletal muscle of cachectic rats bearing a hepatoma. *Am J Physiol.* 1995;268(5 Pt 1):E996–1006.

44. Goldberg AL, Kettelhut IC, Furuno K, Fagan JM, Baracos V. Activation of protein breakdown and prostaglandin E2 production in rat skeletal muscle in fever is signaled by a macrophage product distinct from interleukin 1 or other known monokines. *J Clin Invest.* 1988;81(5):1378–1383.

45. Baracos V, Rodemann HP, Dinarello CA, Goldberg AL. Stimulation of muscle protein degradation and prostaglandin E2 release by leukocytic pyrogen (interleukin-1). A mechanism for the increased degradation of muscle proteins during fever. *N Engl J Med.* 1983;308(10):553–558.

46. Ruff RL, Secrist D. Inhibitors of prostaglandin synthesis or cathepsin B prevent muscle wasting due to sepsis in the rat. *J Clin Invest.* 1984;73(5):1483–1486.

47. Jepson MM, Pell JM, Bates PC, Millward DJ. The effects of endotoxaemia on protein metabolism in skeletal muscle and liver of fed and fasted rats. *Biochem J.* 1986;235(2):329–336.

48. Rock KL et al. Inhibitors of the proteasome block the degradation of most cell proteins and the generation of peptides presented on MHC class I molecules. *Cell.* 1994;78(5):761–771.

49. Jagoe RT, Goldberg AL. What do we really know about the ubiquitin-proteasome pathway in muscle atrophy? *Current opinion in clinical nutrition and metabolic care.* 2001;4(3):183–190.

50. Llovera M, García-Martínez C, Agell N, Lopez-Soriano FJ, Argilés JM. Muscle wasting associated with cancer cachexia is linked to an important activation of the ATP-dependent ubiquitin-mediated proteolysis. *Int J Cancer.* 1995;61(1):138–141.

51. Temparis S et al. Increased ATP-ubiquitin-dependent proteolysis in skeletal muscles of tumor-bearing rats. *Cancer Res.* 1994;54(21):5568–5573.

52. Mitch WE et al. Metabolic acidosis stimulates muscle protein degradation by activating the adenosine triphosphate-dependent pathway involving ubiquitin and proteasomes. *J Clin Invest.* 1994;93(5):2127–2133.

53. Wing SS, Goldberg AL. Glucocorticoids activate the ATP-ubiquitin-dependent proteolytic system in skeletal muscle during fasting. *Am J Physiol.* 1993;264(4 Pt 1):E668–76.

54. Medina R, Wing SS, Haas A, Goldberg AL. Activation of the ubiquitin-ATP-dependent proteolytic system in skeletal muscle during fasting and denervation atrophy. *Biomed Biochim Acta.* 1991;50(4-6):347–356.

55. Taillandier D et al. Coordinate activation of lysosomal, Ca 2+-activated and ATP-ubiquitin-dependent proteinases in the unweighted rat soleus muscle. *Biochem J.* 1996;316 (Pt 1):65–72.

56. Price SR et al. Muscle wasting in insulinopenic rats results from activation of the ATP-dependent, ubiquitin-proteasome proteolytic pathway by a mechanism including gene transcription. *J Clin Invest.* 1996;98(8):1703–1708.

57. Bailey JL et al. The acidosis of chronic renal failure activates muscle proteolysis in rats by augmenting transcription of genes encoding proteins of the ATP-dependent ubiquitin-proteasome pathway. *J Clin Invest.* 1996;97(6):1447–1453.

58. Gomes MD, Lecker SH, Jagoe RT, Navon A, Goldberg AL. Atrogin-1, a muscle-specific F-box protein highly expressed during muscle atrophy. *Proc Natl Acad Sci USA.* 2001;98(25):14440–14445.

59. Bodine SC et al. Identification of ubiquitin ligases required for skeletal muscle atrophy. *Science*. 2001;294(5547):1704–1708.

60. Centner T et al. Identification of muscle specific ring finger proteins as potential regulators of the titin kinase domain. *J Mol Biol*. 2001;306(4):717–726.

61. Hirner S et al. MuRF1-dependent regulation of systemic carbohydrate metabolism as revealed from transgenic mouse studies. *J Mol Biol*. 2008;379(4):666–677.

62. Cohen S et al. During muscle atrophy, thick, but not thin, filament components are degraded by MuRF1-dependent ubiquitylation. *J Cell Biol*. 2009;185(6):1083–1095.

63. Clarke BA et al. The E3 Ligase MuRF1 degrades myosin heavy chain protein in dexamethasone-treated skeletal muscle. *Cell Metab*. 2007;6(5):376–385.

64. Kedar V et al. Muscle-specific RING finger 1 is a bona fide ubiquitin ligase that degrades cardiac troponin I. *Proc Natl Acad Sci USA*. 2004;101(52):18135–18140.

65. Polge C et al. Muscle actin is polyubiquitinylated in vitro and in vivo and targeted for breakdown by the E3 ligase MuRF1. *FASEB J*. 2011;25(11):3790–3802.

66. Lagirand-Cantaloube J et al. The initiation factor eIF3-f is a major target for atrogin1/MAFbx function in skeletal muscle atrophy. *EMBO J*. 2008;27(8):1266–1276.

67. Lagirand-Cantaloube J et al. Inhibition of atrogin-1/MAFbx mediated MyoD proteolysis prevents skeletal muscle atrophy in vivo. *PLoS ONE*. 2009;4(3):e4973.

68. Usui S et al. Endogenous muscle atrophy F-box mediates pressure overload-induced cardiac hypertrophy through regulation of nuclear factor-kappaB. *Circ Res*. 2011;109(2):161–171.

69. Li H-H et al. Atrogin-1 inhibits Akt-dependent cardiac hypertrophy in mice via ubiquitin-dependent coactivation of Forkhead proteins. *J Clin Invest*. 2007;117(11):3211–3223.

70. Sandri M et al. Foxo transcription factors induce the atrophy-related ubiquitin ligase atrogin-1 and cause skeletal muscle atrophy. *Cell*. 2004;117(3):399–412.

71. Norton JA, Moley JF, Green MV, Carson RE, Morrison SD. Parabiotic transfer of cancer anorexia/cachexia in male rats. *Cancer Res*. 1985;45(11 Pt 1):5547–5552.

72. Fulks RM, Li JB, Goldberg AL. Effects of insulin, glucose, and amino acids on protein turnover in rat diaphragm. *J Biol Chem*. 1975;250(1):290–298.

73. Brüning JC et al. A muscle-specific insulin receptor knockout exhibits features of the metabolic syndrome of NIDDM without altering glucose tolerance. *Mol Cell*. 1998;2(5):559–569.

74. Musarò A et al. Localized Igf-1 transgene expression sustains hypertrophy and regeneration in senescent skeletal muscle. *Nat Genet*. 2001;27(2):195–200.

75. Coleman ME et al. Myogenic vector expression of insulin-like growth factor I stimulates muscle cell differentiation and myofiber hypertrophy in transgenic mice. *J Biol Chem*. 1995;270(20):12109–12116.

76. Song Y-H et al. Muscle-specific expression of IGF-1 blocks angiotensin II-induced skeletal muscle wasting. *J Clin Invest*. 2005;115(2):451–458.

77. Rommel C et al. Mediation of IGF-1-induced skeletal myotube hypertrophy by PI(3)K/Akt/mTOR and PI(3)K/Akt/GSK3 pathways. *Nat Cell Biol*. 2001;3(11):1009–1013.

78. Shi J, Luo L, Eash J, Ibebunjo C, Glass DJ. The SCF-Fbxo40 complex induces IRS1 ubiquitination in skeletal muscle, limiting IGF1 signaling. *Dev Cell*. 2011;21(5):835–847.

79. Bodine SC et al. Akt/mTOR pathway is a crucial regulator of skeletal muscle hypertrophy and can prevent muscle atrophy in vivo. *Nat Cell Biol*. 2001;3(11):1014–1019.

80. Frost RA, Lang CH. mTor signaling in skeletal muscle during sepsis and inflammation: where does it all go wrong? *Physiology (Bethesda)*. 2011;26(2):83–96.

81. Shimizu N et al. Crosstalk between glucocorticoid receptor and nutritional sensor mTOR in skeletal muscle. *Cell Metab*. 2011;13(2):170–182.

82. Bentzinger CF et al. Skeletal muscle-specific ablation of raptor, but not of rictor, causes metabolic changes and results in muscle dystrophy. *Cell Metab*. 2008;8(5):411–424.

83. Brunet A et al. Akt promotes cell survival by phosphorylating and inhibiting a Forkhead transcription factor. *Cell*. 1999;96(6):857–868.

84. Waddell DS et al. The glucocorticoid receptor and FOXO1 synergistically activate the skeletal muscle atrophy-associated MuRF1 gene. *Am J Physiol Endocrinol Metab*. 2008;295(4):E785–97.

85. Reed SA, Sandesara PB, Senf SM, Judge AR. Inhibition of FoxO transcriptional activity prevents muscle fiber atrophy during cachexia and induces hypertrophy. *FASEB J*. 2012;26(3):987–1000.

86. Stitt TN et al. The IGF-1/PI3K/Akt pathway prevents expression of muscle atrophy-induced ubiquitin ligases by inhibiting FOXO transcription factors. *Mol Cell*. 2004;14(3):395–403.

87. Kamei Y et al. Skeletal muscle FOXO1 (FKHR) transgenic mice have less skeletal muscle mass, down-regulated Type I (slow twitch/red muscle) fiber genes, and impaired glycemic control. *J Biol Chem*. 2004;279(39):41114–41123.

88. Smith IJ et al. Sepsis increases the expression and activity of the transcription factor Forkhead Box O 1 (FOXO1) in skeletal muscle by a glucocorticoid-dependent mechanism. *Int J Biochem Cell Biol*. 2010;42(5):701–711.

89. Sacheck JM et al. Rapid disuse and denervation atrophy involve transcriptional changes similar to those of muscle wasting during systemic diseases. *FASEB J.* 2007;21(1):140–155.

90. Black PH. Stress and the inflammatory response: a review of neurogenic inflammation. *Brain Behav Immun.* 2002;16(6):622–653.

91. McCarthy JJ et al. Identification of the circadian transcriptome in adult mouse skeletal muscle. *Physiol Genomics.* 2007;31(1):86–95.

92. Latres E et al. Insulin-like growth factor-1 (IGF-1) inversely regulates atrophy-induced genes via the phosphatidylinositol 3-kinase/Akt/mammalian target of rapamycin (PI3K/Akt/mTOR) pathway. *J Biol Chem.* 2005;280(4):2737–2744.

93. Tiao G et al. Energy-ubiquitin-dependent muscle proteolysis during sepsis in rats is regulated by glucocorticoids. *J Clin Invest.* 1996;97(2):339–348.

94. Tessitore L, Costelli P, Baccino FM. Humoral mediation for cachexia in tumour-bearing rats. *Br J Cancer.* 1993;67(1):15–23.

95. Hu Z, Wang H, Lee IH, Du J, Mitch WE. Endogenous glucocorticoids and impaired insulin signaling are both required to stimulate muscle wasting under pathophysiological conditions in mice. *J Clin Invest.* 2009;119(10):3059–3069.

96. May RC, Kelly RA, Mitch WE. Metabolic acidosis stimulates protein degradation in rat muscle by a glucocorticoid-dependent mechanism. *J Clin Invest.* 1986;77(2):614–621.

97. Llovera M et al. Muscle hypercatabolism during cancer cachexia is not reversed by the glucocorticoid receptor antagonist RU38486. *Cancer Lett.* 1996;99(1):7–14.

98. Tessitore L, Costelli P, Baccino FM. Pharmacological interference with tissue hypercatabolism in tumour-bearing rats. *Biochem J.* 1994;299 (Pt 1):71–78.

99. Li W, Moylan JS, Chambers MA, Smith J, Reid MB. Interleukin-1 stimulates catabolism in C2C12 myotubes. *Am J Physiol, Cell Physiol.* 2009;297(3):C706–14.

100. Moylan JS, Smith JD, Chambers MA, McLoughlin TJ, Reid MB. TNF induction of atrogin-1/MAFbx mRNA depends on Foxo4 expression but not AKT-Foxo1/3 signaling. *Am J Physiol, Cell Physiol.* 2008;295(4):C986–93.

101. Fujita J et al. Anti-interleukin-6 receptor antibody prevents muscle atrophy in colon-26 adenocarcinoma-bearing mice with modulation of lysosomal and ATP-ubiquitin-dependent proteolytic pathways. *Int J Cancer.* 1996;68(5):637–643.

102. Bakkar N et al. IKKα and alternative NF-κB regulate PGC-1β to promote oxidative muscle metabolism. *J Cell Biol.* 2012;196(4):497–511.

103. Bakkar N, Guttridge DC. NF-kappaB signaling: a tale of two pathways in skeletal myogenesis. *Physiol Rev.* 2010;90(2):495–511.

104. Cai D et al. IKKbeta/NF-kappaB activation causes severe muscle wasting in mice. *Cell*. 2004;119(2):285–298.

105. Li Y-P et al. TNF-alpha acts via p38 MAPK to stimulate expression of the ubiquitin ligase atrogin1/MAFbx in skeletal muscle. *FASEB J*. 2005;19(3):362–370.

106. Doyle A, Zhang G, Abdel Fattah EA, Eissa NT, Li Y-P. Toll-like receptor 4 mediates lipopolysaccharide-induced muscle catabolism via coordinate activation of ubiquitin-proteasome and autophagy-lysosome pathways. *FASEB J*. 2011;25(1):99–110.

107. Zhang G, Jin B, Li Y-P. C/EBPβ mediates tumour-induced ubiquitin ligase atrogin1/MAFbx upregulation and muscle wasting. *EMBO J*. 2011;30(20):4323–4335.

108. McPherron AC, Lawler AM, Lee SJ. Regulation of skeletal muscle mass in mice by a new TGF-beta superfamily member. *Nature*. 1997;387(6628):83–90.

109. Zimmers TA et al. Induction of cachexia in mice by systemically administered myostatin. *Science*. 2002;296(5572):1486–1488.

110. Murphy KT, Cobani V, Ryall JG, Ibebunjo C, Lynch GS. Acute antibody-directed myostatin inhibition attenuates disuse muscle atrophy and weakness in mice. *J Appl Physiol*. 2011;110(4):1065–1072.

111. Murphy KT et al. Antibody-directed myostatin inhibition enhances muscle mass and function in tumor-bearing mice. *Am J Physiol Regul Integr Comp Physiol*. 2011;301(3):R716–26.

112. Benny Klimek ME et al. Acute inhibition of myostatin-family proteins preserves skeletal muscle in mouse models of cancer cachexia. *Biochem Biophys Res Commun*. 2010;391(3):1548–1554.

113. Zhang L et al. Pharmacological inhibition of myostatin suppresses systemic inflammation and muscle atrophy in mice with chronic kidney disease. *FASEB J*. 2011;25(5):1653–1663.

114. Gilson H et al. Myostatin gene deletion prevents glucocorticoid-induced muscle atrophy. *Endocrinology*. 2007;148(1):452–460.

115. Tanaka Y et al. Experimental cancer cachexia induced by transplantable colon 26 adenocarcinoma in mice. *Cancer Res*. 1990;50(8):2290–2295.

116. Li Q et al. Prevention of cachexia-like syndrome development and reduction of tumor progression in inhibin-deficient mice following administration of a chimeric activin receptor type II-murine Fc protein. *Mol Hum Reprod*. 2007;13(9):675–683.

117. Raje N, Vallet S. Sotatercept, a soluble activin receptor type 2A IgG-Fc fusion protein for the treatment of anemia and bone loss. *Curr Opin Mol Ther*. 2010;12(5):586–597.

118. Sartori R et al. Smad2 and 3 transcription factors control muscle mass in adulthood. *Am J Physiol, Cell Physiol*. 2009;296(6):C1248–57.

119. McFarlane C et al. Myostatin induces cachexia by activating the ubiquitin proteolytic system through an NF-kappaB-independent, FoxO1-dependent mechanism. *J Cell Physiol*. 2006;209(2):501–514.

120. Levine B, Kroemer G. Autophagy in the pathogenesis of disease. *Cell*. 2008;132(1):27–42.

121. Sandri M. Autophagy in health and disease. 3. Involvement of autophagy in muscle atrophy. *Am J Physiol, Cell Physiol*. 2010;298(6):C1291–7.

122. Lecker SH et al. Multiple types of skeletal muscle atrophy involve a common program of changes in gene expression. *FASEB J*. 2004;18(1):39–51.

123. Mammucari C et al. FoxO3 controls autophagy in skeletal muscle in vivo. *Cell Metab*. 2007;6(6):458–471.

124. Criollo A et al. The IKK complex contributes to the induction of autophagy. *EMBO J*. 2009;29(3):619–631.

125. Comb WC, Cogswell P, Sitcheran R, Baldwin AS. IKK-dependent, NF-κB-independent control of autophagic gene expression. *Oncogene*. 2011;30(14):1727–1732.

126. Masiero E et al. Autophagy is required to maintain muscle mass. *Cell Metab*. 2009;10(6):507–515.

127. Ogimoto K, Harris MK, Wisse BE. MyD88 is a key mediator of anorexia, but not weight loss, induced by lipopolysaccharide and interleukin-1 beta. *Endocrinology*. 2006;147(9):4445–4453.

128. Wisse BE et al. Evidence that lipopolysaccharide-induced anorexia depends upon central, rather than peripheral, inflammatory signals. *Endocrinology*. 2007;148(11):5230–5237.

129. Whitaker KW, Reyes TM. Central blockade of melanocortin receptors attenuates the metabolic and locomotor responses to peripheral interleukin-1beta administration. *Neuropharmacology*. 2008;54(3):509–520.

130. Sonti G, Ilyin SE, Plata-Salamán CR. Anorexia induced by cytokine interactions at pathophysiological concentrations. *Am J Physiol*. 1996;270(6 Pt 2):R1394–402.

131. Grossberg AJ et al. Arcuate nucleus proopiomelanocortin neurons mediate the acute anorectic actions of leukemia inhibitory factor via gp130. *Endocrinology*. 2010;151(2):606–616.

132. Bodnar RJ et al. Mediation of anorexia by human recombinant tumor necrosis factor through a peripheral action in the rat. *Cancer Res.* 1989;49(22):6280–6284.

133. Morgan JI, Curran T. Role of ion flux in the control of c-fos expression. *Nature.* 1986;322(6079):552–555.

134. Elmquist JK, Scammell TE, Jacobson CD, Saper CB. Distribution of Fos-like immunoreactivity in the rat brain following intravenous lipopolysaccharide administration. *J Comp Neurol.* 1996;371(1):85–103.

135. Opara EI, Laviano A, Meguid MM, Yang ZJ. Correlation between food intake and CSF IL-1 alpha in anorectic tumor bearing rats. *Neuroreport.* 1995;6(5):750–752.

136. Layé S et al. Endogenous brain IL-1 mediates LPS-induced anorexia and hypothalamic cytokine expression. *Am J Physiol Regul Integr Comp Physiol.* 2000;279(1):R93–8.

137. Plata-Salamán CR, Ilyin SE, Gayle D. Brain cytokine mRNAs in anorectic rats bearing prostate adenocarcinoma tumor cells. *Am J Physiol.* 1998;275(2 Pt 2):R566–73.

138. Ropelle ER et al. A central role for neuronal adenosine 5'-monophosphate-activated protein kinase in cancer-induced anorexia. *Endocrinology.* 2007;148(11):5220–5229.

139. Arruda AP et al. Hypothalamic actions of tumor necrosis factor alpha provide the thermogenic core for the wastage syndrome in cachexia. *Endocrinology.* 2010;151(2):683–694.

140. Hill AG et al. Chronic central nervous system exposure to interleukin-1 beta causes catabolism in the rat. *Am J Physiol.* 1996;271(5 Pt 2):R1142–8.

141. Plata-Salamán CR, Sonti G, Borkoski JP, Wilson CD, French-Mullen JM 04189 brahmsudeledu. Anorexia induced by chronic central administration of cytokines at estimated pathophysiological concentrations. *Physiol Behav.* 1996;60(3):867–875.

142. Beretta E, Dhillon H, Kalra PS, Kalra SP. Central LIF gene therapy suppresses food intake, body weight, serum leptin and insulin for extended periods. *Peptides.* 2002;23(5):975–984.

143. Layé S et al. Subdiaphragmatic vagotomy blocks induction of IL-1 beta mRNA in mice brain in response to peripheral LPS. *Am J Physiol.* 1995;268(5 Pt 2):R1327–31.

144. Hansen MK, Taishi P, Chen Z, Krueger JM. Vagotomy blocks the induction of interleukin-1beta (IL-1beta) mRNA in the brain of rats in response to systemic IL-1beta. *J Neurosci.* 1998;18(6):2247–2253.

145. Hansen MK et al. Effects of vagotomy on lipopolysaccharide-induced brain interleukin-1beta protein in rats. *Auton Neurosci.* 2000;85(1-3):119–126.

146. Bret-Dibat JL, Bluthé RM, Kent S, Kelley KW, Dantzer R. Lipopolysaccharide and interleukin-1 depress food-motivated behavior in mice by a vagal-mediated mechanism. *Brain Behav Immun.* 1995;9(3):242–246.

147. Porter MH, Hrupka BJ, Langhans W, Schwartz GJ. Vagal and splanchnic afferents are not necessary for the anorexia produced by peripheral IL-1beta, LPS, and MDP. *Am J Physiol.* 1998;275(2 Pt 2):R384–9.

148. Pitterman AB et al. Abdominal vagotomy does not modify endotoxic shock in rats. *Life Sci.* 1983;33(11):1033–1037.

149. Bernstein IL. Neutral mediation of food aversions and anorexia induced by tumor necrosis factor and tumors. *Neurosci Biobehav Rev.* 1996;20(1):177–181.

150. Cheung W et al. Role of leptin and melanocortin signaling in uremia-associated cachexia. *J Clin Invest.* 2005;115(6):1659–1665.

151. Doehner W et al. Leptin, insulin sensitivity and growth hormone binding protein in chronic heart failure with and without cardiac cachexia. *Eur J Endocrinol.* 2001;145(6):727–735.

152. La Cava A, Matarese G. The weight of leptin in immunity. *Nat Rev Immunol.* 2004;4(5):371–379.

153. Münzberg H. Differential leptin access into the brain--a hierarchical organization of hypothalamic leptin target sites? *Physiol Behav.* 2008;94(5):664–669.

154. Cone RD et al. The arcuate nucleus as a conduit for diverse signals relevant to energy homeostasis. *Int J Obes Relat Metab Disord.* 2001;25 Suppl 5:S63–7.

155. Laviano A et al. Effects of intra-VMN mianserin and IL-1ra on meal number in anorectic tumor-bearing rats. *J Investig Med.* 2000;48(1):40–48.

156. Dhillon H et al. Leptin directly activates SF1 neurons in the VMH, and this action by leptin is required for normal body-weight homeostasis. *Neuron.* 2006;49(2):191–203.

157. Banks WA, Kastin AJ. Blood to brain transport of interleukin links the immune and central nervous systems. *Life Sci.* 1991;48(25):PL117–21.

158. Zlokovic BV et al. Differential regulation of leptin transport by the choroid plexus and blood-brain barrier and high affinity transport systems for entry into hypothalamus and across the blood-cerebrospinal fluid barrier. *Endocrinology.* 2000;141(4):1434–1441.

159. Banks WA, Ortiz L, Plotkin SR, Kastin AJ. Human interleukin (IL) 1 alpha, murine IL-1 alpha and murine IL-1 beta are transported from blood to brain in the mouse by a shared saturable mechanism. *J Pharmacol Exp Ther.* 1991;259(3):988–996.

160. Banks WA, Kastin AJ, Gutierrez EG. Penetration of interleukin-6 across the murine blood-brain barrier. *Neurosci Lett.* 1994;179(1-2):53–56.

161. Gutierrez EG, Banks WA, Kastin AJ. Murine tumor necrosis factor alpha is transported from blood to brain in the mouse. *J Neuroimmunol.* 1993;47(2):169–176.

162. Elmquist JK et al. Intravenous lipopolysaccharide induces cyclooxygenase 2-like immunoreactivity in rat brain perivascular microglia and meningeal macrophages. *J Comp Neurol.* 1997;381(2):119–129.

163. Ericsson A, Arias C, Sawchenko PE. Evidence for an intramedullary prostaglandin-dependent mechanism in the activation of stress-related neuroendocrine circuitry by intravenous interleukin-1. *J Neurosci.* 1997;17(18):7166–7179.

164. Nadeau S, Rivest S. Effects of circulating tumor necrosis factor on the neuronal activity and expression of the genes encoding the tumor necrosis factor receptors (p55 and p75) in the rat brain: a view from the blood-brain barrier. *Neuroscience.* 1999;93(4):1449–1464.

165. Ek M et al. Inflammatory response: pathway across the blood-brain barrier. *Nature.* 2001;410(6827):430–431.

166. Herkenham M, Lee HY, Baker RA. Temporal and spatial patterns of c-fos mRNA induced by intravenous interleukin-1: a cascade of non-neuronal cellular activation at the blood-brain barrier. *J Comp Neurol.* 1998;400(2):175–196.

167. Nakamura K et al. Immunohistochemical localization of prostaglandin EP3 receptor in the rat nervous system. *J Comp Neurol.* 2000;421(4):543–569.

168. Serrats J et al. Dual roles for perivascular macrophages in immune-to-brain signaling. *Neuron.* 2010;65(1):94–106.

169. Shimomura Y et al. Both cyclooxygenase and lipoxygenase inhibitor partially restore the anorexia by interleukin-1 beta. *Life Sci.* 1992;51(18):1419–1426.

170. Langhans W, Harlacher R, Scharrer E. Verapamil and indomethacin attenuate endotoxin-induced anorexia. *Physiol Behav.* 1989;46(3):535–539.

171. Johnson PM, Vogt SK, Burney MW, Muglia LJ. COX-2 inhibition attenuates anorexia during systemic inflammation without impairing cytokine production. *Am J Physiol Endocrinol Metab.* 2002;282(3):E650–6.

172. Strelkov AB, Fields AL, Baracos VE. Effects of systemic inhibition of prostaglandin production on protein metabolism in tumor-bearing rats. *Am J Physiol.* 1989;257(2 Pt 1):C261–9.

173. Davis TW et al. Inhibition of cyclooxygenase-2 by celecoxib reverses tumor-induced wasting. *J Pharmacol Exp Ther.* 2004;308(3):929–934.

174. Piffar PM et al. Naproxen, clenbuterol and insulin administration ameliorates cancer cachexia and reduce tumor growth in Walker 256 tumor-bearing rats. *Cancer Lett.* 2003;201(2):139–148.

175. Pecchi E, Dallaporta M, Jean A, Thirion S, Troadec JD. mPGES-1 knock-out mice are resistant to cancer-induced anorexia despite the absence of central mPGES-1 up-regulation in wild-type anorexic mice. *J Neuroimmunol*. 2008;199(1-2):104–114.

176. Cone RD. Anatomy and regulation of the central melanocortin system. *Nat Neurosci*. 2005;8(5):571–578.

177. Kishi T et al. Expression of melanocortin 4 receptor mRNA in the central nervous system of the rat. *J Comp Neurol*. 2003;457(3):213–235.

178. Fan W, Boston BA, Kesterson RA, Hruby VJ, Cone RD. Role of melanocortinergic neurons in feeding and the agouti obesity syndrome. *Nature*. 1997;385(6612):165–168.

179. Frigeri LG, Wolff GL, Teguh C. Differential responses of yellow Avy/A and agouti A/a (BALB/c X VY) F1 hybrid mice to the same diets: glucose tolerance, weight gain, and adipocyte cellularity. *Int J Obes*. 1988;12(4):305–320.

180. Pritchard LE, Turnbull AV, White A. Pro-opiomelanocortin processing in the hypothalamus: impact on melanocortin signalling and obesity. *J Endocrinol*. 2002;172(3):411–421.

181. Ollmann MM et al. Antagonism of central melanocortin receptors in vitro and in vivo by agouti-related protein. *Science*. 1997;278(5335):135–138.

182. Jacobowitz DM, O'Donohue TL. alpha-Melanocyte stimulating hormone: immunohistochemical identification and mapping in neurons of rat brain. *Proc Natl Acad Sci USA*. 1978;75(12):6300–6304.

183. Bagnol D et al. Anatomy of an endogenous antagonist: relationship between Agouti-related protein and proopiomelanocortin in brain. *J Neurosci*. 1999;19(18):RC26.

184. Haskell-Luevano C et al. Characterization of the neuroanatomical distribution of agouti-related protein immunoreactivity in the rhesus monkey and the rat. *Endocrinology*. 1999;140(3):1408–1415.

185. Cowley MA et al. Leptin activates anorexigenic POMC neurons through a neural network in the arcuate nucleus. *Nature*. 2001;411(6836):480–484.

186. Scarlett JM et al. Regulation of central melanocortin signaling by interleukin-1 beta. *Endocrinology*. 2007;148(9):4217–4225.

187. Scarlett JM et al. Regulation of agouti-related protein messenger ribonucleic acid transcription and peptide secretion by acute and chronic inflammation. *Endocrinology*. 2008;149(10):4837–4845.

188. Marks DL, Butler AA, Turner R, Brookhart G, Cone RD. Differential role of melanocortin receptor subtypes in cachexia. *Endocrinology*. 2003;144(4):1513–1523.

189. Joppa MA et al. Central administration of peptide and small molecule MC4 receptor antagonists induce hyperphagia in mice and attenuate cytokine-induced anorexia. *Peptides*. 2005;26(11):2294–2301.

190. Markison S et al. The regulation of feeding and metabolic rate and the prevention of murine cancer cachexia with a small-molecule melanocortin-4 receptor antagonist. *Endocrinology*. 2005;146(6):2766–2773.

191. Nicholson JR et al. Peripheral administration of a melanocortin 4-receptor inverse agonist prevents loss of lean body mass in tumor-bearing mice. *J Pharmacol Exp Ther*. 2006;317(2):771–777.

192. Weyermann P et al. Orally available selective melanocortin-4 receptor antagonists stimulate food intake and reduce cancer-induced cachexia in mice. *PLoS ONE*. 2009;4(3):e4774.

193. Cheung WW, Rosengren S, Boyle DL, Mak RH. Modulation of melanocortin signaling ameliorates uremic cachexia. *Kidney Int*. 2008;74(2):180–186.

194. Cheung WW et al. Peripheral administration of the melanocortin-4 receptor antagonist NBI-12i ameliorates uremia-associated cachexia in mice. *J Am Soc Nephrol*. 2007;18(9):2517–2524.

195. Chee MJS, Colmers WF. Y eat? *Nutrition*. 2008;24(9):869–877.

196. Sergeyev V, Broberger C, Hökfelt T. Effect of LPS administration on the expression of POMC, NPY, galanin, CART and MCH mRNAs in the rat hypothalamus. *Brain Res Mol Brain Res*. 2001;90(2):93–100.

197. Gayle D, Ilyin SE, Plata-Salamán CR. Central nervous system IL-1 beta system and neuropeptide Y mRNAs during IL-1 beta-induced anorexia in rats. *Brain Res Bull*. 1997;44(3):311–317.

198. Makarenko IG, Meguid MM, Gatto L, Chen C, Ugrumov MV. Decreased NPY innervation of the hypothalamic nuclei in rats with cancer anorexia. *Brain Res*. 2003;961(1):100–108.

199. Nara-ashizawa N et al. Response of hypothalamic NPY mRNAs to a negative energy balance is less sensitive in cachectic mice bearing human tumor cells. *Nutr Cancer*. 2001;41(1-2):111–118.

200. Chance WT et al. Assessment of feeding response of tumor-bearing rats to hypothalamic injection and infusion of neuropeptide Y. *Peptides*. 1996;17(5):797–801.

201. Chance WT, Balasubramaniam A, Fischer JE. Neuropeptide Y and the development of cancer anorexia. *Ann Surg*. 1995;221(5):579–87; discussion 587–9.

202. Castañeda TR, Tong J, Datta R, Culler M, Tschöp MH. Ghrelin in the regulation of body weight and metabolism. *Front Neuroendocrinol*. 2010;31(1):44–60.

203. Willesen MG, Kristensen P, Rømer J. Co-localization of growth hormone secretagogue receptor and NPY mRNA in the arcuate nucleus of the rat. *Neuroendocrinology*. 1999;70(5):306–316.

204. Dixit VD et al. Ghrelin inhibits leptin- and activation-induced proinflammatory cytokine expression by human monocytes and T cells. *J Clin Invest*. 2004;114(1):57–66.

205. Otero M et al. Chronic inflammation modulates ghrelin levels in humans and rats. *Rheumatology (Oxford)*. 2004;43(3):306–310.

206. Basa NR et al. Bacterial lipopolysaccharide shifts fasted plasma ghrelin to postprandial levels in rats. *Neurosci Lett*. 2003;343(1):25–28.

207. Madison LD et al. Prostacyclin signaling regulates circulating ghrelin during acute inflammation. *J Endocrinol*. 2008;196(2):263–273.

208. Nagaya N et al. Chronic administration of ghrelin improves left ventricular dysfunction and attenuates development of cardiac cachexia in rats with heart failure. *Circulation*. 2001;104(12):1430–1435.

209. Shimizu Y et al. Increased plasma ghrelin level in lung cancer cachexia. *Clin Cancer Res*. 2003;9(2):774–778.

210. Wolf I et al. Adiponectin, ghrelin, and leptin in cancer cachexia in breast and colon cancer patients. *Cancer*. 2006;106(4):966–973.

211. Takahashi M et al. Ghrelin and leptin levels in cachectic patients with cancer of the digestive organs. *Int J Clin Oncol*. 2009;14(4):315–320.

212. Legakis I, Stathopoulos J, Matzouridis T, Stathopoulos GP. Decreased plasma ghrelin levels in patients with advanced cancer and weight loss in comparison to healthy individuals. *Anticancer Res*. 2009;29(10):3949–3952.

213. Hanada T et al. Anti-cachectic effect of ghrelin in nude mice bearing human melanoma cells. *Biochem Biophys Res Commun*. 2003;301(2):275–279.

214. Perboni S, Bowers C, Kojima S, Asakawa A, Inui A. Growth hormone releasing peptide 2 reverses anorexia associated with chemotherapy with 5-fluoruracil in colon cancer cell-bearing mice. *World J Gastroenterol*. 2008;14(41):6303–6305.

215. Deboer MD et al. Ghrelin treatment of chronic kidney disease: improvements in lean body mass and cytokine profile. *Endocrinology*. 2008;149(2):827–835.

216. Barazzoni R et al. Combined effects of ghrelin and higher food intake enhance skeletal muscle mitochondrial oxidative capacity and AKT phosphorylation in rats with chronic kidney disease. *Kidney Int*. 2010;77(1):23–28.

217. Akashi YJ et al. No effects of human ghrelin on cardiac function despite profound effects on body composition in a rat model of heart failure. *Int J Cardiol.* 2009;137(3):267–275.

218. Wahl SM, Altman LC, Rosenstreich DL. Inhibition of in vitro lymphokine synthesis by glucocorticosteroids. *J Immunol.* 1975;115(2):476–481.

219. Besedovsky H, Sorkin E, Keller M, Müller J. Changes in blood hormone levels during the immune response. *Proc Soc Exp Biol Med.* 1975;150(2):466–470.

220. Shek PN, Sabiston BH. Neuroendocrine regulation of immune processes: change in circulating corticosterone levels induced by the primary antibody response in mice. *Int J Immunopharmacol.* 1983;5(1):23–33.

221. Besedovsky H, del Rey A, Sorkin E. Immunoregulatory feedback between interleukin-1 and glucocorticoid hormones. *Science.* 1986;

222. Sapolsky R, Rivier C, Yamamoto G, Plotsky P, Vale W. Interleukin-1 stimulates the secretion of hypothalamic corticotropin-releasing factor. *Science.* 1987;238(4826):522–524.

223. Berkenbosch F, van Oers J, del Rey A, Tilders F, Besedovsky H. Corticotropin-releasing factor-producing neurons in the rat activated by interleukin-1. *Science.* 1987;238(4826):524–526.

224. Wang J, Dunn AJ. Mouse interleukin-6 stimulates the HPA axis and increases brain tryptophan and serotonin metabolism. *Neurochem Int.* 1998;33(2):143–154.

225. Van der Meer MJ, Sweep CG, Pesman GJ, Borm GF, Hermus AR. Synergism between IL-1 beta and TNF-alpha on the activity of the pituitary-adrenal axis and on food intake of rats. *Am J Physiol.* 1995;268(4 Pt 1):E551–7.

226. Akita S et al. Human and murine pituitary expression of leukemia inhibitory factor. Novel intrapituitary regulation of adrenocorticotropin hormone synthesis and secretion. *J Clin Invest.* 1995;95(3):1288–1298.

227. Bethin KE, Vogt SK, Muglia LJ. Interleukin-6 is an essential, corticotropin-releasing hormone-independent stimulator of the adrenal axis during immune system activation. *Proc Natl Acad Sci USA.* 2000;97(16):9317–9322.

228. Ericsson A, Liu C, Hart RP, Sawchenko PE. Type 1 interleukin-1 receptor in the rat brain: distribution, regulation, and relationship to sites of IL-1-induced cellular activation. *J Comp Neurol.* 1995;361(4):681–698.

229. Ericsson A, Kovács KJ, Sawchenko PE. A functional anatomical analysis of central pathways subserving the effects of interleukin-1 on stress-related neuroendocrine neurons. *J Neurosci.* 1994;14(2):897–913.

230. Ching S et al. Endothelial-specific knockdown of interleukin-1 (IL-1) type 1 receptor differentially alters CNS responses to IL-1 depending on its route of administration. *J Neurosci.* 2007;27(39):10476–10486.

231. Elander L et al. Inducible prostaglandin E2 synthesis interacts in a temporally supplementary sequence with constitutive prostaglandin-synthesizing enzymes in creating the hypothalamic-pituitary-adrenal axis response to immune challenge. *J Neurosci.* 2009;29(5):1404–1413.

232. Nogueiras R et al. The central melanocortin system directly controls peripheral lipid metabolism. *J Clin Invest.* 2007;117(11):3475–3488.

233. Perez-Tilve D et al. Melanocortin signaling in the CNS directly regulates circulating cholesterol. *Nat Neurosci.* 2010;13(7):877–882.

234. Song CK et al. Melanocortin-4 receptor mRNA expressed in sympathetic outflow neurons to brown adipose tissue: neuroanatomical and functional evidence. *Am J Physiol Regul Integr Comp Physiol.* 2008;295(2):R417–28.

235. Song CK, Jackson RM, Harris RBS, Richard D, Bartness TJ. Melanocortin-4 receptor mRNA is expressed in sympathetic nervous system outflow neurons to white adipose tissue. *Am J Physiol Regul Integr Comp Physiol.* 2005;289(5):R1467–76.

236. Brito MN, Brito NA, Baro DJ, Song CK, Bartness TJ. Differential activation of the sympathetic innervation of adipose tissues by melanocortin receptor stimulation. *Endocrinology.* 2007;148(11):5339–5347.

237. Bowers RR et al. Sympathetic innervation of white adipose tissue and its regulation of fat cell number. *Am J Physiol Regul Integr Comp Physiol.* 2004;286(6):R1167–75.

238. Kim YS, Sainz RD, Molenaar P, Summers RJ. Characterization of beta 1- and beta 2-adrenoceptors in rat skeletal muscles. *Biochem Pharmacol.* 1991;42(9):1783–1789.

239. Martin WH, Murphree SS, Saffitz JE. Beta-adrenergic receptor distribution among muscle fiber types and resistance arterioles of white, red, and intermediate skeletal muscle. *Circ Res.* 1989;64(6):1096–1105.

240. Ryall JG, Gregorevic P, Plant DR, Sillence MN, Lynch GS. Beta 2-agonist fenoterol has greater effects on contractile function of rat skeletal muscles than clenbuterol. *Am J Physiol Regul Integr Comp Physiol.* 2002;283(6):R1386–94.

241. Ryall JG, Sillence MN, Lynch GS. Systemic administration of beta2-adrenoceptor agonists, formoterol and salmeterol, elicit skeletal muscle hypertrophy in rats at micromolar doses. *Br J Pharmacol.* 2006;147(6):587–595.

242. Rattigan S et al. Alpha-adrenergic receptors in rat skeletal muscle. *Biochem Biophys Res Commun.* 1986;136(3):1071–1077.

243. Portillo MP, Martínez JA, Larralde J. Repartitioning effect of a mixed beta-agonist on body composition. *Rev Esp Fisiol.* 1990;46(2):191–196.

244. Lynch GS, Ryall JG. Role of beta-adrenoceptor signaling in skeletal muscle: implications for muscle wasting and disease. *Physiol Rev*. 2008;88(2):729–767.

245. Stallion A, Foley-Nelson T, Chance WT, James JH, Fischer JE. Anticatabolic effect of the beta 2-agonist cimaterol in vivo in tumor-bearing animals. *J Surg Res*. 1995;59(3):387–392.

246. Stallion A, Foley-Nelson T, Chance WT, Fischer JE. Effects of increased beta 2-agonist dose in tumor-bearing animals. *Nutr Cancer*. 1993;20(3):251–260.

247. Oya Y, Ogawa M, Kawai M. [Therapeutic trial of beta 2-adrenergic agonist clenbuterol in muscular dystrophies]. *Rinsho Shinkeigaku*. 2001;41(10):698–700.

248. Carter WJ, Lynch ME. Comparison of the effects of salbutamol and clenbuterol on skeletal muscle mass and carcass composition in senescent rats. *Metab Clin Exp*. 1994;43(9):1119–1125.

249. Ryall JG, Plant DR, Gregorevic P, Sillence MN, Lynch GS. Beta 2-agonist administration reverses muscle wasting and improves muscle function in aged rats. *J Physiol (Lond)*. 2004;555(Pt 1):175–188.

250. Martineau L, Little RA, Rothwell NJ, Fisher MI. Clenbuterol, a beta 2-adrenergic agonist, reverses muscle wasting due to scald injury in the rat. *Burns*. 1993;19(1):26–34.

251. Navegantes LC, Resano NM, Migliorini RH, Kettelhut IC. Effect of guanethidine-induced adrenergic blockade on the different proteolytic systems in rat skeletal muscle. *Am J Physiol*. 1999;277(5 Pt 1):E883–9.

252. Navegantes LCC, Resano NMZ, Baviera AM, Migliorini RH, Kettelhut IC. Effect of sympathetic denervation on the rate of protein synthesis in rat skeletal muscle. *Am J Physiol Endocrinol Metab*. 2004;286(4):E642–7.

253. Minokoshi Y et al. Leptin stimulates fatty-acid oxidation by activating AMP-activated protein kinase. *Nature*. 2002;415(6869):339–343.

254. Morley JE, Thomas DR, Wilson M-MG. Cachexia: pathophysiology and clinical relevance. *Am J Clin Nutr*. 2006;83(4):735–743.

255. Llovera M et al. Role of TNF receptor 1 in protein turnover during cancer cachexia using gene knockout mice. *Mol Cell Endocrinol*. 1998;142(1-2):183–189.

256. Strassmann G, Fong M, Kenney JS, Jacob CO. Evidence for the involvement of interleukin 6 in experimental cancer cachexia. *J Clin Invest*. 1992;89(5):1681–1684.

257. Zamir O et al. Reduced muscle protein breakdown in septic rats following treatment with interleukin-1 receptor antagonist. *Int J Biochem*. 1994;26(7):943–950.

258. Lloyd CE, Palopoli M, Vary TC. Effect of central administration of interleukin-1 receptor antagonist on protein synthesis in skeletal muscle, kidney, and liver during sepsis. *Metab Clin Exp*. 2003;52(9):1218–1225.

259. Almon RR, DuBois DC, Jusko WJ. A microarray analysis of the temporal response of liver to methylprednisolone: a comparative analysis of two dosing regimens. *Endocrinology*. 2007;148(5):2209–2225.

260. Wu Y et al. REDD1 is a major target of testosterone action in preventing dexamethasone-induced muscle loss. *Endocrinology*. 2010;151(3):1050–1059.

261. Romero LI, Kakucska I, Lechan RM, Reichlin S. Interleukin-6 (IL-6) is secreted from the brain after intracerebroventricular injection of IL-1 beta in rats. *Am J Physiol*. 1996;270(3 Pt 2):R518–24.

262. Kovács KJ, Földes A, Sawchenko PE. Glucocorticoid negative feedback selectively targets vasopressin transcription in parvocellular neurosecretory neurons. *J Neurosci*. 2000;20(10):3843–3852.

263. Scheinman RI, Cogswell PC, Lofquist AK, Baldwin AS. Role of transcriptional activation of I kappa B alpha in mediation of immunosuppression by glucocorticoids. *Science*. 1995;270(5234):283–286.

264. Shiuchi T et al. Hypothalamic orexin stimulates feeding-associated glucose utilization in skeletal muscle via sympathetic nervous system. *Cell Metab*. 2009;10(6):466–480.

265. Konsman JP, Tridon V, Dantzer R. Diffusion and action of intracerebroventricularly injected interleukin-1 in the CNS. *Neuroscience*. 2000;101(4):957–967.

266. Gourine AV, Leon LR, Rudolph K, Korsak AS, Kluger MJ. Anterior hypothalamic interleukin-1 receptors are involved in mediation of fever during bacterial sepsis in rats. *Ann N Y Acad Sci*. 1998;856:266–269.

267. Paul PK et al. Targeted ablation of TRAF6 inhibits skeletal muscle wasting in mice. *J Cell Biol*. 2010;191(7):1395–1411.

268. Hunter RB, Kandarian SC. Disruption of either the Nfkb1 or the Bcl3 gene inhibits skeletal muscle atrophy. *J Clin Invest*. 2004;114(10):1504–1511.

269. Mourkioti F et al. Targeted ablation of IKK2 improves skeletal muscle strength, maintains mass, and promotes regeneration. *J Clin Invest*. 2006;116(11):2945–2954.

270. Rivadeneira DE et al. Glucocorticoid blockade does not abrogate tumor-induced cachexia. *Nutr Cancer*. 1999;35(2):202–206.

271. Heikinheimo O, Pesonen U, Huupponen R, Koulu M, Lähteenmäki P. Hepatic metabolism and distribution of mifepristone and its metabolites in rats. *Hum Reprod*. 1994;9 Suppl 1:40–46.

272. Jagoe RT, Lecker SH, Gomes M, Goldberg AL. Patterns of gene expression in atrophying skeletal muscles: response to food deprivation. *FASEB J*. 2002;16(13):1697–1712.

273. Sofer A, Lei K, Johannessen CM, Ellisen LW. Regulation of mTOR and cell growth in response to energy stress by REDD1. *Mol Cell Biol*. 2005;25(14):5834–5845.

274. Budanov AV, Karin M. p53 target genes sestrin1 and sestrin2 connect genotoxic stress and mTOR signaling. *Cell*. 2008;134(3):451–460.

275. Huszar D et al. Targeted disruption of the melanocortin-4 receptor results in obesity in mice. *Cell*. 1997;88(1):131–141.

276. Pruett SB, Padgett EL. Thymus-derived glucocorticoids are insufficient for normal thymus homeostasis in the adult mouse. *BMC Immunol*. 2004;5:24.

277. Anker S, Ponikowski P, Varney S, Chua T. ScienceDirect - The Lancet : Wasting as independent risk factor for mortality in chronic heart failure. *The Lancet*. 1997;

278. Reid WD, MacGowan NA. Respiratory muscle injury in animal models and humans. *Mol Cell Biochem*. 1998;179(1-2):63–80.

279. Braun TP et al. Central nervous system inflammation induces muscle atrophy via activation of the hypothalamic-pituitary-adrenal axis. *J Exp Med*. 2011;208(12):2449–2463.

280. Perretti M, Duncan GS, Flower RJ, Peers SH. Serum corticosterone, interleukin-1 and tumour necrosis factor in rat experimental endotoxaemia: comparison between Lewis and Wistar strains. *Br J Pharmacol*. 1993;110(2):868–874.

281. Adachi O et al. Targeted disruption of the MyD88 gene results in loss of IL-1- and IL-18-mediated function. *Immunity*. 1998;9(1):143–150.

282. Kawai T, Adachi O, Ogawa T, Takeda K, Akira S. Unresponsiveness of MyD88-deficient mice to endotoxin. *Immunity*. 1999;11(1):115–122.

283. Haddad F, Zaldivar F, Cooper DM, Adams GR. IL-6-induced skeletal muscle atrophy. *J Appl Physiol*. 2005;98(3):911–917.

284. Masferrer JL, Seibert K, Zweifel B, Needleman P. Endogenous glucocorticoids regulate an inducible cyclooxygenase enzyme. *Proc Natl Acad Sci USA*. 1992;89(9):3917–3921.

285. Zamir O, Hasselgren PO, Higashiguchi T, Frederick JA, Fischer JE. Tumour necrosis factor (TNF) and interleukin-1 (IL-1) induce muscle proteolysis through different mechanisms. *Mediators Inflamm*. 1992;1(4):247–250.

286. Zamir O, Hasselgren PO, Allmen von D, Fischer JE. In vivo administration of interleukin-1 alpha induces muscle proteolysis in normal and adrenalectomized rats. *Metab Clin Exp*. 1993;42(2):204–208.

287. Dantzer R et al. Cytokines and sickness behavior. *Ann N Y Acad Sci*. 1998;840:586–590.

288. Ridder DA et al. TAK1 in brain endothelial cells mediates fever and lethargy. *J Exp Med*. 2011;208(13):2615–2623.

289. Davis CN et al. MyD88-dependent and -independent signaling by IL-1 in neurons probed by bifunctional Toll/IL-1 receptor domain/BB-loop mimetics. *Proc Natl Acad Sci USA*. 2006;103(8):2953–2958.

290. Kleinridders A et al. MyD88 signaling in the CNS is required for development of fatty acid-induced leptin resistance and diet-induced obesity. *Cell Metab*. 2009;10(4):249–259.

291. Grossberg AJ et al. Inflammation-induced lethargy is mediated by suppression of orexin neuron activity. *J Neurosci*. 2011;31(31):11376–11386.

292. Murray RZ, Kay JG, Sangermani DG, Stow JL. A role for the phagosome in cytokine secretion. *Science*. 2005;310(5753):1492–1495.

293. Hill JW et al. Acute effects of leptin require PI3K signaling in hypothalamic proopiomelanocortin neurons in mice. *J Clin Invest*. 2008;118(5):1796–1805.

294. Lazarus M et al. EP3 prostaglandin receptors in the median preoptic nucleus are critical for fever responses. *Nat Neurosci*. 2007;10(9):1131–1133.

295. Plata-Salamán CR, Oomura Y, Kai Y. Tumor necrosis factor and interleukin-1 beta: suppression of food intake by direct action in the central nervous system. *Brain Res*. 1988;448(1):106–114.

296. Balthasar N et al. Leptin receptor signaling in POMC neurons is required for normal body weight homeostasis. *Neuron*. 2004;42(6):983–991.

297. Castle WE. Size Genes of Mice. *Proc Natl Acad Sci USA*. 1942;28(3):69–72.

298. Farooqi IS et al. Clinical spectrum of obesity and mutations in the melanocortin 4 receptor gene. *N Engl J Med*. 2003;348(12):1085–1095.

299. Joppa MA, Gogas KR, Foster AC, Markison S. Central infusion of the melanocortin receptor antagonist agouti-related peptide (AgRP(83-132)) prevents cachexia-related symptoms induced by radiation and colon-26 tumors in mice. *Peptides*. 2007;28(3):636–642.

300. Scarlett JM et al. Genetic and pharmacologic blockade of central melanocortin signaling attenuates cardiac cachexia in rodent models of heart failure. *J Endocrinol*. 2010;206(1):121–130.

301. Laviano A et al. Neural control of the anorexia-cachexia syndrome. *Am J Physiol Endocrinol Metab*. 2008;295(5):E1000–8.

302. Ahn JD, Dubern B, Lubrano-Berthelier C, Clement K, Karsenty G. Cart overexpression is the only identifiable cause of high bone mass in melanocortin 4 receptor deficiency. *Endocrinology*. 2006;147(7):3196–3202.

303. Glatt V, Canalis E, Stadmeyer L, Bouxsein ML. Age-related changes in trabecular architecture differ in female and male C57BL/6J mice. *J Bone Miner Res.* 2007;22(8):1197–1207.

304. Bouxsein ML et al. Guidelines for assessment of bone microstructure in rodents using micro-computed tomography. *J Bone Miner Res.* 2010;25(7):1468–1486.

305. Farooqi IS et al. Dominant and recessive inheritance of morbid obesity associated with melanocortin 4 receptor deficiency. *J Clin Invest.* 2000;106(2):271–279.

306. Tanaka T et al. Central melanocortin signaling restores skeletal muscle AMP-activated protein kinase phosphorylation in mice fed a high-fat diet. *Cell Metab.* 2007;5(5):395–402.

307. Martinelli CE et al. Obesity due to melanocortin 4 receptor (MC4R) deficiency is associated with increased linear growth and final height, fasting hyperinsulinemia, and incompletely suppressed growth hormone secretion. *J Clin Endocrinol Metab.* 2011;96(1):E181–8.

308. Zhao L-J et al. Relationship of obesity with osteoporosis. *J Clin Endocrinol Metab.* 2007;92(5):1640–1646.

309. Cawley NX et al. Obese carboxypeptidase E knockout mice exhibit multiple defects in peptide hormone processing contributing to low bone mineral density. *Am J Physiol Endocrinol Metab.* 2010;299(2):E189–97.

310. Zhong Q et al. Multiple melanocortin receptors are expressed in bone cells. *Bone.* 2005;36(5):820–831.

311. Dumont LM, Wu C-SJ, Tatnell MA, Cornish J, Mountjoy KG. Evidence for direct actions of melanocortin peptides on bone metabolism. *Peptides.* 2005;26(10):1929–1935.

312. Tallam LS, da Silva AA, Hall JE. Melanocortin-4 receptor mediates chronic cardiovascular and metabolic actions of leptin. *Hypertension.* 2006;48(1):58–64.

313. Greenfield JR et al. Modulation of blood pressure by central melanocortinergic pathways. *N Engl J Med.* 2009;360(1):44–52.

314. Nagaya N, Kojima M, Kangawa K. Ghrelin, a novel growth hormone-releasing peptide, in the treatment of cardiopulmonary-associated cachexia. *Intern Med.* 2006;45(3):127–134.

315. Nagaya N et al. Treatment of cachexia with ghrelin in patients with COPD. *Chest.* 2005;128(3):1187–1193.

316. Brüning JC et al. Role of brain insulin receptor in control of body weight and reproduction. *Science.* 2000;289(5487):2122–2125.

317. Lee J-Y et al. Loss of cytokine-STAT5 signaling in the CNS and pituitary gland alters energy balance and leads to obesity. *PLoS ONE*. 2008;3(2):e1639.

318. Hou B et al. Selective utilization of Toll-like receptor and MyD88 signaling in B cells for enhancement of the antiviral germinal center response. *Immunity*. 2011;34(3):375–384.

319. Hou B, Reizis B, DeFranco AL. Toll-like receptors activate innate and adaptive immunity by using dendritic cell-intrinsic and -extrinsic mechanisms. *Immunity*. 2008;29(2):272–282.

320. Henao-Mejia J et al. Inflammasome-mediated dysbiosis regulates progression of NAFLD and obesity. *Nature*. 2012;482(7384):179–185.

321. Bence KK et al. Neuronal PTP1B regulates body weight, adiposity and leptin action. *Nat Med*. 2006;12(8):917–924.

322. Qian S et al. Neither agouti-related protein nor neuropeptide Y is critically required for the regulation of energy homeostasis in mice. *Mol Cell Biol*. 2002;22(14):5027–5035.

323. Luquet S, Perez FA, Hnasko TS, Palmiter RD. NPY/AgRP neurons are essential for feeding in adult mice but can be ablated in neonates. *Science*. 2005;310(5748):683–685.

324. Tong Q, Ye C-P, Jones JE, Elmquist JK, Lowell BB. Synaptic release of GABA by AgRP neurons is required for normal regulation of energy balance. *Nat Neurosci*. 2008;11(9):998–1000.

325. Wu Q, Boyle MP, Palmiter RD. Loss of GABAergic signaling by AgRP neurons to the parabrachial nucleus leads to starvation. *Cell*. 2009;137(7):1225–1234.

326. Mitch WE et al. Evaluation of signals activating ubiquitin-proteasome proteolysis in a model of muscle wasting. *Am J Physiol*. 1999;276(5 Pt 1):C1132–8.

327. SLUSHER MA, ROBERTS S. Fate of adrenal ascorbic acid: relationship to corticosteroid secretion. *Endocrinology*. 1957;61(1):98–105.

328. Hyde SR, McCallum RE. Lipopolysaccharide-tumor necrosis factor-glucocorticoid interactions during cecal ligation and puncture-induced sepsis in mature versus senescent mice. *Infect Immun*. 1992;60(3):976–982.

329. Konagaya M, Bernard PA, Max SR. Blockade of glucocorticoid receptor binding and inhibition of dexamethasone-induced muscle atrophy in the rat by RU38486, a potent glucocorticoid antagonist. *Endocrinology*. 1986;119(1):375–380.

330. Heikinheimo O, Kekkonen R, Lähteenmäki P. The pharmacokinetics of mifepristone in humans reveal insights into differential mechanisms of antiprogestin action. *Contraception*. 2003;68(6):421–426.

331. Frost RA, Lang CH. Regulation of muscle growth by pathogen-associated molecules. *J Anim Sci.* 2008;86(14 Suppl):E84–93.

332. Mathison JC, Ulevitch RJ, Fletcher JR, Cochrane CG. The distribution of lipopolysaccharide in normocomplementemic and C3-depleted rabbits and rhesus monkeys. *Am J Pathol.* 1980;101(2):245–264.

333. Van Gammeren D, Damrauer JS, Jackman RW, Kandarian SC. The I B kinases IKK and IKK are necessary and sufficient for skeletal muscle atrophy. *FASEB J.* 2008;23(2):362–370.

334. Hunter RB et al. Activation of an alternative NF-kappaB pathway in skeletal muscle during disuse atrophy. *FASEB J.* 2002;16(6):529–538.

335. Muller FL et al. Denervation-induced skeletal muscle atrophy is associated with increased mitochondrial ROS production. *Am J Physiol Regul Integr Comp Physiol.* 2007;293(3):R1159–68.

336. Semprun-Prieto LC et al. Angiotensin II induced catabolic effect and muscle atrophy are redox dependent. *Biochem Biophys Res Commun.* 2011;409(2):217–221.

337. Li YP, Schwartz RJ, Waddell ID, Holloway BR, Reid MB. Skeletal muscle myocytes undergo protein loss and reactive oxygen-mediated NF-kappaB activation in response to tumor necrosis factor alpha. *FASEB J.* 1998;12(10):871–880.

338. Li Y-P, Chen Y, Li AS, Reid MB. Hydrogen peroxide stimulates ubiquitin-conjugating activity and expression of genes for specific E2 and E3 proteins in skeletal muscle myotubes. *Am J Physiol, Cell Physiol.* 2003;285(4):C806–12.

339. Furukawa-Hibi Y, Yoshida-Araki K, Ohta T, Ikeda K, Motoyama N. FOXO forkhead transcription factors induce G(2)-M checkpoint in response to oxidative stress. *J Biol Chem.* 2002;277(30):26729–26732.

340. Moldawer LL, Svaninger G, Gelin J, Lundholm KG. Interleukin 1 and tumor necrosis factor do not regulate protein balance in skeletal muscle. *Am J Physiol.* 1987;253(6 Pt 1):C766–73.

341. De Bosscher K, Vanden Berghe W, Haegeman G. The interplay between the glucocorticoid receptor and nuclear factor-kappaB or activator protein-1: molecular mechanisms for gene repression. *Endocr Rev.* 2003;24(4):488–522.

342. Sorrells SF, Sapolsky RM. An inflammatory review of glucocorticoid actions in the CNS. *Brain Behav Immun.* 2007;21(3):259–272.

343. Terada Y et al. Aldosterone stimulates nuclear factor-kappa B activity and transcription of intercellular adhesion molecule-1 and connective tissue growth factor in rat mesangial cells via serum- and glucocorticoid-inducible protein kinase-1. *Clin Exp Nephrol.* 2012;16(1):81–88.

344. Irita J et al. Osteopontin deficiency protects against aldosterone-induced inflammation, oxidative stress, and interstitial fibrosis in the kidney. *Am J Physiol Renal Physiol.* 2011;301(4):F833–44.

345. Fukuda S et al. Aldosterone-induced kidney injury is mediated by NFκB activation. *Clin Exp Nephrol.* 2011;15(1):41–49.

346. Gilbert KC, Brown NJ. Aldosterone and inflammation. *Curr Opin Endocrinol Diabetes Obes.* 2010;17(3):199–204.

347. Nishiyama A et al. Possible contributions of reactive oxygen species and mitogen-activated protein kinase to renal injury in aldosterone/salt-induced hypertensive rats. *Hypertension.* 2004;43(4):841–848.

348. Leroy V et al. Aldosterone activates NF-kappaB in the collecting duct. *J Am Soc Nephrol.* 2009;20(1):131–144.

349. Lang F et al. (Patho)physiological significance of the serum- and glucocorticoid-inducible kinase isoforms. *Physiol Rev.* 2006;86(4):1151–1178.

350. Tai DJC, Su C-C, Ma Y-L, Lee EHY. SGK1 phosphorylation of IkappaB Kinase alpha and p300 Up-regulates NF-kappaB activity and increases N-Methyl-D-aspartate receptor NR2A and NR2B expression. *J Biol Chem.* 2009;284(7):4073–4089.

351. Nishi M, Tanaka M, Matsuda K-I, Sunaguchi M, Kawata M. Visualization of glucocorticoid receptor and mineralocorticoid receptor interactions in living cells with GFP-based fluorescence resonance energy transfer. *J Neurosci.* 2004;24(21):4918–4927.

352. Ullrich S et al. Serum- and glucocorticoid-inducible kinase 1 (SGK1) mediates glucocorticoid-induced inhibition of insulin secretion. *Diabetes.* 2005;54(4):1090–1099.

353. Almeida M, Han L, Ambrogini E, Weinstein RS, Manolagas SC. Glucocorticoids and tumor necrosis factor α increase oxidative stress and suppress Wnt protein signaling in osteoblasts. *J Biol Chem.* 2011;286(52):44326–44335.

354. Iuchi T et al. Glucocorticoid excess induces superoxide production in vascular endothelial cells and elicits vascular endothelial dysfunction. *Circ Res.* 2003;92(1):81–87.

355. Reichardt HM et al. Repression of inflammatory responses in the absence of DNA binding by the glucocorticoid receptor. *EMBO J.* 2001;20(24):7168–7173.

356. Reichardt HM et al. DNA binding of the glucocorticoid receptor is not essential for survival. *Cell.* 1998;93(4):531–541.

357. Kleiman A, Tuckermann JP. Glucocorticoid receptor action in beneficial and side effects of steroid therapy: lessons from conditional knockout mice. *Mol Cell Endocrinol.* 2007;275(1-2):98–108.

358. Varga G et al. Glucocorticoids induce an activated, anti-inflammatory monocyte subset in mice that resembles myeloid-derived suppressor cells. *J Leukoc Biol.* 2008;84(3):644–650.

359. Vanden Berghe W, Francesconi E, De Bosscher K, Resche-Rigon M, Haegeman G. Dissociated glucocorticoids with anti-inflammatory potential repress interleukin-6 gene expression by a nuclear factor-kappaB-dependent mechanism. *Mol Pharmacol.* 1999;56(4):797–806.

360. Vayssière BM et al. Synthetic glucocorticoids that dissociate transactivation and AP-1 transrepression exhibit antiinflammatory activity in vivo. *Mol Endocrinol.* 1997;11(9):1245–1255.

361. Lin CW et al. trans-Activation and repression properties of the novel nonsteroid glucocorticoid receptor ligand 2,5-dihydro-9-hydroxy-10-methoxy-2,2,4-trimethyl-5-(1-methylcyclohexen-3-y1)-1H-[1]benzopyrano[3,4-f]quinoline (A276575) and its four stereoisomers. *Mol Pharmacol.* 2002;62(2):297–303.

362. Coghlan MJ et al. A novel antiinflammatory maintains glucocorticoid efficacy with reduced side effects. *Mol Endocrinol.* 2003;17(5):860–869.

363. Beck IME et al. Crosstalk in inflammation: the interplay of glucocorticoid receptor-based mechanisms and kinases and phosphatases. *Endocr Rev.* 2009;30(7):830–882.

364. De Bosscher K et al. A fully dissociated compound of plant origin for inflammatory gene repression. *Proc Natl Acad Sci USA.* 2005;102(44):15827–15832.

365. Dewint P et al. A plant-derived ligand favoring monomeric glucocorticoid receptor conformation with impaired transactivation potential attenuates collagen-induced arthritis. *J Immunol.* 2008;180(4):2608–2615.

366. Miner JN et al. Antiinflammatory glucocorticoid receptor ligand with reduced side effects exhibits an altered protein-protein interaction profile. *Proc Natl Acad Sci USA.* 2007;104(49):19244–19249.

367. Belvisi MG et al. Therapeutic benefit of a dissociated glucocorticoid and the relevance of in vitro separation of transrepression from transactivation activity. *J Immunol.* 2001;166(3):1975–1982.

368. Busquets S et al. Myostatin blockage using actRIIB antagonism in mice bearing the Lewis lung carcinoma results in the improvement of muscle wasting and physical performance. *J Cachex Sarcopenia Muscle.* 2012;3(1):37–43.

369. Op den Kamp CM et al. Pre-cachexia in patients with stages I-III non-small cell lung cancer: Systemic inflammation and functional impairment without activation of skeletal muscle ubiquitin proteasome system. *Lung Cancer.* 2012;76(1):112–117.

370. Stephens NA et al. Using transcriptomics to identify and validate novel biomarkers of human skeletal muscle cancer cachexia. *Genome Med.* 2010;2(1):1.

APPENDIX A

Supplemental Figures referred to in main text.

Figure 28. Melanocortin Blockade Protects Lean Mass, but Not Skeletal Muscle Mass in Experimental Cancer Cachexia

Figure 29. Ghrelin treatment fails to improve muscle mass and lean mass in chronic renal failure independent from food intake

Figure 30. Low Dose Dexamethasone Does Not Restore the Catabolic Response to i.c.v. IL-1β in ADX Mice

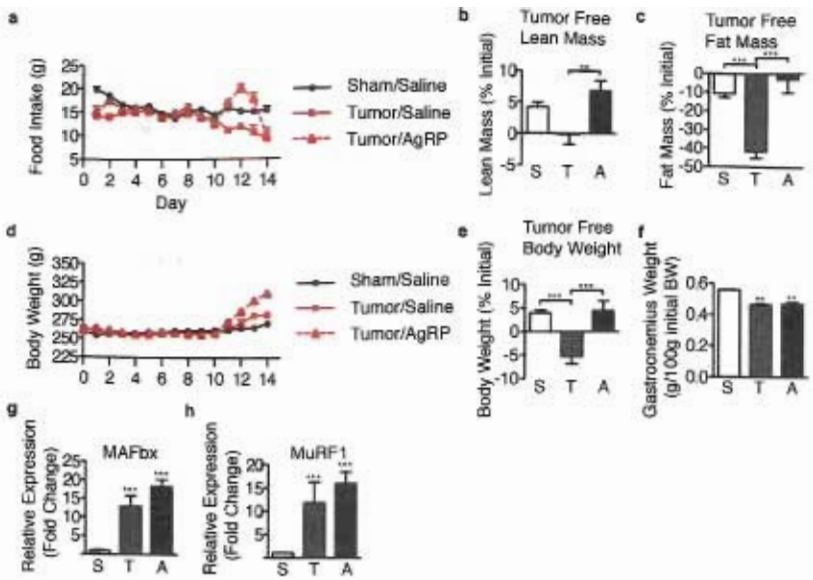

Figure 28. Melanocortin blockade protects lean mass, but not skeletal muscle mass in experimental cancer cachexia

Male F344 rats were implanted with a syngenic methyl cholanthrene induced sarcoma or were subject to a sham surgery (n=7). Tumor bearing rats were treated with 1 nmol AgRP (n=8) or saline (n=8) by i.c.v. injection in the evening starting on day 10. (**a**) Food intake and (**d**) body weight were measured daily. (**b**) AgRP treatment improved tumor free lean mass, (**c**) fat mass and (**e**) Body weight on the final day of the experiment as measured by NMR. (**f**) AgRP did not prevent the loss of skeletal muscle mass or (**g**) the induction of MAFbx or (**h**) MuRF1 mRNA in gastrocnemius muscle. **= P<0.01, ***=P<0.001 as calculated by one way ANOVA with Bonferroni post-test. S=Sham/Saline, T=Tumor/Saline, A=Tumor/AgRP.

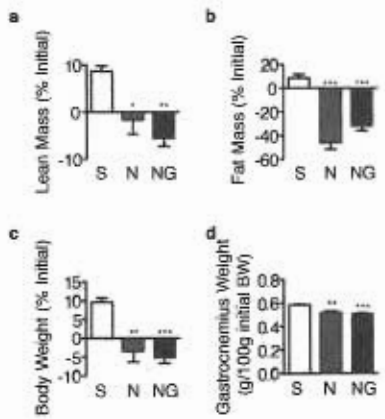

Figure 29. Ghrelin treatment fails to improve muscle mass and lean mass in chronic renal failure independent from food intake

Male F344 rats were subjected to 5/6th nephrectomy or sham surgery (n=5). Nephrectomized rats were treated with ghrelin (n=10) or saline (n=9) by subcutaneous osmotic mini pump. Ghrelin treated animals were pair fed to the saline/nehrectomy group. (**a**) Ghrelin treatment failed to improve lean mass, (**b**) fat mass and (**c**) body weight on the final day of the experiment as measured by NMR. (**d**) Ghrelin did not prevent the loss of skeletal muscle mass. *=P<0.05, **= P<0.01, ***=P<0.001 as calculated by one way ANOVA with Bonferroni post-test. S=Sham/Saline, N=Nephrectomy/Saline, NG=Nephrectomy/Ghrelin/Pair Fed.

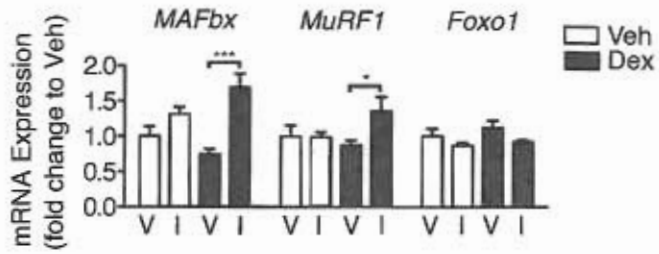

Figure 30. Low dose dexamethasone does not restore the catabolic response to i.c.v. IL-1β in ADX mice

Male C57BL/6 mice were adrenalectomized, replaced with low endogenous corticosterone, and injected i.c.v. with IL-1β (10 ng, n=5-6/group). A subset of the animals were injected with low-dose dexamethasone (20 µg/kg). Atrophy gene expression in gastrocnemius muscle 8 h after injection relative to GAPDH as an endogenous control. *= P<0.05, ***=P<0.001 as calculated by one way ANOVA with Bonferroni post-test. V=Vehicle, I=IL-1β.

APPENDIX B

Studies examining the role of glucocorticoid signaling in skeletal muscle in experimental models of muscle atrophy.

Background

Our studies utilizing ADX animals as well as the mGRKO mouse have demonstrated that muscle atrophy in response to LPS depends on intact glucocorticoid signaling in muscle (Figure 14). Further, levels of circulating corticosterone similar to those seen in a multitude of disease states are sufficient to produce significant atrophy in isolation. Therefore, in the studies detailed below, we attempted to extrapolate these findings in two disease models.

Study 1- *LLC Cancer Cachexia in mGRKO Mice.*

Materials and Methods

Six-week old male mGRKO and $GR^{Lox/Lox}$ littermates were injected subcutaneously with $5x10^7$ LLC cells in 100 µL PBS, in the left flank. Animals were sacrificed 16 days after injection, as some animals had begun to demonstrate significant weight loss. Food intake and body weight were recorded daily. Gastrocnemius muscles were weighed at the time of sacrifice and preserved in RNALater (Ambion). Real time PCR was performed as described in chapter 2.

Results

Similar to our previous experiments with the LLC tumor (Figure 2), tumors were palpable several days after implantation. After one week of growth, the skin overlying the tumor began to ulcerate in some animals in a manner unrelated to genotype. This was not seen when the tumors were implanted suprascapularly (Figure 2). Food intake and body weight were unaffected throughout the course of the experiment, until the final day of the experiment where several LLC/mGRKO animals unexpectedly lost weight overnight (Figure 31 a, b). Weight loss was not observed at this or any tumor size in previous experiments with suprascapular tumors. At the time of sacrifice, many of the tumor bearing animals were profoundly anemic, in a manner that appeared to correlate more with the degree of ulceration than with tumor burden. Specifically, the three animals that were undergoing rapid weight loss were most affected. While weight loss is a feature of cachexia, the rapid weight loss seen in these animals is atypical of LLC cachexia. When these animals are included in the data, few differences are evident between genotypes. However, when these animals are excluded, trends become evident which suggest that mGRKO mice may resist LLC cachexia to some degree. Tumor weight was roughly equivalent between groups (Figure 31 c). Muscle weight was significantly reduced in $GR^{Lox/Lox}$ mice, which lost ~8% muscle mass relative to controls (Figure 31 d, e). In contrast, mGRKO mice lost ~4% muscle mass. When skeletal muscle gene expression is examined however, tumor growth increased MAFbx gene expression in both $GR^{Lox/lox}$ and mGRKO mice (Figure 31 f). MuRF1 and Foxo1 were not significantly induced by tumor growth, likely owing to the small tumor size at which this experiment was terminated.

Conclusions

The involvement of glucocorticoids in cancer cachexia is a subject of debate in the literature. Unfortunately, this study cannot shed any definitive light on the subject owing to the presence of anemia and ulceration. The LLC tumor line is syngenic to C57/BL6 mice. However, our mGRKO mice were only ~90% BL6, owing to the contribution of the FBV line in which the MCK-Cre transgenic was derived. It is possible that the ulceration and anemia are a result of this minor histoincompatability. Alternately, it is possible that these findings are the result of the tumor site (flank vs suprascapular), although the flank is the most common site of implantation for this tumor. Regardless, due to the development of anemia, this experiment had to be stopped early prior to the full development of wasting. When animals exhibiting the worst anemia (and weight loss) were excluded, mGRKO mice appeared to experience a 50% protection of muscle mass. However, due to the large variability of muscle mass lost in response to tumor growth in both genotypes, and the relatively small absolute magnitude of weight loss exhibited, it is difficult to make any definitive statements about this finding.

The E3 ligases expression, in contrast, did not reflect this protection of muscle mass. MAFbx was the only atrophy gene induced by LLC growth, in contrast with our published study in chapter 2 (Figure 2), likely owing to the relatively small tumor mass achieved by this study. Both genotypes exhibited an equal induction of MAFbx, demonstrating that the induction of this gene by tumor growth does not depend on glucocorticoids. The dissociation between the degree of wasting and the expression of the E3 ubiquitin ligases is not surprising given our experience with tumor models. In the MCA sarcoma model and also the walker 256 tumor model in rats, muscle mass loss is evident prior to significant inductions in E3 ligase expression. As it is the general habit to push tumor models as close as possible to the end of life, E3 ligases

are generally elevated in experimental models of cancer cachexia, despite not being present longitudinally. Furthermore, a recently published report using the LLC model demonstrated that myostatin antagonism reverses muscle mass loss but not atrophy gene expression in mice growing LLC tumors (368). In human cancer cachexia, MAFbx and MuRF1 expression has not been associated with ongoing weight loss (369, 370). Therefore, it is unclear whether E3 ligase expression truly is a marker of ongoing muscle loss in response to tumor growth, or whether it simply represents elevated proteolysis in response to multi system organ failure in the hours preceding death. This question is unanswerable without the development of animal models that more closely recapitulate the human condition. Regardless, while these data are suggestive of a contribution of glucocorticoids to muscle wasting in cancer cachexia, further studies are required to explore this subject.

Study 2- *Experimental Sepsis in mGRKO Mice.*

Materials and Methods

Female mGRKO mice at 12-14 weeks of age were subject to cecal ligation and puncture (CLP). Under isoflurane anesthesia, a midline laparotomy was performed, and the cecum was externalized and ligated just proximal to the ileocecal valve. The cecum was punctured through and through with a 19 gauge needle, and intestinal contents were extruded to maintain patency of the needle tract. The cecum was then returned to the abdominal cavity and the wound was closed with 4/0 silk suture. Mice received 1 cc of sterile normal saline subcutaneously immediately following the procedure. Sham surgeries were performed in the same manner except that the cecum was neither ligated nor punctured. Survival, food intake and body weight were followed daily. Muscle mass was recorded at the time of sacrifice.

Results

Significant mortality was observed in both genotypes on the second day after CLP (Figure 32 a). Food intake and body weight were both significantly decreased from baseline in both genotypes (Figure 32 b, c). At sacrifice, muscle mass was higher in mGRKO mice compared with littermate $GR^{Lox/Lox}$ mice (Figure 32 d), although this did not rise to the level of statistical significance. In some cohorts of mGRKO mice, significantly increased muscle mass is observed at baseline. Therefore, it is unclear whether this trend toward increased muscle mass in the mGRKO mouse after CLP is the result of a baseline phenotype in this cohort of animals, or a differential response to sepsis.

To avoid the mortality associated with the CLP procedure, and the complication of 3 days with near zero food intake, we examined mice at a 24 hour time point after CLP. At this time point, CLP has been demonstrated to significantly increase proteolysis in rat muscle in a manner dependent on glucocorticoids (93). CLP lead to an equivalent suppression of food intake in both genotypes relative to sham operated control animals (Figure 32 e). Interestingly, body weight was lost equally in all 4 groups (Figure 32 f). Consistent with this, muscle mass was not different between sham and CLP animals within a genotype, although mGRKO mice had larger muscles irrespective of treatment (Figure 32 g).

Discussion

Despite the clearly established role for glucocorticoids in mediating increases in muscle proteolysis in experimental sepsis, we were unable to demonstrate protection from muscle atrophy in the mGRKO mouse in response to CLP. One possible explanation is the significant stress of laparotomy. Mice are extremely

sensitive to stress, which is marked by increased levels of circulating glucocorticoids. Thus, one possible interpretation of the data in Figure 32 g is that both sham and CLP $GR^{Lox/Lox}$ animals experienced significant atrophy. It is likely that if a longer time point were examined, sham animals would have recovered from the stress of surgery, and differences in atrophy would have become apparent. However, in order to accomplish this, the CLP model would need to be titrated to increase survival at longer time points. Unfortunately, due to time constraints, this was not possible. Therefore, conclusive evidence linking glucocorticoids to muscle atrophy in sepsis cannot be found in this data.

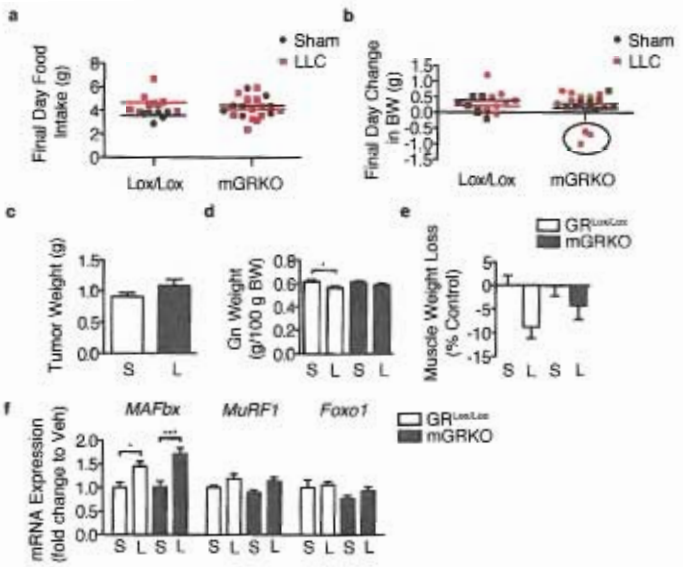

Figure 31. Glucocorticoids and muscle atrophy in cancer cachexia

Male mGRKO mice and $GR^{Lox/Lox}$ littermate controls were implanted with the lewis lung carcinoma ($5X10^7$) cells or were subject to a sham surgery (n=6-12/group). (**a**) Food intake was measured daily and was normal until the final day of the experiment. (**b**) Body weight was normal until several animals in the mGRKO/LLC group lost weight (circled). These animals were profoundly anemic at sacrifice and are excluded from the results below. (**c**) Tumor weight was slightly higher in mGRKO mice. (**d**) Gastrocnemius muscle weight normalized to initial body weight and (**e**) muscle mass loss relative to controls. (**f**) Atrophy gene expression in gastrocnemius muscle relative to GAPDH as an endogenous control. *= P<0.05, ***=P<0.001 as calculated by two-way ANOVA with Bonferroni post-test. S=Sham, L=Lewis Lung Carcinoma.

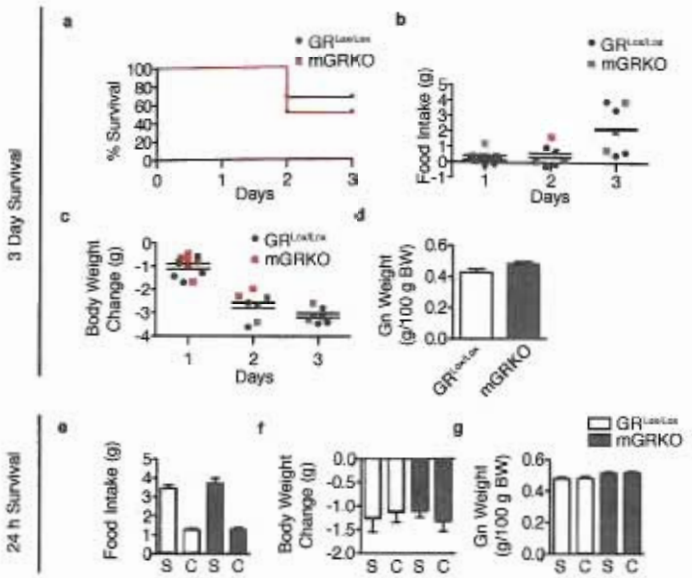

Figure 32. Glucocorticoids and muscle atrophy in sepsis

Male mGRKO mice and $GR^{Lox/Lox}$ littermate controls were subjected to cecal ligation and puncture or were subject to a sham surgery (n=5-6/group). Two time points were examined: a 3-day time point and a 24 h time point. (**a**) Survival, (**b**) Food intake and (**c**) body were measured daily. (**d**) Gastrocnemius muscle weight normalized to initial body weight. (**e**) Food intake 24 h after CLP. (**f**) Body Weight change 24 h after CLP. (**g**) Gastrocnemius muscle weight normalized to initial body weight. S=Sham, C=Lewis Lung Carcinoma.